1-1-2007

Design and structural analysis of sofa frames

Li Dai

DESIGN AND STRUCTURAL ANALYSIS OF SOFA FRAMES

By

Li Dai

A Dissertation
Submitted to the Faculty of
Mississippi State University
in Partial Fulfillment of the Requirements
for the Degree of Doctor of Philosophy
in Forest Products
in the Department of Forest Products

Mississippi State, Mississippi

December 2007

DESIGN AND STRUCTURAL ANALYSIS OF SOFA FRAMES

By

Li Dai

Approved:

Jilei Zhang
Associate Professor of Forest Products
(Director of Dissertation)

Steve L. Hunter
Associate Professor of Forest Products
(Committee Member)

Harry A. Cole
Associate Professor of Civil Engineering
(Committee Member)

Yibin Xue
Assistant Research Professor of
Center for Advanced Vehicular Systems
(Committee Member)

Gary Daniels
General Manager, Frame Operations
Schnadig Cooperation
(Committee Member)

Rubin Shmulsky
Associate Professor of Forest Products
Interim Department Head /Graduate
Coordinator of the Department of Forest
Products

George M. Hopper
Dean of the College of Forest Resources

Name: Li Dai

Date of Degree: December 14, 2007

Institution: Mississippi State University

Major Field: Forest Products

Major Professor: Dr. Jilei Zhang

Title of Study: DESIGN AND STRUCTURAL ANALYSIS OF SOFA FRAMES

Pages in Study: 153

Candidate for Degree of Doctor of Philosophy

This project's goals are to evaluate the structure and strength design of *Schnadig* three-seat sofa frames and improve the design to meet product performance requirement specified by *Schnadig*. The target goal of medium or above acceptance level of General Service Administration (GSA) performance test was expected for the improved design. The design procedures and testing results in the study are also applicable to other frames. In this study, the mechanical and strength properties of frames, and members and joints, were evaluated.

Schnadig three-seat sofa frames were evaluated by the performance tests. The critical joints and members were identified. Generally the frames did not reach the anticipated medium acceptance level. The inadequate connection of joints and the weak member were the major cause of failure.

Next, the static and fatigue properties of selected plywood, oriented strand board (OSB) and particle board (PB) were investigated. The regression equations of *S-N* (stress

versus number of cycles to failure) through low 5% points (i.e., the 5th percentile) were derived for all selected wood composite materials and proposed as design equations for achieving a conservative design of furniture frame structural members considering fatigue effects. Analysis results indicted that when cyclic stepped load effects were considered, the allowable design stress for plywood, OSB, and PB should not exceed respectively, 54%, 64%, and 68% of their MOR.

Experiments were also designed to investigate the lateral shear and direct withdraw load resistances of face-to-face and end-to-face joints. Two types of connection, glue and single staple, were studied. Load direction relative to grain direction was considered. Statistical analyses were implemented to study the effect on the load resistance of the joints.

Lastly, a solid 3D frame model was developed in I-DEAS to obtain the internal forces on critical components. Suggestions on the constructions of critical components were made based on internal forces obtained from computer modeling, as well as the laboratory results of frames, members, joints. One result of this study is the recommendations for improved construction details.

Key words: furniture frame, structural analysis, wood composite

ACKNOWLEDGEMENTS

I would like to take this opportunity to acknowledge those people who gave their support and motivation in the pursuit of my doctoral degree.

First and foremost, I want to give my deepest thanks to my husband, Yufeng Ge, my mom, Xinbao Tu, and my dad, Xianguo Dai. I appreciate their understanding for all the time I was away from them. This dissertation could not be possible without their unconditional understanding and support.

Next, I would like to express my greatest appreciation to my committee chair, Dr. Jilei Zhang. Dr. Zhang's consistent motivation and direction played a key role throughout my Ph.D. program. More importantly, I learned from him the qualities a good researcher must have: passion, perseverance, discipline, patience, and intelligence. Dr. Zhang's philosophy and attitude toward science and research will have a far-reaching influence on me in my career.

Also, I would like to extend appreciation to my committee members, Dr. Yibin Anna Xue, Dr. Steve Hunter, Dr. Harry Cole, and Mr. Gary Daniels. I thank them for their time and efforts in serving on my graduate committee and reviewing my dissertation. Their wisdom and professionalism are reflected in every single line throughout this dissertation

In addition, my appreciations go out to the staff working in furniture testing lab, Mr. Bob Tackett and Mr. Franklin Quin. They provided a huge amount of assistance in experimental design and data collection.

Last but not least, I want to thank *Schnadig* Corporation and Franklin Furniture Institute for their financial support and research funding.

TABLE OF CONTENTS

LIST OF TABLES

LIST OF FIGURES

CHAPTER I

INTRODUCTION

Background

Strength and durability performance of an upholstered furniture frame is dependent on how well its structural design is performed and its manufacturing process is executed to ensure all engineering design specifications are satisfied. Structural design of a piece of furniture, like that of most structures of historical origin, evolved through experience gained by trial and error. Whereas analytical procedures have been developed and incorporated into the design of other structures such as bridges and buildings, they have not been systematically introduced into the design of furniture frames. Even though in the past few decades extensive research has been carried out on the strength properties of furniture, most work had been focusing on frame component performance studies such as joint moment resistance and member material strength and stiffness. Current furniture strength design practice is still mostly based on a mixture of experience and trial and error. No research has been done to relate frame service loads required to its frame component design in terms of design loads corresponding to different service load levels. In other words, design loads for strength and durability design of upholstered furniture frames are not available. The reason for lack of design load information is due to the fact that internal forces at critical joints and members in a sofa frame have never been

analyzed. However, furniture designers need this information to optimize their design and achieve desired product performance and quality requirements with minimum materials and manufacturing costs.

This research focused on the development of analysis methods and design procedures for three-seat sofa frames, which represent a complex structural system consisting of members and joints, and are prone to multi-phase failures under repeated loading. Once the methods and procedures had been developed, they were applied to an industry frame evaluation and design project to achieve optimum design, which requires information such as design loads, material strength properties, and joint load resistance capacities.

The three-seat sofa frame studied in the project was manufactured by *Schnadig*, one of the largest family owned furniture manufacturers in the United States. Figure 1.1 shows the overall construction of the frame, including the sizes of key members, and the constructions of joints. In general, the frame is 90.5 inches long, 31 inches deep, and 33 inches high. The frame is constructed with 28 parts, all of which are made from 3/4-inch-thick six-ply southern yellow pine plywood except for the front and back spring rails, which are made from 7/8-inch-thick hardwood plywood. Appendix A lists the name, material type, and sizes of each part. The members were mainly connected by glue and staples. The staples used were SENCOTE 16 gage galvanized chisel-end-point types with leg length of 1.5 inches. The glue was polyvinyl acetate (PVA) wood glue with solids content of 40%.

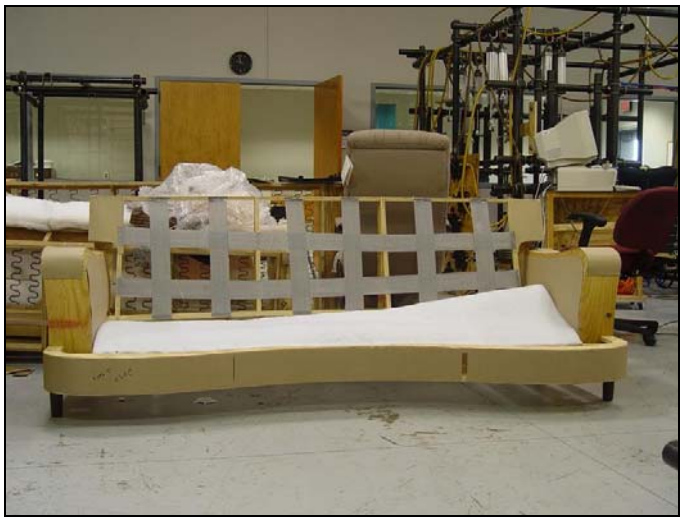

Figure 1.1 The three-seat sofa frame by *Schnadig*

The component behaviors of the *Schnadig* frame subjected to the GSA (GSA 1981 and 1989) testing loads and boundary conditions were studied. Member material and joint mechanical properties were evaluated, and the Finite Element Method (FEM) was applied to develop a simulation model, which was expected to predict the internal forces at critical joints and members. Static and fatigue data of frame components obtained from research during the past six years at the Franklin Furniture Institute, Mississippi State University were incorporated with simulation results to derive loads for design upholstered furniture frames.

Objectives

The main objectives of this research were to perform design and structural analysis of the *Schnadig* sofa frame, summarize current available information on engineering design, derive cyclic schedules for durability evaluation of frame

components, and propose optimization of current frame constructions. It aimed to evaluate and improve the structural design of *Schnadig* three-seat frame so that the medium or above acceptance levels according to the GSA standard would be economically achieved.

The overall goal can be broken down into the following objectives:

1) Evaluate *Schnadig* three-seat sofa frame construction performance.
    - Understand and document current frame performance levels, constructions, and specifications.
    - Identify critical structural components of sofa frames.
2) Analyze *Schnadig* three-seat sofa frame structures.
    - Develop frame structural analysis models.
    - Analyze internal forces at each critical structural component.
    - Establish fatigue test matrix for critical structural components.
    - Combine the results of the static and fatigue properties on the components from this study and previous studies into the frame analysis.
3) Improve *Schnadig* three-seat sofa frames based on design targets and analysis data.
    - Propose optimization of current frame constructions or new frame design to satisfy the same level of performance as the frame design supplied as the base line.
    - Optimize design to achieve maximum performance/cost ratio.

Procedures

There are existing general testing standards for the performance of sofa frames, such as GSA performance regime FNAE-80-214A (GSA 1998), which are evaluated by cyclic loading rather than static loading. Strength design of sofa frames to satisfy GSA performance test standards needs information related to the fatigue strength properties of their components. In the previous studies, *S-N* curves (stress versus number of cycles to failure) were proposed to describe the fatigue properties of wood composites subjected to zero-to-maximum repeated cyclic loading. Most recently, the Palmgren-Miner (Miner 1945, Palmgren 1924) rule was proposed to estimate the fatigue life of wood composites as upholstered furniture stock subjected to cyclic stepped loads based on the stepped load schedule and *S-N* curves of material (Zhang et al. 2005).

The *S-N* curves can be obtained by applying zero-to-maximum constant amplitude cyclic loads tests, so the remaining problem is to determine the stepped load schedule for each component under GSA loads and boundary conditions. One method is to treat the main structure members as simplified beam models, so that the moment in the beam at different GAS load schedule can be calculated. This simplified method can be used by the furniture manufacturers as a quick estimation without tedious computation. The other method is to simulate the frames and the boundary conditions by using computer finite element (FE) software. The load distribution in the frames under GSA boundary conditions obtained from FE simulation is considered as more accurate than simplified method because it is more representative of the real-world situation. Once the fatigue

load schedules for critical members are obtained, the sizes of structural members can be estimated using the Palmgren-Miner rule equation if the *S-N* curve of the material is known. Then the equivalent moment value used as design loads for each member can be calculated based on estimated member cross section dimensions, and the static/fatigue ratio can be obtained dividing the static loads by fatigue loads for each member.

With regard to the design of joints subjected to GSA performance tests, experience has shown that the cyclic strength of the joints is no more than fifty percent of static strength (Eckelman and Erdil 2000). In other words, to design an upholstered furniture joint to meet a specified GSA performance level of a given stepped load schedule, its load capacity should be at least twice the strength under the same static load. Zhang et al. (2003) proposed a ratio of 2.2 for the design of T-shaped, end-to-side, two-pin dowel joints. In this research, static load test on the joints were performed in addition to performance test. The results obtained from this study were compared with experience and the previous study, and a ratio was proposed for the design of joints when cyclic load effects are considered.

In this project, tests were carried out on frames and the components. Tests on frames were GSA performance tests, through which the frames were evaluated and weak parts were identified. Mechanical experiments on components, including members and joints, were designed, with the purpose of attaining preliminary data pertinent to the strength properties of sofa frame components, and providing basic guidelines for sofa frame design. The mechanical tests on members included: (1) static center load bending

tests to obtain the Modulus of Elasticity (MOE) and Modulus of Rupture (MOR) of selected wood composite materials, (2) constant amplitude cyclic load tests on selected wood composites to derive the *S-N* equations, and (3) cyclic stepped load tests on selected wood composite members to validate the aforementioned procedure used to predict the member fatigue life. The mechanical tests on joints include: (1) shear and direct withdraw load tests on glued face-to-face and end-to-face joints, and (2) shear and direct withdraw load tests on single stapled face-to-face and end-to-face joints. Lastly FE models were developed to simulate the frames under GSA loads and boundary conditions in order to explore the stresses in the critical components. Therefore, the cause of structure failure of the frames could be manifested by incorporating the performance tests and their simulation results with the experiments on individual components.

The dissertation is ordered as follows. Chapter II reviews the current literature relating to the performance on frames, the properties of members, fasteners and joints, and numerical methods used to analyze the frame structures. Chapters III to V describes the tests implemented on frames, members, and joints, respectively. Chapter VI presents the FE models developed to predict the internal forces at critical components. Finally, conclusions are summarized in Chapter VII with the recommendations of the *Schnadig* frames.

CHAPTER II

LITERATURE REVIEW

Performance Tests

Performance tests may be defined as accelerated use tests that predict the ability of a product to fulfill its intended function. The characteristics of good furniture performance tests are: (1) a performance test method should be universal in its geographical range of application; (2) the tests should be of such a nature that they provide the maximum amount of engineering design information concerning the furniture per unit cost; (3) the tests should provide manufacturers with the information needed to market their products and customers with the information needed to purchase them; (4) it is important that the tests should provide a means of quantifying experience, i.e., the tests must provide a means of quantifying the strength characteristics of furniture that fails in service, as well as the strength of furniture that is able to survive generations of use; and, (5) the tests should provide a means for determining the key strength parameters of furniture in an unequivocal manner (Eckelman 1988a).

The prime requirement for a universal, multipurpose test method is that the load model incorporated into it must readily take into account the differences in how the furniture is used, in order to realistically reproduce the differences in how the furniture fails. In most instances, failures of furniture are due to fatigue as a result of repeated use.

Owing to the fact, Eckelman (1988b) proposed a “cyclic stepped load” method. The critical parameters of the process are: (1) the cyclic load rate; (2) the initial starting load; (3) the load increments; and (4) the number of cycles to be completed at each load level. Extensive structural testing has shown that furniture should be subjected to about 25,000 test cycles at each load level before it is subjected to the next higher level at the rate of 20 cycles per minute. A cyclic stepped load model was incorporated into the performance test method developed by the General Service Administration of the federal government for the evaluation of upholstered furniture. Eckelman and Zhang (1995) described six specific tests for upholstered sofa, i.e., seat load foundation test, backrest foundation test, backrest frame test, horizontal side thrust arm load test, front to back load test for legs, and horizontal side thrust test on legs. Tests carried out on hundreds of sofas indicate that the six tests evaluate the most important strength characteristics of the furniture and are equally effective in discovering weakness and hidden defects in design. Figure 2.1 illustrates six test configurations for evaluating structural durable performance characteristics of upholstered furniture frames. Table 2.1 gives detailed cyclic load schedules of these tests. The schedules include initial load, load increments, number of loads, and service acceptance levels.

In addition to the testing program on upholstered frames, there is also a testing program designed for bare frames, which was undertaken at Purdue University in cooperation with the National Furniture Center (NFC). For bare frame testing, instead of backrest and seat foundation tests, there are vertical load test on arms, vertical load test

on front rail, and torsional inward pull test on seat rails. Figure 2.2 illustrates the test configurations for evaluating bare furniture frames, and Table 2.2 lists the schedule of NFC testing schedule on bare frames (Eckelman and Winandy 1978).

Table 2.1 Typical upholstered furniture frame loading schedules and performance-acceptance levels

Test	Initial load (lb.)	Load increments (lb.)	Number of loads	Light-service acceptance level	Medium-service acceptance level	Heavy-service acceptance level
				---------- (lb.) ----------		
Seat Load Foundation Test*	100/50	25/12.5	3	200/100	250/125	275/137.5
Backrest Foundation Test	50	12.5	3	112.5	125	150
Backrest Frame Test	75	25	3	75	100	150
Horizontal Side-thrust Test on Arms - Outward	50	25	1	75	150	200
Front to Back Load test on Legs	100	50	2	150	200	300
Side-thrust Load Test on Legs - Inward	100	50	1	200	250	350

* Seat load test is begun with 100 pounds applied to the rear load position of the load head and with 50 pounds applied to the front position. Rear loadings are increased in increments of 25 pounds and front loadings in increments of 12.5 pounds after 25,000 cycles have been completed at each preceding load level.

Table 2.2 National Furniture Center (NFC) loading schedules and performance-acceptance levels for bare frames

Test	Initial load (lb.)	Load increments (lb.)	Number of loads	Light-service acceptance level	Medium-service acceptance level	Heavy-service acceptance level
				---------- (lb.) ----------		
Cyclic Front to Back Load Test on Top Rails	75	25	3	75	100	150
Cyclic Side-thrust Load Test on Arms						
Outward	50	25	1	75	150	200
Inward				75	175	225
Cyclic Vertical Load Test on Arms	100	100	1	400	600	800
Cyclic Vertical Load Test on						
Front Rail	100	100	3	300	400	600
Back Rail				200	300	500
Cyclic Torsional Inward Pull Test on Seat Rails	100	100	1	300	400	600
Cyclic Front to Back Load Test on Legs	100	50	2	150	200	300
Side-thrust Load Test on Legs						
Outward	100	50	1	100	150	250
Inward				200	250	350

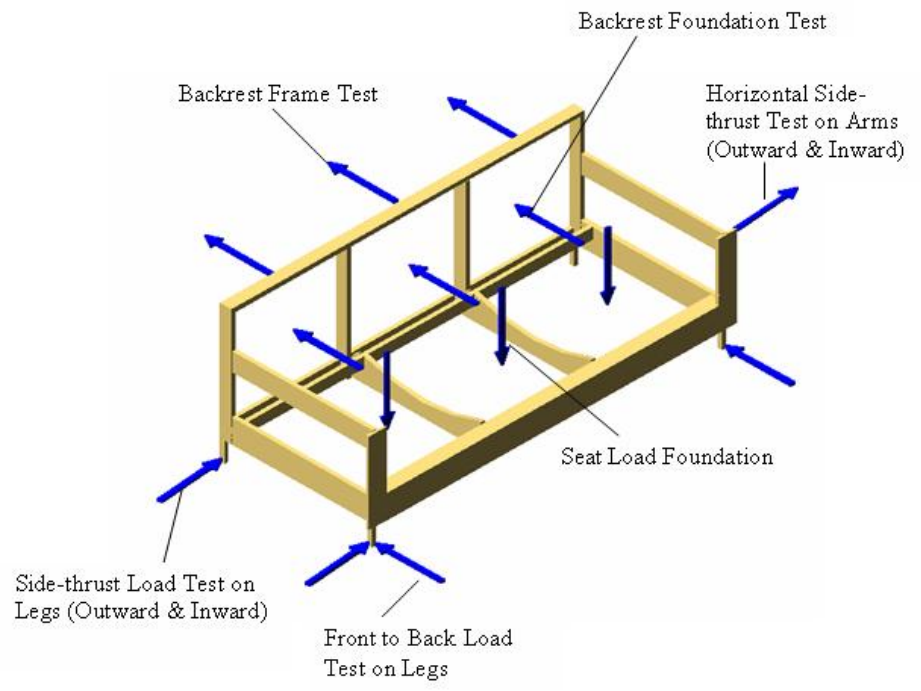

Figure 2.1 Structural performance test loads of three-seat upholstered sofa frames

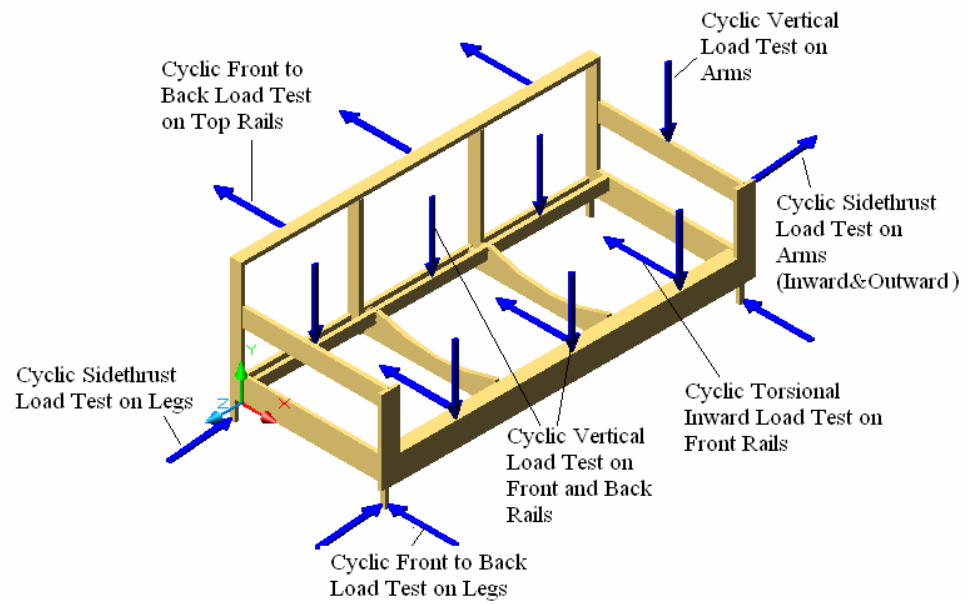

Figure 2.2 Structural performance test loads of three-seat bare sofa frames

Frame Member Material Properties

Furniture is designed primarily for aesthetic appearance by design artists. In most cases the implementation of the design is left to individuals familiar with the performance of materials, the production facilities available to produce the piece of furniture, and the production costs for alternative implementations of the design. These individuals perform the engineering design function. Increasingly, they are applying engineering techniques (Hoover et al. 1987). With the increased use of engineered wood composites, such as plywood, OSB, and particleboard, in upholstered frames, much research is needed to evaluate these products since these products were designed and manufactured initially not for furniture frame stock purposes. In this part, the research on the strength properties such as static, fatigue, impact, and creep, of wood material are reviewed.

Static

Hoover et al. did research on laminate-veneer-lumber (LVL) as the substitute material in furniture production from both a structural and an economical point of view (Hoover et al. 1987, Hoover et al. 1988). A regression model was developed to predict the effect of size, number, and location of holes on maximum load. Angled grain significantly reduced the properties of LVL.

Fatigue

Strength design of upholstered furniture frames should take into account member material fatigue strength properties since most service failures of the frames appear to be

fatigue related (Eckelman and Zhang 1995). The furniture procurement programs of the US government require that upholstered furniture manufacturers conduct the GSA performance test regimen FNAE-80-214A (GSA 1998), and provide furniture performance data to prove satisfaction of performance specifications suitable for use by the federal government. Performance tests are based on a zero-to-maximum cyclic stepped load (variable amplitude loading) method rather than a static load or constant amplitude cycling load method (Eckelman 1988a, 1988b). Strength and durability design of upholstered furniture frames, to satisfy performance test standards such as GSA performance test regimen, need information regarding fatigue strength properties of their components. Also, Eckelman and Zhang (1995) pointed out that it would be necessary to establish a relationship between the static strength of the frames and their fatigue strength.

Although fatigue studies have been carried on wood composites as structural components for airplanes, roofs, walls, and floors, this information has not been systematically introduced into the design of furniture required to resist repeated loads as structures. As more wood composites such as plywood and OSB are used for furniture frame stock, the information related to fatigue strength properties of various types of wood composites becomes more essential. However, the strength properties available for the design of upholstered furniture frames have primarily been determined by static load tests. Research to determine the fatigue properties of wood composites subjected to cyclic loads in furniture applications, especially, stepped cyclic loads, has been minimal.

Fatigue performance of plywood subjected to repeated and reversed flat-wise bending stresses 1,790 cycles per minute (Kommers 1943) was evaluated for aircraft applications. The fatigue strength for 50 million cycles of reversed stress is approximately 27% of the static MOR for the species investigated (yellow birch, yellow-poplar, Sitka spruce, and Douglas fir).

Shear fatigue properties of 23/32 inch commercial OSB were investigated (Cai et al. 1996) under repeated sinusoidal loading using a five-point flat-wise bending test. Regression of the fatigue data of stress-level (the percentage of the static shear strength) versus the log number of cycles-to-failure resulted in a linear *S*-*N* curve.

In an effort to understand fatigue behavior of wood composites as furniture frame stock, Bao and Eckelman (1995) investigated the edgewise fatigue bending resistance of medium density fiberboard (MDF), OSB, and particle board (PB) with the stress-based constant amplitude cycling load and matched piece approach. Experimental results indicated that all three materials would be expected to have fatigue lives of at least 200,000 cycles at the load stress levels of 40 percent of MOR or less. No mathematical representations were derived to approximate *S*-*N* curves of evaluated materials.

To develop an experimental design procedure for furniture frame engineering design considering the fatigue effects, Zhang et al. (2005) evaluated edgewise bending fatigue performances of three wood composites, southern yellow pine plywood, OSB and PB, by subjecting them to zero-to-maximum constant amplitude and stepped cyclic

bending loads. Regression analysis of *S-N* data indicated a linear relationship between applied nominal stress and the logarithm of number of cycles to failure.

Also, in this study, the Adkins' method (1988) was applied to derive the fitting constants *E* and *H* for the Adkins' equation, $S = \sigma_u (E - H \times \log_{10} N_f)$, where σ_u was the ultimate bending strength (MOR). It was found that the constant *E* values were 0.9, 0.9, and 1.0 for plywood, OSB, and PB, respectively. The constant *H* values were 0.05, 0.07, and 0.09 for plywood, OSB, and PB, respectively. It seemed that the constant *H* was correlated with basic wood element sizes of composite raw material such as veneer and particles. It was suggested that the equation $S = MOR(1 - H \times \log_{10} N_f)$ would estimate *S-N* curves of plywood, OSB, and PB if their MOR values were known, where *H* values were 0.05, 0.07, and 0.09 for plywood, OSB, and PB, respectively. This implied that once the MOR was known for a given wood composite, its *S-N* curve could be determined.

Cyclic stepped load tests of full-size specimens showed that the Palmgren-Miner rule was an effective method to estimate the fatigue life of wood composites subjected to the edgewise cyclic stepped bending stresses using their *S-N* curves. But, it tended to overestimate the fatigue life of plywood as being used for three-seat sofa frame top rails to satisfy heavy duty service acceptance level, and fatigue life for OSB to satisfy medium duty service acceptance level. This was due to the fact that the derived *S-N* curve equations estimated mean values of fatigue life (Zhang et al. 2005).

Dynamic Behavior of Materials

Research (Janowiak and Pellerin 1990) was conducted to evaluate the response of reconstituted wood plates to impact loading. The research presented examines an empirical approach to characterize impact response for purposes of investigating initial plate failure followed by evaluation of reductions in ultimate load-carrying capacity. Empirically, the impact response problem for a flexible plate requires examining two deformation systems. Analytical solution of the problem was examined using both an approximate static and a more rigorous dynamic analysis. Exact plate theory, which accounts for transverse shear deformation, was used to evaluate impact-induced stresses given the contact force derived from the static or dynamic plate response analysis. Two program codes, Plate Analysis for Static and Dynamic Loading (PASADL1) and PASADL2, were assembled for examining static, dynamic, and impact loading. A selective subroutine (FAIL), structured within the PASADL codes, was designed to predict failure for thin orthotropic plates where the induced-stress field is dominated by deflection stresses. Experiments were conducted where simply supported plate specimens were impacted according to PASADL FAIL analysis predictions. Three different types of reconstituted wood plates were tested at 16 and 24-inch spans. Initial plate failure was observed for the predicted impact loading cycles. The impacted specimens were statically tested to determine the remaining ultimate plate load-carrying capacity. Similarly, control specimens were tested to provide a comparative database for statistical inferences. Small numerical differences were found between average ultimate

load-carrying capacities of control and impacted specimens. Greater sensitivity was observed in reductions of plate stiffness.

Creep

Wood is a viscoelastic material and, therefore, creep must be accounted for in the design of wood structure when sustained loads are present. The National Forest Products Association Design Specification for Wood Construction suggests a creep factor of 1.5 for glued laminated timber and seasoned sawn lumber, and 2.0 for unseasoned sawn lumber. That is, deflection due to long-term or permanent loads is assumed to be 1.5 to 2.0 times the immediate elastic deflection caused by the load (Fridley 1992). No research was found concerning with the creep factor of wood material used in sofa.

Fasteners and Joints

The design of joints is the most important step in the entire design process for a piece of furniture. Even though the members may have enough strength to carry the forces imposed upon them, if the joints are weak, the structure may still fail. It is probably safe to say that more structural failures occur in furniture because of weak joints than from any other single cause. It is important, therefore, that the joints be properly designed so that they can safely carry the forces imposed upon them in service (Eckelman 2003).

In discussing furniture construction, it is necessary to differentiate between the terms fasteners and joints. Staples, nails, screws, and dowel pins are all examples of

fasteners. When any of these fasteners are used to join two or more members together, they form what is termed a joint. Each type of fastener has its own unique strength characteristics such as ultimate withdrawal strength, shear strength, and bending moment. And ideally, it should be possible to design a complete joint from a consideration of the strength of the individual fasteners used in its construction (Eckelman 2003). The following are previous studies on the mechanical and strength properties of fasteners joints.

Fasteners

Staples

Staples are used in a variety of ways in frame construction. They are frequently used to hold glue blocks in place until the adhesive dries, hold joints such as dowel joints together until the glue dries, and bridge members together. Other uses include attaching plywood gussets to joints to form staple-glued gusset type of joints and also to attach large panels to frames or panels to backs of cases (Eckelman 2003).

Results of direct withdrawal strength of single-staple joints in plywood study (Zhang et al. 2002a) showed that the withdrawal load ranged from 126 to 135 pounds for 16-gage staples with 0.5 inch penetration, 204 to 224 pounds with 0.75 inch penetration, 234 to 316 pounds with 1.0 inch penetration, and 297 to 336 pounds with 1.25 inch penetration. For 15-gage staples, the withdrawal load ranged from 107 to 166 pounds with 0.5 inch penetration, 175 to 250 pounds with 0.75 inch penetration, 234 to 325

pounds for 1.0 inch penetration, and 342 to 365 pounds for 1.25 inch penetration. The withdrawal strength of the single-staple joints could be predicted by a first-order multiple regression equation that included depth of penetration, gage, and staple crown orientation.

The additive effects of staples on the edge direct withdrawal resistance of multi-staple joints constructed of pine plywood have been investigated in Zhang et al. (2002b). Test results indicated that the number of staples positively affected the joint direct withdrawal resistance. The withdrawal resistance of multi-staple joints could be estimated from the withdrawal resistance of single-staple joints and the multi-staple correction factor. The withdrawal resistance was found to be proportional to the number of staples raised to the 0.75 power.

Zhang and Maupin (2004) evaluated the face lateral and withdrawal resistances of face-to-face single and multi-staple joints in furniture-grade, 3/4-inch 5-ply southern yellow pine plywood. Single-staple joint experimental results indicated that staple crown orientation influenced the lateral and withdrawal resistances of single-staple joints in pine plywood. Multi-staple joint experimental results indicated, in general, that the number of staples positively affected the joint lateral and withdrawal resistances.

Zhang et al (2004) also evaluated the edgewise lateral resistances of T-shaped, face-to-edge single and multi-staple joints in furniture-grade, 3/4-inch 5-ply southern yellow pine plywood. Experimental results indicated that staple penetration depth and the number of staples positively affected the edge lateral resistance of staple joints. Tested joints tended to show higher lateral resistances when they were subjected to loads

perpendicular to the fastening member thickness direction, compared to when they were subjected to parallel loads.

Screws

Screws are frequently used to reinforce critically stressed corners with blocks which are glued and screwed in place. Also many of the highly stressed braces used in furniture construction such as the center rail to center upright braces and front rail to stretcher braces are attached with screws. Eckelman (2003) put forward the formulas in computing withdrawal strength of screws from the side grain of solid wood, withdrawal strength of screws from the end grain of solid wood, lateral strength of screws in side grain of solid wood.

Tests were carried out by Eckelman (1988) to determine the holding strengths of various sizes of sheet metal type screws in the face of a commercially available medium density fiberboard (MDF). Similarly, tests were carried out to determine holding strength in the edge of the MDF. Expressions were obtained.

Erdil et al. (2002) did tests to determine the holding strength of screws in the face and edges of plywood and oriented strandboard. Predictive expressions were fitted to the results, which enable the withdrawal strengths of screws embedded in these materials to be predicted as a function of screw diameter and depth of penetration, and density of the board material. The edge withdrawal strength of the 10AB gage screws embedded 1 inch in Douglas-fir plywood ranged from 385 pounds to 532 pounds.

Kurt (2003) studied the effects of screw-gluing and gap-filling phenol resorcinol formaldehyde (GPRF) adhesive using different glue line thicknesses on the shear strength of wood-plywood joints to determine the use of screw-gluing fastening (SG) method and GPRF adhesive. The specimens were manufactured using either SG method with GPRF adhesive and fine threaded dry-wall screws or press-gluing (PG) method with GPRF adhesive. The Analysis of Covariance (ANCOVA) was used for statistical analyses. The results showed that the strength among fastening methods was significantly affected by the glue line thickness, so the strength decreased as the glue line thickness increase. The SG fastening method was found to be as effective as the PG method without thick glue adhesion, but more effective when thick glue lines present. The method can be successfully used to bond wood to plywood for wooden panels, i.e., stressed skin and sandwich panels.

Joints

Dowel Joint

Because of their favorable cost and production characteristics, dowel pins have long been a favorite connector used in furniture industry. The dowel pins themselves are ordinarily subjected to only shear and axial force. Eckelman (2003) put forward the formulas of withdrawal strength of dowel pins from side grain surfaces, withdrawal strength of dowel pins from end grain surfaces, withdrawal strength of end to side grain dowel joints, withdrawal strength of side grain to side grain dowel joints, withdrawal of

end grain to end grain joints, bending strength of two-pin moment-resisting dowel joints, and shear strength of two-pin end-to-side grain dowel joints. However, these expressions were based on a limited number of tests and were intended only to provide estimates. Later research was performed to determine the strength characteristics of dowel joints.

Zhang et al. (2001) conducted tests to determine the bending strength and moment-rotation characteristics of T-type, two-pin dowel joints constructed of red oak, yellow-poplar, southern pine plywood, aspen engineered strand lumber, and particle board. Experimental results indicated that joints constructed of red oak and plywood had the highest bending strength, and that joints of particleboard had the weakest bending resistance. No significant differences in bending strength between joints constructed of oak and plywood were observed. The results for joint stiffness Z-values indicated that the joint stiffness was in the magnitude of 10^{-6} rad./lb.-in. It was also found that the bending strength (M) of the joint could be predicted by means of the formula $M = (d_1/2 + w/3 + e/3)T$, where T = the ultimate direct withdrawal strength of a single dowel, w = the width of the rail, e = the distance from the rail centerline to the neutral axis, and d_1 is the spacing between two dowels (d_1 = 2 in.). The range of ultimate bending strength is from 1,850 lb.-in. (particleboard) to 2,875 lb.-in. (red oak).

A study was undertaken by Zhang et al. (2002) to determine the ability of plywood and OSB to resist lateral forces. These tests developed basic strength data for dowel joints constructed of plywood and OSB in furniture frames.

Eckelman et al. (2002) conducted studies to obtain fundamental information about the withdrawal and bending strength of dowel joints constructed of plywood and oriented strandboard that would be useful in the engineering design of upholstered furniture frames. Results of the withdrawal tests were incorporated into predictive expressions that allow designers to estimate withdrawal strength as a function of the diameter of the dowel, their depth of embedment, and the density of the composite material. Results of the two-pin moment-resisting joint tests indicate that the bending strength of two-pin dowel joints constructed of plywood and OSB may be estimated by means of the same expression developed for solid wood. The average bending strengths of 4-inch wide rails varied from a low of 2,490 lb.-in. for OSB-2 to a high of 3,480 lb.-in. for OSB-1. The average bending strengths of 6-inch wide rails varied from a low of 4,430 lb.-in. for OSB-2 to a high of 5,900 lb.-in. for HP-1.

Torsional strength of dowel joints is an important consideration in the design of furniture frames constructed of plywood and OSB because several members, esp. the seat rails of sofa frames, may be subjected to substantial torsional forces. Zhang et al. (2002) investigated the torsional strength of two-pin dowel joints constructed of plywood and OSB. Experimental results showed that when the dowel spacing or rail width increased, the torsional strength of the joints increased significantly, and this increase was linear with the dowel spacing or rail width. Specimens loaded in the flat position yielded significantly lower torsional strength values than specimens loaded in edge position. Joints subjected to high torsional forces such as the front rail to stump joints in smooth-

front sofas or the side rails in T-front sofas should be reinforced with glue blocks or gusset plates in order to develop the strength needed to resist in-service loads.

Zhang et al. (2003a) investigated the withdrawal and bending performance of wood dowel joints in furniture-grade, 3/4-inch-thick, 5-ply southern yellow pine plywood. Withdrawal tests results indicated that ply-grain orientation had no significant influence on the strength of single dowel withdrawal from edges of 5-ply pine plywood. The withdrawal strength increased significantly as dowel penetration increased from 0.5 to 1.75 inches at the increments of 0.25 inch, but the rate was reduced. The withdrawal strength could be reasonably estimated by means of the power equation including dowel penetration depth. Bending test results indicated that joint bending strength and stiffness increased significantly from 2,471 lb.-in. to 5,541 lb-in. as rail widths increased from four to seven inches, in an increment of one inch.

All aforementioned researches are concerned with static strength of joints. Information about joint fatigue failure also should be taken into account because most service failures of the frames appear to be fatigue related and the most common failure to the frames occurs at the joints. Zhang et al. (2001) investigated fatigue strength properties of T-type, two-pin moment-resisting dowel joints subjected to constant and stepped cyclic bending loads. Red oak, yellow-poplar, plywood, aspen Engineered Strand Lumber (ESL), and particleboard were tested in the construction of joints. Regression of *M-N* data (moment versus log number of cycles to failure) of each joint material type subjected to constant cyclic bending loads resulted in linear equations for

M-N curves. Joints constructed of particleboard had significantly lower fatigue life than joints of red oak, yellow-poplar, plywood, and ESL. No evidence of significant differences existed in fatigue life among joints constructed of red oak, yellow-poplar, plywood, and ESL, but results of static bending tests showed significant differences in bending strength among them. Joint resistance to fatigue failure should be taken into account in strength design of furniture frames that are subjected to repeated loading.

Similar research was conducted on furniture grade, 3/4-inch, 5-ply southern yellow pine plywood by Zhang et al. (2003b). Regression of *M-N* data also indicated a linear relationship existed between the fatigue bending moment applied to joints and the log number of cycles to failure. A simplified method of deriving the fatigue life estimation equation based on known information such as joint static bending strength was proposed. Cyclic stepped load tests verified that Palmgren-Miner rule was an effective method in estimating fatigue life of two-pin dowel joints subjected to cyclic stepped bending moments based on their *M-N* curves. Fatigue life comparisons among joint groups with different static bending strengths indicated that a significant increase in static bending strength might not yield a significant fatigue life increase when a joint was subjected to cyclic stepped loads. Joint resistance to fatigue failure should be taken into account in strength design of furniture frames that are subjected to repeated loading.

Gusset-plate

Only limited information is available concerning bending resistance of gusset-plate joints constructed of wood composites. To study the strength and stiffness of joints

with gusset-plates, Eckelman (1971) constructed T-shaped joints of Douglas-fir with different configurations of gusset-plates: right-rail-fit gussets, oversize rectangular gussets, and triangular-shaped gussets. Experimental results indicated that the joints were not particularly sensitive to construction variables such as the number of staples and how tightly they were pulled down. Rather, the strength of the joints was limited by the strength of the gusset-plate materials, and in particular, by the rolling shear strength and the shear strength of the plywood. The bending strength of the joints improved considerably when width and length of gusset-plates were increased. The joints constructed with the 3/8 inch plywood plates were 1.26 times as strong as the joints constructed with 1/4-inch plates.

Zhang et al. (2001) investigated the bending strength of T-type, staple-glued plywood gusset-plate joints constructed of wood composites. Test results indicated that the bending strength of gusset-plate joints was significantly affected by gusset-plate thickness, width, and length. Among the plate size parameters, plate width affected joint bending strength the most. Joint member material type and the number of staples had no effect on bending strength. The bending strength of joints constructed with five-inch-wide plates averaged two times as strong as joints constructed of the three-inch-wide plates for the same plate length and thickness. Joint member material and the number of staples had no effect on bending strength. The average bending strength of the joints ranged from 6,073 to 18,528 lb.-in. with plate sizes from 1/4 by 3 by 6 in. to 3/8 by 5 by

10 inches. In general, the bending strength of gusset-late joints could be predicted by means of an expression relating width, length, and thickness.

Mortise and Tenon

Mortise and tenon joints have been widely used for centuries, and despite the increasing use of dowel joints, they are still favored for many types of construction. Numerous variations of the basic joint exist including the blind, stub, keyed, pinned or pegged, open or slip, and haunched mortise-and-tenon joints (Eckelman 2003). Eckelman (2003) put forward the expression for computing the bending strength of mortise-and-tenon joints constructed with 3/8- inch tenons.

Rectangular mortise and tenon construction has been widely used in barns and other buildings and furniture. Round mortise and tenon joints are essentially a modern variation of this construction. They are much easier to manufacture. Potentially, this provides an outlet for small-diameter tree stems that are presently of essentially no economic value (Eckelman et al. 2002).

Eckelman et al. (2004a) conducted tests to determine the withdrawal capacity of cross-pinned round mortise and tenon joints. Tenon diameters ranged from a nominal 0.6 to 1.0 inch. Cross-pins were about one-half the diameter of the tenons. Both wood and steel cross-pins were included. Glued but unpinned joints were included to provide a basis for comparison. Joints with wood cross-pins developed about one-third the capacity of comparable glued but unpinned tenons; joints with steel cross-pins developed over one-half the capacity. Offsetting the cross-pins toward the root of the tenon

increased withdrawal capacity, whereas offsetting the cross-pin toward the tip of tenon decreased capacity. Shrink-fit techniques were found to provide a simple means of producing uniformly tight fitting joints. Shrink-fit joints produce significant levels of withdrawal capacity but likely should not be used alone without adhesives or cross-pins.

Tests were conducted on the same round mortise and tenon joints (Eckelman et al. 2004b) to determine the effect of cross pinning the tenons of round mortise and tenon joints on the bending moment capacity of the joints. It was found that cross pinning reduced the bending moment capacity of red oak joints by 33 percent and yellow-poplar joints by 38 percent. Smaller cross-pins had less effect than larger cross-pins, and offsetting the pins toward the tip of the tenon also caused less reduction in bending moment capacity. Results also tended to indicate that the form factor for round beams, i.e., 1.18, should be incorporated into the flexure formula when estimating the bending moment capacity of round tenons. Finally, the results indicated that the shoulders on tenons significantly increase the bending moment capacity of a joint when the shoulders of the tenon fit firmly against the side of the member in which the tenon was inserted.

T-type End-to-side-grain Furniture Joint

The bending moment capacity of traditional and alternative T-type end-to-side-grain joints constructed of Oriental beech, European oak, and Scotch pine were investigated by Efe et al. (2005). Two-pin dowel and mortise-and-tenon joints assembled with polyvinyl acetate adhesive were considered as traditional adhesive-based joints, and minifix plus dowel and screw joins were considered alternative non-adhesive-based joints.

Experimental results indicated traditional adhesive-based mortise-and-tenon joins yielded the highest bending moment capacity among the four types of tested joints, varying from 2,266 lb-in for Scotch pine to 3,956 lb-in for Oriental beech. Minifix plus dowel joints had the lowest bending moment capacity, varying from 434 lb-in for Scotch pine to 584 lb-in for European oak. Screw joints could produce higher bending moment capacities than traditional glued dowel joints. The bending moment capacity of minifix plus dowel joints was less sensitive to wood species change than mortise-and-tenon joints, dowel joints, and screw joints.

Metal-plate-connected Joint

Metal plates are commonly chosen to connect critical joints, such as front post-front rail and side rail-back post joints, in upholstered furniture frame construction since those joints are highly stressed and difficult to reinforce. Metal plates have unique features of high uniform load resistance, rapid production, and easy connection of members with uniform thickness. With the increased use of engineered composite panel products, such as plywood, as upholstered furniture frame stock, loading capacity data such as moment capacity of joints connected with metal plates is critical for furniture manufacturers to conduct engineering design of upholstered furniture frames on a rational basis.

Zhang et al. (2005) investigated the effects of metal plate length and width, and joint rail width on the moment capacity of the T-shaped, end-to-side, metal-plate-connected (MPC) joints in furniture grade, 3/4 –inch 7-ply southern yellow pine plywood.

Experimental results indicated that metal-plate and rail widths affected the moment capacity of MPC plywood joints the most compared to other factors. The average moment capacity of tested joints ranged from 2,863 lb.-in. to 13,721 lb.-in. The minimum metal-plate length to prevent having joints with tooth withdrawal failure and to have joints fail with plate yield mode is six inch. The moment capacity of MPC joints in pine plywood can be reasonably estimated with existing mechanics based models.

Through-bolts with Dowel-nuts

Through bolts with dowel-nuts are used in furniture construction, both as primary connectors and also to reinforce weaker joints. Through bolts with dowel-nuts are commonly used in chair construction, for example, to reinforce the critical seat side rail to back post joints. They are also commonly used in bulky furniture such as tables. These fasteners also have significant potential value in upholstered furniture frame construction in similar situations where strength and reliability are needed.

Erdil et al. (2003) studied the pull-out strength of dowel-nuts from the ends of plywood and oriented strandboard and the strength of two-bolt moment-resisting joints constructed with this fastener. Results indicated that maximum pull-out strength was obtained with placement of the dowel-nut as close as one inch to the end of the rail in oriented strandboard and 1.5 inches in plywood. Bending tests showed that ultimate bending moments of two-bolt moment-resisting joints up to 9,180 lb.-in. could be obtained with 6-inch-wide rails connected with two fasteners.

Numerical Analysis of Furniture Frames

A piece of furniture is structurally complex because frame components contain curvatures and varying cross sections. Connections are semi-rigid rather than rigid and behave as non-linear structures and their dimensions must not be disregarded in comparison to the dimensions of the frame. In this situation, in engineering computations, simplifying assumptions were adopted in which the connections were assumed either ideally rigid or articulated (Smardzewski 1998). The reason for the lack of systematic analysis of frame structure is that most furniture is a complex system which requires considerable technical experience and involves substantial numbers of tedious computations. Therefore, the analytical methods are far from being commonly employed by furniture designers. In this situation, it appears that numerical methods of rigidity-strength analysis may become the most effective tools for furniture designers.

Research by Gustafsson on structural design of chairs showed how simple finite element calculations lead to a totally different design of a chair. He also emphasized the need for more research on wood in "furniture size" and not only as part of building structures (Gustafasson 1995). Gustafsson (1996a) studied a simple chair, made of birch, where the emphasis was laid on its ability to carry different loads. Using finite element analysis, he predicted the strain and stress at different points on the chair structure. Furthermore, a chair was made and exposed to the same load pattern as used in finite element calculations. The strain was monitored and compared to the calculated value at the points of most interest. The results showed that part of the calculations corresponded

fairly well with the monitored values but also much work still remained in order to totally predict the accurate structural behavior. He also mentioned the difference between tensile and compression strength properties in wood, which made ordinary FEM programs hazardous to use because the background theory assumed that these properties were equal in magnitude (Gustafsson 1996b).

Gustafsson (1997) used different element types to analyze the chair structure. One conclusion was that the overall structure was preferably analyzed by beam element while details such as joints can be studied by plain stress element. Results showed that ordinary chairs were overbuilt and material was wasted from the viewpoint of solid mechanics. He also concluded that much more knowledge was needed about the material wood.

A research project was undertaken by Smardzewski (1998) with the objective to develop and test the effectiveness of a program designed for rigidity-strength analysis of furniture side frames constructions. The program provided results of computation of values of cross section forces, node translocations and dimensions of connectors (dowels or tenons) in selected places of connection of component elements. It was found that tenon connections in constructions of chair side frames ensure sufficient strength and rigidity of the system and maintain optimal dimensions of cross sections of component elements. Dowel connections could replace tenon joints reaching the same strength, but the areas of cross sections of the elements to be joined would have to increase from 18% to 45%. The strength of connections and their dimensions were not as important as the

connecting member in the chair. The rigidity of the chair side frame depended directly on the position of the connecting member and increased as the position of this element was lowered.

CHAPTER III

GSA TESTS ON *SCHNADIG* FRAMES

Frame Testing Plan

Eight sets of performance tests conducted on the three seat sofa frames. Six were the GSA tests on upholstered frames listed in Table 2.1. These were horizontal side-thrust arm load test (outward), seat load foundation test, backrest frame test, backrest foundation test, front to back load test on legs, and side-thrust load test on legs (inward). The other two were the tests on bare frames shown in Table 2.2. These were side-thrust arm load test (inward) and cyclic vertical load test on arms. Through conducting performance tests, critical members and joints can be identified so that measures can be taken to strengthen those weak parts. After the performance tests, static load tests were performed on the intact joints in order to relate the strength properties of the joints under cyclic stepped load and static load. Altogether, there were twelve frames, numbered from #1 to #12, provided by *Schnadig* for frame evaluation. For each test, three replicates were performed. Table 3.1 lists the performance testing plan and the acceptance level.

For the legs tests, the test could not be completed because the plastic legs were too weak. For both tests of front to back load test on legs, and side-thrust load test on legs, the testing was forced to stop after just a few cycles. Therefore, no more tests on legs were performed.

Table 3.1 Performance testing plan on *Schnadig* frames

Performance Test	Frame No.	Light acceptance level	Medium acceptance level	Heavy acceptance level
		(lb.)		
Arm-inward	#1, #5, #6	75	175	225
Arm-outward	#2, #3, #7	75	150	200
Seat load foundation	#2, #5, #6	200/100	250/125	275/137.5
Backrest frame	#2, #4, #8	75	100	150
Back rest foundation	#9, #10, #11	112.5	125	150
Arm -Vertical	Frame #11, #12 (both arms)	400	600	800
Front to back load test on legs	Tests were forced to stop after a few cycles due to the weak plastic leg.			
Side-thrust load test on legs				

Frames #1, #5, and #6 (Table 3.1) were tested under side-thrust inward load acting upon the arm rails. The test consists of subjecting one arm of the frame to a horizontal force in an inward direction as shown in Figure 3.1. The force was applied to the outside surface of an arm at a point as near as possible to the intersection of the stump with the arm. Test was started at 50 pound load level; and the load was increased in increments of 25 pounds after 25,000 cycles had been completed at each preceding load level. The test was continued until the arm suffered disabling damage or until a desired load level had been achieved.

Frames #2, #3, and #7 (Table 3.1) were tested under side-thrust outward load acting upon the arm rails. The test consists of subjecting one arm of the frame to a

horizontal force in an outward direction as shown in Figure 3.2. The force was applied to the inside surface of an arm at a point as near as possible to the intersection of the stump with the arm. Same with side-thrust arm load inward test, outward test was started at 50 pound load level; load was increased in increments of 25 pounds after 25,000 cycles had been completed at each preceding load level. The test was continued until the arm suffered disabling damage or until a desired load level had been achieved.

The three frames subjected to seat load foundation test were Frames #2, #5, and #6 (Table 3.1). Seat load foundation test consists of subjecting the seat of the sofa to the "sitting action" of three identical load heads as shown in Figure 3.3. These loads were applied at the center and at points 1/6th the length of the open face of the sofa from each end. Testing was begun with 100 pounds applied to the rear load position and 50 pounds applied to the front position. Front and rear loads were applied simultaneously. Rear loadings were increased in increments of 25 pounds and front loadings in increments of 12.5 pounds after 25,000 cycles had been completed at each preceding load level. Tests were continued until some type of seat foundation failure such as breakage of a spring occurred, or until a desired level of performance had been achieved.

The frames subjected to backrest frame test were Frames #2, #4, and #8 (Table 3.1). Backrest frame test consists of applying three loads to the top rail of the sofa in a front to back direction. These loads were applied at the center and at points 1/6th the length of the open face of the sofa from each end as shown Figure 3.4. The test was begun at the 75 pound load level, and loads were increased by 25 pounds after 25,000

cycles had been completed at each preceding load level. Testing was continued until the frame suffered disabling damage or until a desired level of performance had been achieved.

Frames #9, #10, and #11 (Table 3.1) were subjected to backrest foundation test. The test consists of applying three loads to the backrest of the sofa in a front to back direction. These loads are applied at the center and at points $1/6^{th}$ the length of the open face of the sofa from each end as shown in Figure 3.5. The test was begun at the 50 pound load level, and loads were increased by 12.5 pounds after 25,000 cycles had been completed at each preceding load level. Testing was continued until some type of physical failure occurred in the backrest foundation system, such as a broken spring, or until a desired level of performance had been achieved.

One arm of Frame #11 and both arms of Frame #12 (Table 3.1) were tested under cyclic vertical load. In vertical load test on arms, a cyclic vertical load is applied downward to each of the sofa at mid span of the arm as shown in Figure 3.6. The test was started at 100 pound load level, and the load was increased by 100 pounds after 25,000 cycles had been completed at each load level. The test was continued until the arm suffered disabling damage.

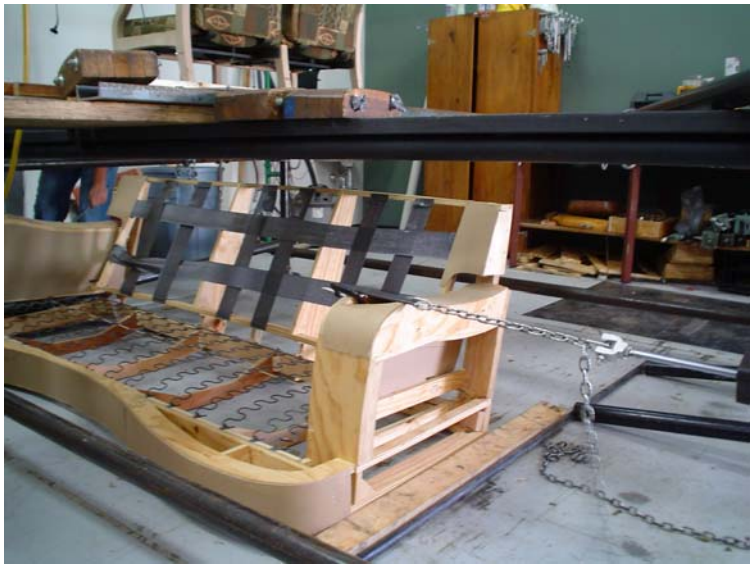

Figure 3.1 Horizontal side-thrust arm load test (inward) setup

Figure 3.2 Horizontal side-thrust arm load test (outward) setup

Figure 3.3 Seat load foundation test setup

Figure 3.4 Backrest frame test setup

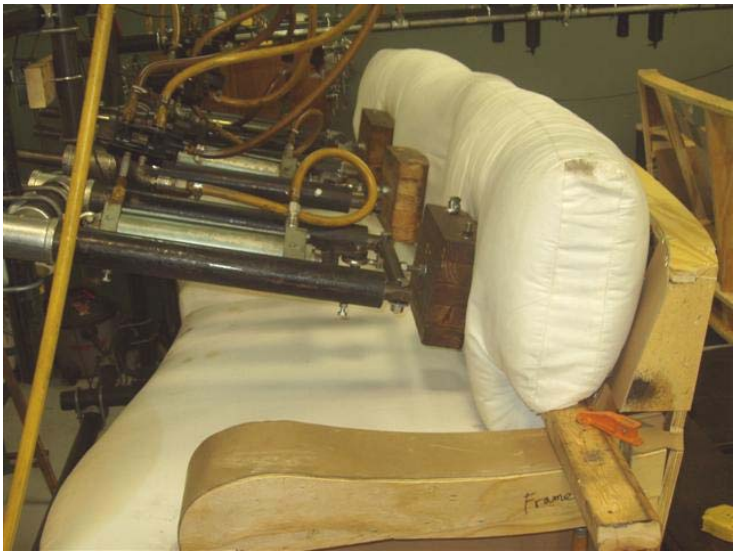

Figure 3.5 Backrest foundation test setup

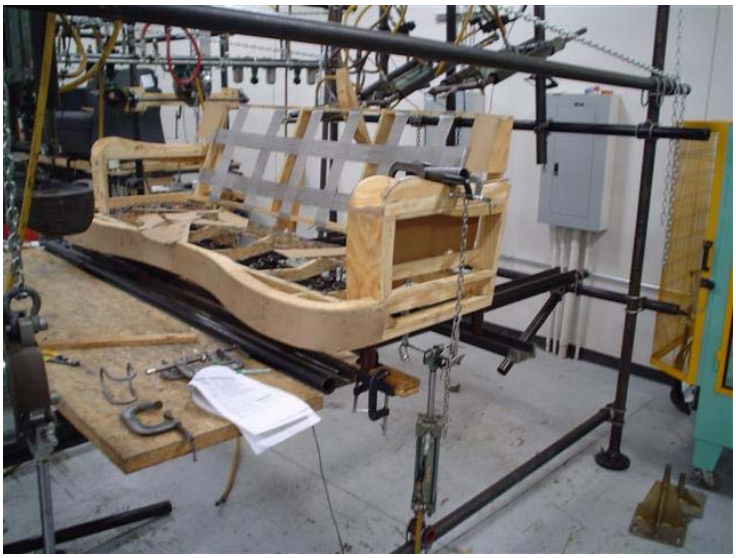

Figure 3.6 Vertical load test on arms setup

Frame Testing Results and Discussion

Table 3.2 lists the summaries of the testing results for each test in terms of acceptance level, passed load level, failed load level, and failure mode. In general, most of the tests did not reach the desired medium acceptance service level except backrest frame test, where the three frames were at three different acceptance levels, and arm vertical test, where all the frames passed heavy acceptance level. The weak joints were observed as the major cause of failure for backrest frame test, backrest foundation test, and horizontal side-thrust arm load test (inward and outward). Only for seat load test was member breakage the cause for failure. The following paragraphs describe each test.

Table 3.2 Summary of performance testing results for *Schnadig* frames

GSA Test	Frame No.	Acceptance Level	Passed load level (lb)	Failure level (lb)	Failure mode
Arm-inward	#1	Light	125	150	Front stump to bottom side rail joint failure
	#5	Light	100	125	
	#6	Light	75	100	
Arm-outward	#2	Light	100	125	Front stump to side center rail joint failure
	#3	Light	75	100	
	#7	Light	75	100	
Seat load foundation	#2	Light	200/100	225/112.5	Back spring rail breakage
	#5	Light	200/100	225/112.5	
	#6	< Light	175/87.5	200/100	
Backrest frame	#2	Heavy	150	-	Top arm rail to back post joint failure
	#4	Medium	100	125	
	#8	Light	75	100	
Back rest foundation	#9	< Light	87.5	100	Top arm rail to back post joint failure
	#10	< Light	-	50	
	#11	< Light	50	62.5	
Arm -Vertical	#11	Heavy	800	-	-
	#12 (left arm)	Heavy	800	-	
	#12 (right arm)	Heavy	800	-	

Horizontal Side-thrust Arm Load Test (Inward)

Frames #1, #5, and #6 failed at the load level of 150, 125, and 100 pounds, respectively. All of them passed light acceptance level (75 lb, Table 3.1) but not medium acceptance level (175 lb, Table 3.1). The three frames had failure of the joint of front stump to bottom side rail as shown in Figure 3.7. At this joint of each frame, there were two staples driven through the reinforcing block to the face of bottom side rail, and two staples driven through the edge of bottom side rail to the end of front stump. The staples were 16-gage with penetration depth into the plywood around 0.5 inches, and no glue was applied to the contact surface between the block and the plywood. The joint failed because the staples were pulled out directly from the face of bottom side rail and the end of front stump. The failure mode of the staples withdrawal from the face of bottom side rail and the end of front stump indicated that the moment capacity of the joint was governed by the direct withdraw load capacities of the staples from plywood face and end.

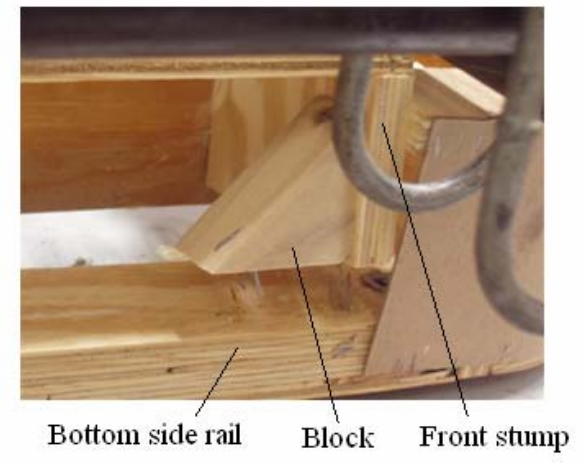

Figure 3.7 Failure mode of staples withdrawal from the bottom side rail face and front stump end in horizontal side-thrust arm load test (inward) (left side view)

Horizontal Side-thrust Arm Load Test (Outward)

The three frames failed at the load level of 125, 100, and 100 pounds, respectively, and all of them achieved light acceptance level (75 lb, Table 3.1) but not medium acceptance level (150 lb, Table 3.1). The weak joint of front stump to side center rail as shown in Figure 3.8 was the common cause for the failure of the three frames. For each frame, there were two staples driven through the side center rail to the front stump edge, and no glue was applied to the contact surface of the two members. The staples were 16-gage with penetration depth of 0.75 inch to the edge of the front stump, and they were directly pulled out of the edge of front stump. The failure mode also indicated that the moment capacity of the joint was affected by the direct withdraw load capacity of the staples from the edge of plywood.

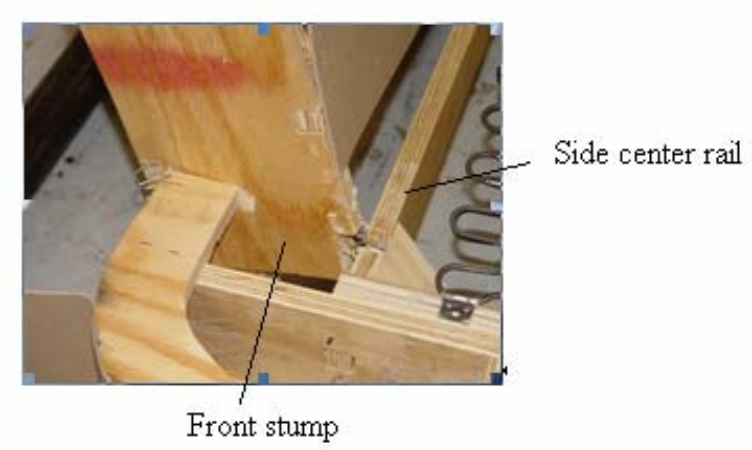

Figure 3.8 Failure mode of staples withdrawal from the front stump edge in horizontal side-thrust arm load test (outward) (front view)

Seat Load Foundation Test

Frames #2, #5, and #6 failed at the load level of 225/112.5, 225/112.5, and 200/100 pounds, respectively. Frame #2 and #5 passed light acceptance level (200/100 lb, Table 3.1) but not medium acceptance level (250/125 lb, Table 3.1), while Frame #6 did not reach light acceptance level. The back spring rail was 3 inches in depth. It fractured near mid-span it fractured due to the bending stress in an edgewise direction as shown in Figure 3.9. No major defects of the plywood were observed around the breakage. The failure mode of the breakage of spring rail due to bending stress indicated that the edgewise MOR of the rail material might govern the foundation strength performance.

Figure 3.9 Failure mode of the back spring rail breakage in seat load foundation test (back view)

Backrest Frame Test

Frame #2 survived the last load level of 150 pounds, and was considered being passed heavy duty (150 lb, Table 3.1) so that the testing stopped. Frames #4 and #8 failed at the load level of 125 pounds and 100 pounds, and achieved medium (100 lb, Table 3.1) and light acceptance level (75 lb, Table 3.1), respectively. Separation of the joint between the top arm rail and the back post at one side was the cause of failure for both frames #4 and #8. The joint type of top arm rail to back post was mortise-and-tenon with glue and staples. Ten, nine and six staples were driven through the back post to the arm rail for frames #2, #4 and #8, respectively. The staples were 16-gage with penetration depth of 0.75 inch to the end of arm rail. As shown in Figure 3.10, for frames #4 and #8, the staples were pulled out from the end of top arm rail. Glue was applied during assembly, however, no glue or very little amount of glue was found at the interfacial bonding between mortise and tenon. It might suggest that the direct withdraw capacity of staples govern the joint strength.

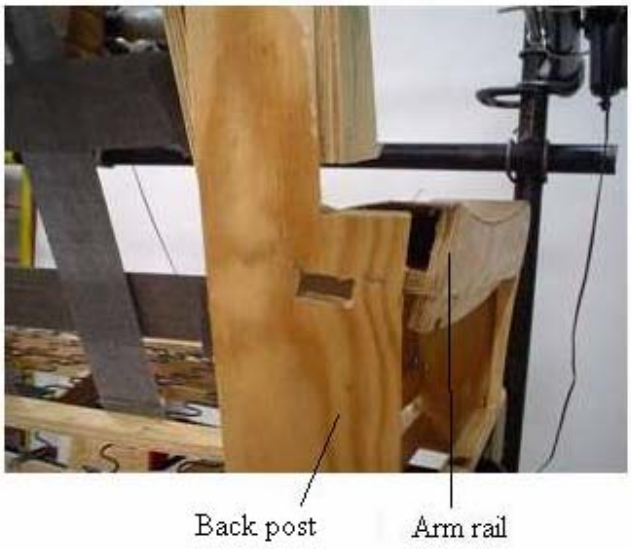

Figure 3.10 Failure mode of staples withdrawal from the arm rail end in backrest frame test (back view)

Backrest Foundation Test

Frames #9, #10, and #11 failed at the load level of 100, 50, and 62.5 pounds, respectively, and all of them did not reach the light acceptance level (112.5 lb, Table 3.1). Similar to the backrest frame test, the weak joint of top arm rail to back post at one side was the cause of failure as shown in Figure 3.11. Staples were pulled out of the end of arm rail. Four or five staples were used to fasten top arm rail to the back post for each frame, and also no glue or, if any, little amount glue was found. The staples were 16-gage with penetration depth of 0.75 inch to the end of arm rail.

For the frames subjected to backrest frame test (Frames #2, #4, #8), there were ten, nine, and six staples on the joint of top arm rail to back post. While for the frames subjected to backrest foundation test (Frames #9, #10, #11), there were only four or five

staples on the same joint. It was obvious that the staples used were not consistent during frame assembly operation, which might cause the frame performance variation.

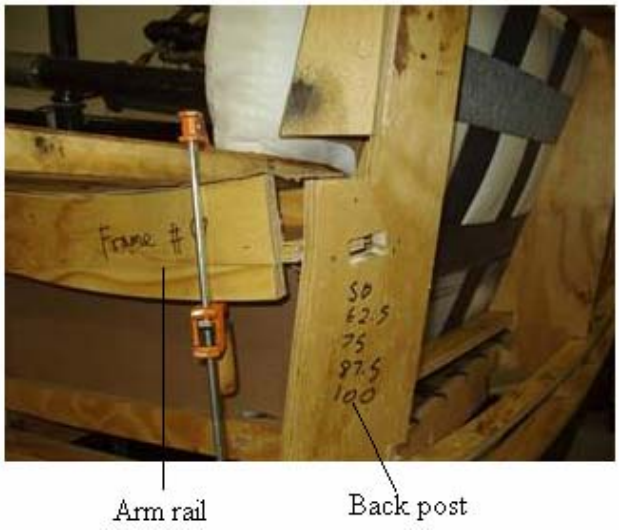

Figure 3.11 Failure mode of staples withdrawal from the arm rail end in backrest foundation test (right side view)

Static Load Test on Joints

Static load tests were performed on some remaining intact joints of the *Schnadig* frames. The purposes were to investigate the load resistances of the joints under static loads, and to correlate the fatigue strength and static strength of the joints, if applicable. Experience has shown that the cyclic strength of frames is no more than fifty percent of static strength (Eckelman and Erdil 2000). The study by Zhang et al. (2003) showed the ratios of the static moment capacities of tested T-shaped, end-to-side, two-pin dowel joints to their corresponding passed stepped moment levels ranged from 2.1 to 2.6, with

an average value of 2.2. Based on the testing results in this study and experience data, a ratio will be proposed for the design of joints when considering cyclic load effects.

The static load tests performed were (1) static load test on arms (inward), (2) static load test on arms (outward), (3) static load test on back uprights, (4) shear load on the joints of top arm rail to back upright, and (5) direct withdrawal load on the joints of top arm rail to back post. For each test, three joints were tested. The results were summarized in Table 3.3.

Table 3.3 Testing plan and summary of the joint static load test

	Critical joint	Mean maximum load (lb.)	Static / P *	Static / F *
Static load on arms (inward)	Y	150	1.5	1.2
Static load on arms (outward)	Y	150	1.8	1.4
Static load on back uprights	N	92	N/A	N/A
Lateral shear load on the joints of top rail to back upright	N	402	N/A	N/A
Direct withdraw load on the joints of arm rail to back post	Y	111	1.2	1.0

* Static/P is equal to mean maximum static load over the mean passed load level in Table 3.1, and Static/F is equal to mean maximum static load over the mean failed load level in Table 3.1 for applicable tests.

Static Load Test on Arms (Inward)

Three frames with intact joints of front stump to bottom side rail were tested under static horizontal side-thrust load in an inward direction. The setup was the same as in GSA horizontal side-thrust arm load test (inward), except that the load was manually adjusted as shown in Figure 3.12. The test was started at 100 pounds, and remained at

that level for one minute. Then the load was increased by 25 pounds, and the procedure repeated until the joint of front stump to bottom side rail broke as shown in Figure 3.13. The three joints failed because of staple withdrawal from the face of bottom side rail, which was the same failure mode observed in cyclic load test. No glue was observed on the contact surface of the block and the bottom side rail. The ultimate load was 200, 125, and 125 pounds for three tested joints, respectively, with an average of 150 pounds (Table 3.3). For the joint of each frame, there were two staples driven through the block to the face of bottom side rail, and two staples driven through the edge of bottom side rail to the end of front stump. The penetration depth of the staples was 0.5 inch. The mean cyclic load level where the frame failed was 125 pounds, and passed was 100 pounds (Table 3.2). The ratio of static load to passed cyclic stepped load was 1.5, and to failed cyclic stepped load was 1.2 (Table 3.3). The joint of front stump to bottom side rail was a critical joint under GSA side-thrust load test (inward) on arms.

Figure 3.12 Static load test on arms (inward) setup

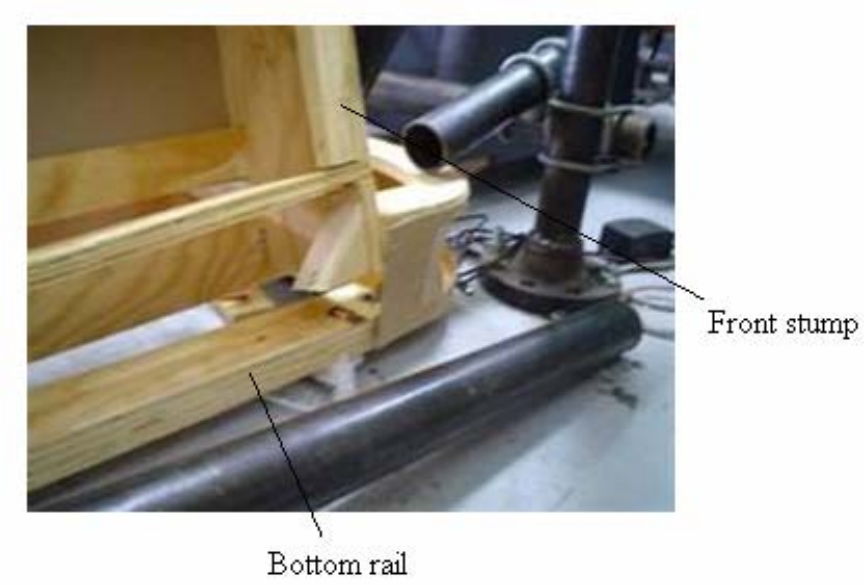

Figure 3.13 Failure mode of staples withdrawal from the bottom side rail face and front stump end in static load test (inward) on arms (left side view)

Static Load Test on Arms (Outward)

Three frames with intact front stump to side center rail joints were tested under static horizontal side-thrust load in an outward direction. The setup was the same with GSA horizontal side-thrust arm load test (outward) as shown in Figure 3.14. The test was started at 100 pounds, and remained at that level for one minute. Then the load was increased by 25 pounds, and remained at 125 pound level for one minute. The procedure repeated until the joint of front stump to side center rail broke as shown in Figure 3.15. The three joints failed because of the staple withdrawal from side center rail edge, which was the same failure mode observed in cyclic load test. No glue was observed on the contact surface of the side center rail to the front stump. The ultimate load was 150, 175,

and 125 pounds for three tested joints respectively, with an average of 150 pounds. Two staples from side center rail to front stump edge were used in the joint for each frame, and the penetration depth was 0.75 inch. The mean stepped cyclic load level where the frame failed was 108 pounds, and passed was 83 pounds (Table 3.2). The ratio of mean static load to passed cyclic load was 1.8, and to failed cyclic load was 1.4. The joint of front stump to side center rail was a critical joint under GSA side-thrust load test (outward) on arms.

Figure 3.14 Static load test on arms (outward) setup

Figure 3.15 Failure mode of staples withdrawal from the front stump edge in static load test (outward) on arms (front view)

Static Load Test on Back Uprights

Three frames with intact joints of back upright to back spring rail were subjected to static loads on the back upright in a backward direction. The joint was separated from the rest of the frame by cutting the top rail apart, and the load was applied at the top end of the back upright as shown in Figure 3.16. The test was started at 25 pound load level, and remained there for one minute. The load was increased by 25 pounds, and the procedure was repeated until the joint of back upright to back spring rail failed as shown in Figure 3.17. There were four staples driven through the back spring rail to the back upright edge and two staples driven through back center rail to back upright edge for each frame, and the penetration depth was 0.75 inch. The joints failed because of the staple direct withdrawal from the edge of the upright. The ultimate load was 75, 100, and 100

pounds, respectively, with an average of 92 pounds. With the back upright 28 inches, the moment at the joint of back upright to back spring rail would be 2,576 lb-in. A finite element model was built in I-DEAS to explore the internal forces at components when the frame was subjected to GSA load. The models were demonstrated in Chapter VI. The simulation of the model indicated that the moment at this joint at medium acceptance load level (100 lb) was 1,307 lb-in. Therefore, the ratio of actual strength of the joint (2,576 lb-in) over the expected strength (1,307 lb-in) was 2. This joint was not a critical joint under GSA backrest frame test.

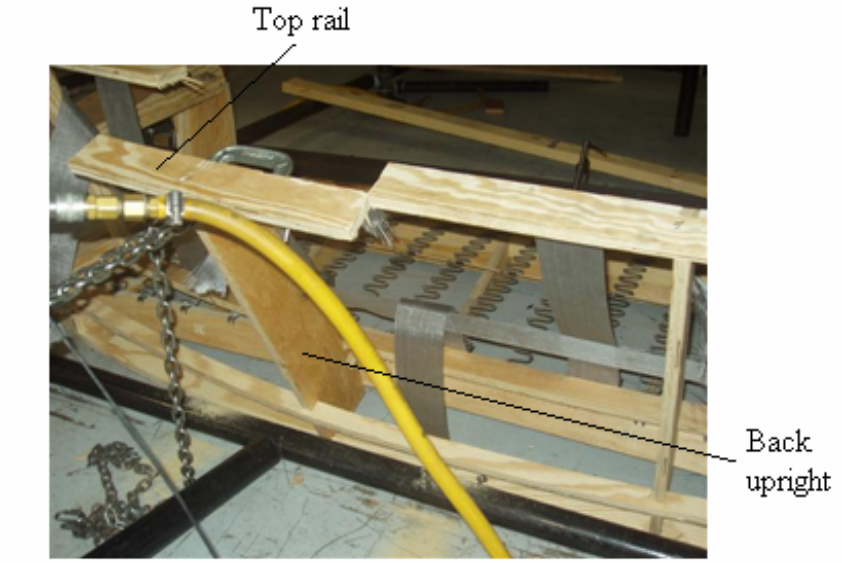

Figure 3.16 Static load test on back uprights setup

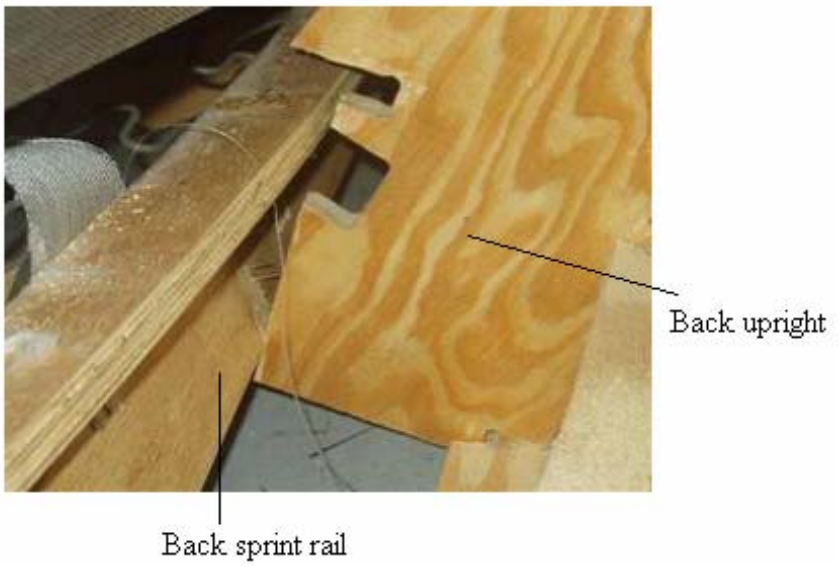

Figure 3.17 Failure mode of the staples withdrawal from the back upright edge in static load on back uprights (back view)

Lateral Shear Load Test on Joints of Top Rail to Back Upright

Three intact joints of top rail to back upright were cut out of the frame to perform the lateral shear load test. The test was conducted on a hydraulic SATEC universal-testing machine at a loading rate of 0.10 in./min, Figure 3.18. The maximum load was 559, 297, and 349 pounds, respectively, with an average of 402 pounds. There were only two staples driven through the top rail into the end of back upright for the latter two joints as shown in Figure 3.19. For the first joint, there were additional two staples driven through the back upright edge to the top rail face. This explained why its maximum load (559 pounds) was much higher than the other two (297 and 349 pounds). The staples were 16-gage with the penetration depth of 0.75 inch. The simulation of the model

indicated that the shear load at this joint at medium acceptance load level (100 lb) was 50 pounds, and at heavy acceptance level (150 lb) was 75 pounds. The ratio of actual lateral shear strength (402 lb) over the expected strength at medium acceptance level (50 lb) was 8.04, and at heavy acceptance level (75 lb) was 5.36, which suggests that the joint of back upright to top rail was over-designed with regard to the lateral shear resistance.

Figure 3.18 Lateral shear load test on the joint of top rail to back upright

Figure 3.19 Failure of the joint of top rail to back upright under static load

Direct Withdraw Load Test on Joints of Arm Rail to Back Post

Three intact joints of arm rail to back post were cut out of the frames to perform the direct withdraw load test. The test was also conducted on a hydraulic SATEC universal-testing machine at a loading rate of 0.10 in./min as shown in Figure 3.20. The maximum load was 105, 67, and 161 pounds, respectively, with an average of 111 pounds. The staples were driven through the back post to the end of arm rail with the penetration depth of 0.75 inch. There were four or five staples connecting the back post to the arm rail for each joint as shown in Figure 3.21. With four or five staples the average load resistance of 111 pounds of the joint, which seemed relatively low. Some of the staples were driven into the wood in an angle and missed the material, which might cause the low load resistance.

In GSA backrest foundation test the load is almost in line with the joint of top arm rail to back post. It is reasonable to assume the load applied to each joint as a direct withdraw load that has a magnitude of half of total load applied on the backrest foundation. The average passed load level was 63 pounds, and failed load level was 71 pounds (Table 3.2), which caused a direct withdraw load at the joint of the magnitude of 95 pounds and 107 pounds respectively. Therefore, the static strength to passed load level was 1.2, and to failed load level was 1.0.

Figure 3.20 Direct withdraw load test on the joint of arm rail to back post

Figure 3.21 Failure of the joint of arm rail to back post under static load

Summary

Six sets of performance tests were implemented on the *Schnadig* frames: (1) horizontal side-thrust arm load test (inward), (2) horizontal side-thrust arm load test (outward), (3) seat load foundation test, (4) backrest frame test, (5) backrest foundation test, and (6) arm vertical test. The testing results indicated that generally the frames did not reach the anticipated medium acceptance level except for the arm vertical test, where all the tested frames passed heavy duty. The inadequate connections at the joints were the major causes of failure. The weak joints identified were front stump to bottom side rail joint, front stump to side center rail joint, and top arm rail to back post joint. Only one member was overstressed for all the tests, which was the back spring rail under the seat load foundation test. Glue was applied to the joints when assembling. However, little or no glue was observed on the joint interfaces. Therefore, only staples were carrying loads. Moreover, the inconstant application of staples appeared to be the cause of various performance behaviors. Table 3.4 summarizes the weak components identified for each test and its failure mode of GSA tests for *Schnadig* frames.

Static load test on the remaining corresponding intact joints were also performed. The results provided as a reference to the performance test results. Among the five joints tested, three were identified as critical joints in performance tests, which were (1) the joint of front stump to bottom side rail, (2) the joint of front stump to side center rail, and (3) the joint of top arm rail to back post. For these three joints, the ratio of static strength to the fatigue strength at failed load level ranged from 1.02 to 1.2, and at passed load

level ranged from1.05 to 1.8. Considering experience and previous study, a ratio of 2 is recommended for the design of joints to account for cyclic load effects. Table 3.4 summarizes the failure mode of each test.

Table 3.4 Summary of the performance tests on frames and static load tests on joints

	Weak component	Failure mode
Cyclic stepped load tests		
Arm-inward	Joint of front stump to bottom side rail	Staple direct withdraw from material face
Arm-outward	Joint of front stump to side center rail	Staple direct withdraw from material edge
Seat load foundation	Back spring rail	Member breakage in edgewise direction
Backrest frame	Joint of arm rail to back post	Staple direct withdraw from material face
Backrest foundation	Joint of arm rail to back post	Staple direct withdraw from material face
Arm-vertical	N/A	N/A
Static load test		
Static load on arms (inward)	N/A	Staple direct withdraw from material face
Static load on arms (outward)		Staple direct withdraw from material edge
Static load on back uprights		Staple direct withdraw from material face
Lateral shear load on the joints of top rail to back upright		Staple lateral shear
Direct withdraw load on the joints of arm rail to back post		Staple direct withdraw from material face

The next two chapters will look into the properties of the members and joints respectively. In Chapter IV the properties of selected wood composites subjected to

static and cyclic load were investigated. In Chapter V the lateral and direct withdraw strength properties of stapled and glued joints were studied.

CHAPTER IV

STATIC AND FATIGUE PROPERTIES OF WOOD COMPOSITES USED AS FRAME MATERIALS

As stated in the literature review, Palmgren-Miner rule is an effective method to estimate the fatigue life of wood composites subjected to the edgewise cyclic stepped bending stresses using their *S-N* curves. Moreover, the *S-N* curves at low 5% were proposed in order to guarantee a conservative criterion. In this study, low limit 5% data points are defined as the 5th percentile, the value of a variable for which 5% of the values of the distribution are smaller (Freund and Wilson 1997). This research recommended that additional experiments were needed to further verify Adkins' equations in terms of their constant values (*E* and *H*) for wood composites. A primary objective of this study was to evaluate the fatigue performance of selected wood materials subjected to edgewise bending fatigue stresses using the stress-based approach, and to further verify the experimental and design procedures proposed in a previous study (Zhang et al. 2005) for estimating the section size of wood composites as furniture frame stock.

In this part of study, the static properties of selected wood composites were first examined to obtain the mechanical properties such as MOR and MOE. Then constant amplitude fatigue load tests were performed on three OSB materials to derive the *S-N* curves at low 5% limit. Combining these test results with those in the study by Zhang et

al. (2005), the section size of selected wood composites were estimated by using Palmgren-Miner rule and low 5% *S-N* curves. Finally cyclic stepped load tests were carried out on the wood composites with calculated section size in order to verify the proposed methods.

Static Load Test

Materials and Methods

Samples of three OSB (OSB#2, #3, and #4), *Schnadig* pine plywood (plywood #2), and *Schnadig* hardwood plywood (plywood #3) were tested in this study. OSB#2 was aspen board supplied by *Weyerhauuser*, and OSB#3 and #4 were southern yellow pine board obtained from *Norboard*. All OSB materials were 23/32 inch thick standard 4 by 8-foot structural grade panels with face grain oriented in the direction parallel to the long side. Plywood #2 was 3/4 inch thick Frame 1 furniture-grade 6-ply southern yellow pine plywood acquired from *Schnadig*. The 4 by 8-foot full size sheet of 6-ply plywood#2 was constructed with two center plies aligned parallel to the face plies, and the one ply adjacent to face ply aligned perpendicular to the face on each side. The face grain was aligned parallel to the long side. *Schnadig* 7-ply hardwood plywood#3 was 7/8 inch thick with one center ply aligned parallel to the face plies, and the two plies adjacent to face ply aligned perpendicular to the face on each side. The face grain was aligned parallel to the long side. Specimens in this study were fabricated from cutting full-size sheets of OSB and plywood randomly selected from panel stacks. All specimens were

conditioned in an 8% equilibrium moisture content chamber prior to tests, and were randomly assigned to testing groups.

Simply-supported center-point loaded edgewise bending tests were performed to obtain the physical and mechanical properties of plywood#2, plywood#3, OSB#2, #3, and #4, such as the mean values of MOR and MOE. In addition, a simply supported center-point loaded flatwise bending test was performed on plywood#2 and plywood#3.

All static testing specimens measured 2-inches wide by 40-inches long, with their long directions parallel to the full size sheet eight foot direction. Specimens were tested according to ASTM D4761 (ASTM 2001a) at a span-to-depth ratio of 18. Twenty replicates were tested for each of the five sample groups. All static bending tests were conducted on a hydraulic SATEC universal-testing machine at a loading rate of 0.25 inch per minute for edgewise bending and 0.37 inch per minute for flatwise bending as shown in Figure 4.1. Load-deflection data of the tested specimens were recorded. Specimen moisture content and density were also measured (ASTM 2001b).

Physical and Mechanical Properties

Table 4.1 summarizes the mean values of the physical and mechanical properties of plywood#2, #3, OSB#2, #3, and #4 in edgewise direction. The data of southern pine plywood#1, OSB#1, and PB from Zhang et al. (2005) were also summarized here. Table 4.2 summarizes the mean values of the physical and mechanical properties of plywood#2 and #3, in flatwise direction.

For each of plywood#2 and #3, two groups of samples were tested, parallel cutting samples and crossing cutting samples. Parallel cutting was to cut the samples along the 8-foot direction, and cross cutting was to cut the samples perpendicular to the 8-foot direction. For 6-ply plywood#2, there were four plies, two face plies and two center plies, aligned parallel to the 8-foot direction, and two plies aligned perpendicular to the 8-foot direction. And the testing results indicated that the parallel-cut samples had a higher MOR (5,796 psi) than that of cross-cut samples (4,293 psi). The hardwood plywood#3 had three plies, two face plies and one center ply, aligned parallel to the 8-foot direction, and four plies aligned perpendicular to the 8-foot direction. The cutting direction of 8-foot direction was its weak direction. As listed in Table 4.1, the MOR of the parallel-cut samples was 5,835 psi, and the MOR of cross-cut samples was 8,547 psi.

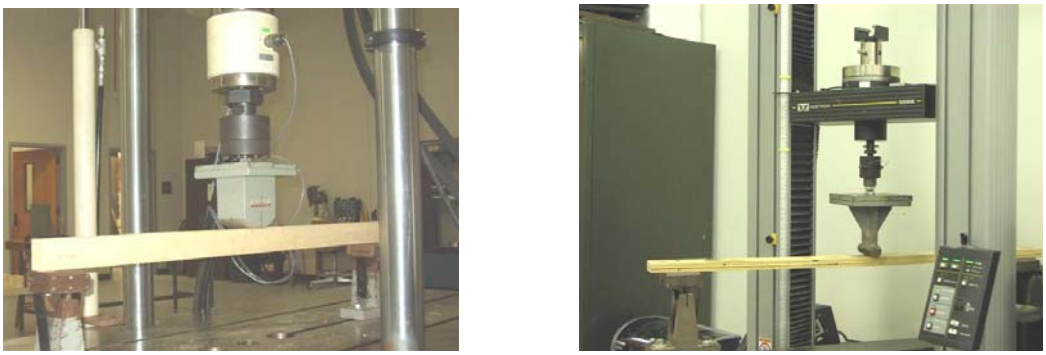

Figure 4.1 Setup of simply support center load, (a) edgewise and (b) flatwise, bending test

Table 4.1 Physical and mechanical properties of edgewise bending strength of wood composites included

Material type	Species	Dimension (in.) thick-ness	Dimension (in.) length by depth	Moisture Content (%)	Density (pcf)	Modulus of Rupture (psi)	Modulus of Elasticity ($\times 10^6$ psi)
Plywood#1[a]	southern yellow pine	3/4		7.8 (4)	42.0 (3)	6,600 (15)	0.99 (17)
OSB#1[a]	southern yellow pine	23/32		6.8 (5)	41.0 (5)	4,200 (16)	0.74 (8)
Particle-board [a]	southern yellow pine	3/4		7.7 (2)	49.0 (3)	1,600 (10)	0.33 (10)
Plywood#2	southern yellow pine	3/4	40 by 2	7.1 (23)	36.9 (16)	5,796[P](6) 4,293[C](13)	0.92[P] (9) 0.66[C] (26)
Plywood#3	hardwood	7/8		6.3 (15)	48.1 (12)	5,835[P] (9) 8,547[C] (30)	0.78[P] (6) 1.1[C] (12)
OSB#2	aspen	23/32		5.8 (4)	42.3 (5)	4,600 (10)	0.94 (5)
OSB#3	southern yellow pine	23/32		6.2 (5)	41.5 (5)	3,600 (9)	0.63 (4)
OSB#4	southern yellow pine	23/32		6.1 (4)	40.1 (5)	2,800 (15)	0.52 (6)

[a] Data were obtained from Zhang et al. (2005); specimens were not tested in this study.
[P] Results were obtained by cutting the samples parallel to the 8-foot direction.
[C] Results were obtained by cutting the samples perpendicular to the 8-foot direction.

Table 4.2 Physical and mechanical properties of flatwise bending strength of plywood #2 and plywood#3

	Modulus of Rupture (psi)	Modulus of Elasticity ($\times 10^6$ psi)
Plywood#2	5,115[P] (31) 3,206[C] (35)	0.89[P] (27) 0.44[C] (16)
Plywood#3	6,933[P] (10) 7,764[C] (10)	1.0[P] (9) 0.77[C] (9)

[P] Results were obtained by cutting the samples parallel to the 8-foot direction.
[C] Results were obtained by cutting the samples perpendicular to the 8-foot direction.

Constant-Amplitude Cyclic Load Test

Materials and Methods

Simply-supported center-point load edgewise constant-amplitude cycle tests were performed on OSB#2, #3, and #4 to investigate their *S-N* curves. The specimens measured 2 inches wide by 40 inches long, and were randomly selected from the same specimen sources of OSB in static tests. The specimens of each OSB material were tested under six nominal stress levels, which were 80, 75, 70, 65, 60, and 55 percent of the mean MOR value obtained from static center load bending test. Ten replicates were tested for each cyclic load level, so that sixty specimens were evaluated for OSB#2, #3, and #4, respectively. Edgewise constant-amplitude cyclic tests were conducted on a specially designed air cylinder and pipe rack system as shown in Figure 4.2. This set up allowed 10 specimens to be tested simultaneously. The specimens were simply supported with a support span of 36 inches and tested edgewise using center point loading. Zero-to-maximum cyclic loads were applied to specimens by air cylinders for each load level at a rate of 20 cycles per minute (GSA 1998). A programmable logic controller (PLC) and electrical re-settable counter system recorded the number of cycles completed. Limit switches actuated and stopped the test when the tested specimen completely broke. The *S-N* curves for each of three OSB materials were derived by regressing the stress levels with the log number of cycles to failure with a least squares method.

S-N Curves

Individual data points of applied nominal stress versus fatigue life (the number of cycles to failure) of OSB#2, #3, and #4 were plotted on a linear-log coordinate system as shown in Figures 4.3. The average coefficients of variation of fatigue life were 109, 113, and 93 percent for OSB#2, OSB#3, and OSB#4, respectively.

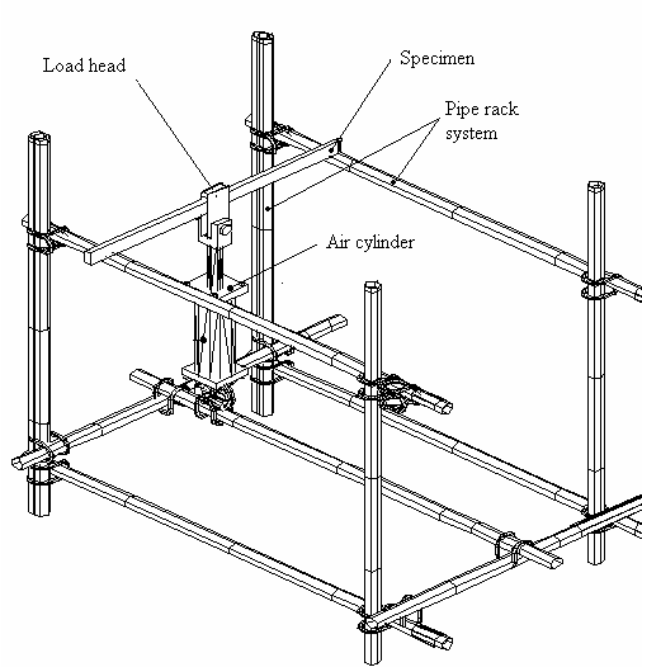

Figure 4.2 A specially designed air cylinder and pipe rack setup for constant amplitude cyclic tests

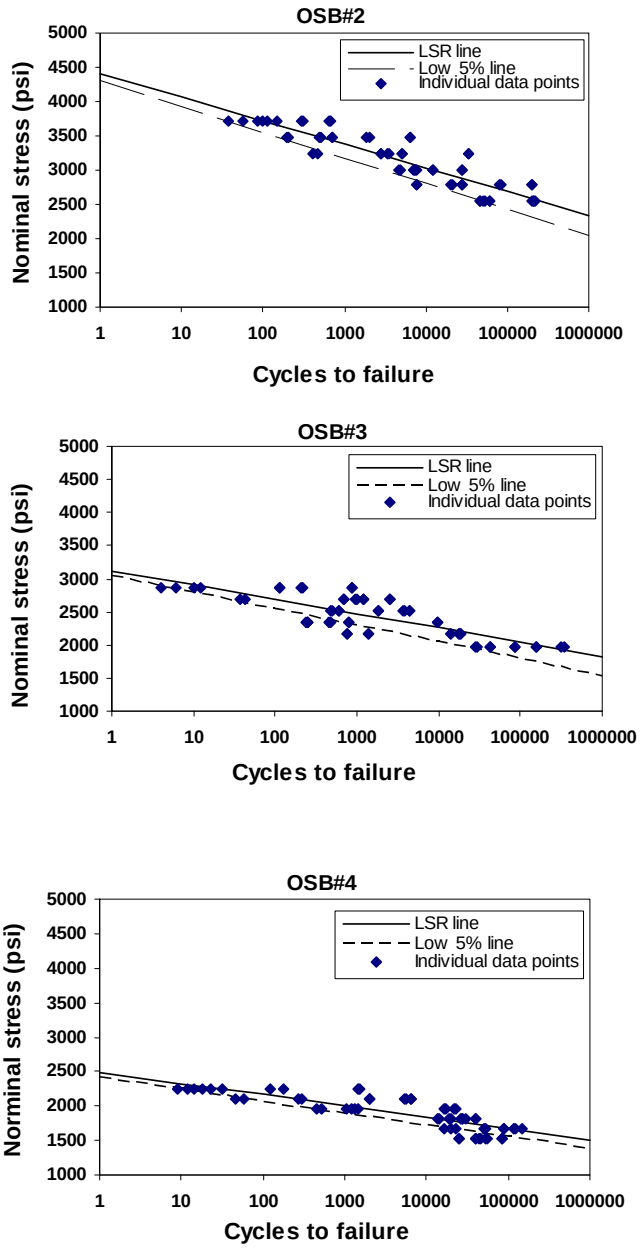

Figure 4.3 Individual data points and regression *S-N* curves of OSB#2,#3 and #4 plotted on linear-log coordinate system

The linear-log plots indicated an approximately linear relationship between nominal stress and log fatigue life. Therefore, the following equation was employed to fit individual data points using the least square regression (LSR) method for each material data set (Dowling 1999):

$$S = C - D \times \log_{10} N_f \tag{4-1}$$

where: S = applied nominal stress (psi.); N_f = number of cycles to failure; C, D = fitting constants.

Table 4.3 gives the regression fitting constant values of C and D, and coefficient of determination r^2 values of derived equations for each of three OSB materials. By setting $C = E \times MOR$, and $D = H \times MOR$, the Adkins' equation with the following format was derived for each of the three OSB materials:

$$S = MOR(E - H \times \log_{10} N_f) \tag{4-2}$$

The results of fitting constants E and H were given in Table 4.2. Both E and H values of three tested OSB sample groups were very close to E and H values of OSB #1 evaluated in the previous study (Zhang et al. 2005). Therefore, the Adkins' equation with the format, $S = MOR(1 - 0.07 \times \log_{10} N_f)$, describes S-N relation for OSB materials.

In order to guarantee a conservative design, low limit regression lines at 5% were derived for materials. For a sample size of ten, the 5 percentile point was the one with the lowest number of cycles to failure. For each load level, a low 5% data point was found, and then equation (4.1) was employed to fit these individual data points, i.e., one data point for each applied load level of each material. Stress-life data of plywood#1,

OSB#1, and PB from the study (Zhang et al. 2005) and OSB#2, #3, and #4 investigated in this study were analyzed.

Table 4.4 shows the results of fitting constants *C* and *D*, and *E* and *H* for the Adkins' equation. Results of derived constants *E* and *H* in Table 4.3 suggest that for practical design purposes the *S-N* curves of wood composites evaluated in this study could be approximated by equation (4.2), where the constant *E* was 0.85, and the constant *H* values were 0.06, 0.08, and 0.10, for plywood, OSB, and particleboard, respectively.

Table 4.3 Constants of estimated *S-N* curve equations derived based on all data points

Material type	MOR (psi)	Regression			Adkins	
		C	D	r^2	E	H
Plywood#1	6,600	5,775	344	0.74	0.9	0.05
OSB#1	4,200	3,959	287	0.76	0.9	0.07
Particleboard	1,600	1,534	149	0.85	1.0	0.09
OSB#2	4,600	4,406	344	0.80	1.0	0.07
OSB#3	3,600	3,116	214	0.62	0.9	0.06
OSB#4	2,800	2,488	163	0.70	0.9	0.06

Table 4.4 Constants of estimated *S-N* curve equations derived based on 5% low limit data points

Material type	MOR (psi)	Regression				Adkins	
		C	D	r^2		E	H
Plywood#1	6,600	5,610	395	0.92		0.85	0.06
OSB#1	4,200	3,823	372	0.93		0.91	0.09
OSB#2	4,600	4,300	375	0.98		0.93	0.08
OSB#3	3,600	3,045	252	0.88		0.85	0.07
OSB#4	2,800	2,404	170	0.92		0.86	0.06
				Avg.	=	0.89	0.08
Particleboard	1,600	1,410	154	0.94		0.88	0.10

Cyclic Stepped Load Test

Materials and Methods

Edgewise cyclic stepped load tests were performed on the full size top rail of a three-seat sofa frame to verify the Palmgren-Miner rule in estimating the fatigue life of wood composites subjected to a cyclic stepped fatigue load schedule. As shown in Figure 2.1, the backrest frame test consisted of applying three loads to the top rail of the sofa in a front to back direction. These loads were applied at the center and at points 1/6th the length of the open face of the sofa from each end. The test was begun at the 75 pound load level, and loads are increased by 25 pounds after 25,000 cycles have been completed at each preceding load level (Table 2.1). Testing was continued until the frame suffered disabling damage or until a desired level of performance had been achieved.

Testing specimens were cut from plywood#2, OSB#2, #3, and #4 sheets, and measured 80-inches long, with their length directions parallel to the full size sheet 8-foot direction. The depth of each material was listed in Table 4.5, and the algorithm for specimen depth determination will be given in the following paragraphs. The specimens were simply-supported with a support span of 72 inches, which is the common length of a three-sofa frame. Three identical loads were applied by the air cylinders at the center point of the rail and at points 1/6 of the span from the support end as shown in Figure 4.4 in an edgewise direction. The specimens were tested under the load schedule listed in Table 4.6. There were three replicates for each material at each load level. The last

column of Table 4.6 shows the bending moment of the beam under the external load conditions.

A programmable logic controller (PLC) and electrical re-settable counter system recorded the number of cycles completed. After 25,000 cycles had been completed at a prescribed load level, the limit switches actuated and stopped the test. The load was increased by 25 pounds, and the procedure was repeated until the beam broke. For all the static tests and fatigue tests, the specimens were tested in a laboratory where the temperature was maintained at 74 ± 2°F and the relative humidity at 50 ± 2 percent.

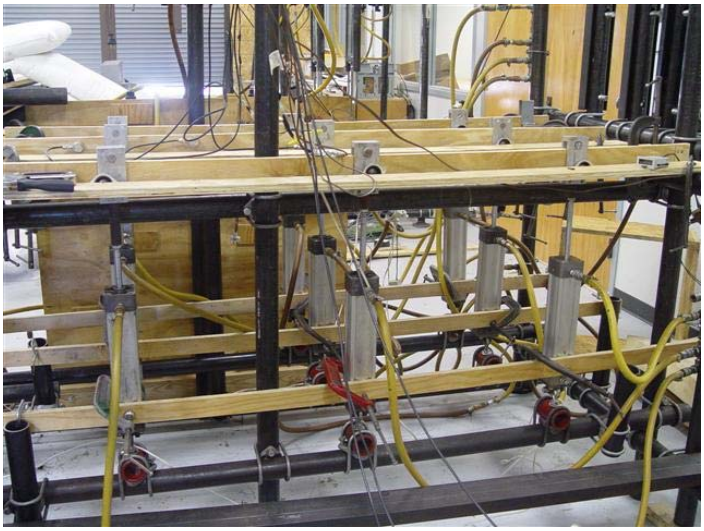

Figure 4.4 Test setup for stepped cyclic load tests

Table 4.5 lists the cross section dimensions of the specimens subjected to the cyclic stepped load schedule (Table 4.6) tests. The depth of each material at each service acceptance level was estimated using the Palmgren-Miner rule based on its low 5% limit

S-N curve equation, $S = MOR(0.85 - H \times \log_{10} N_f)$ with *H* equal to 0.06, 0.08, and 0.10 for plywood, OSB, and PB, respectively.

Table 4.5 Depths of full-size back top rail specimens subjected to stepped load schedule

Material type	MOR (psi)	Thickness (in.)	E	H	Depths for different service acceptance level (in.)		
					Light	Medium	Heavy
Plywood#2	5,796	3/4		0.06	2.302	2.658	3.257
OSB#2	4,600		0.85		2.862	3.309	4.062
OSB#3	3,600	23/32		0.08	3.236	3.740	4.592
OSB#4	2,800				3.669	4.241	5.207

Table 4.6 Cyclic stepped loading schedule for 72-inch-long back top rail fatigue tests and calculated maximum moments in back top rails for each fatigue load level under the simple-support boundary condition

j	P (lb.)	Number of loads	Cumulative cycles	Service-acceptance level	M_j (lb.-in.)
1	75	3	25,000	Light-Service	2,250
2	100	3	50,000	Medium-Service	3,000
3	125	3	75,000		3,750
4	150	3	100,000	Heavy-Service	4,500

The depth of a 72-inch-long back top rail of a three seat sofa frame needed to meet the heavy-service acceptance level of the cyclic stepped load schedule was calculated to illustrate the steps to estimate member sizes based on *S-N* curves and fatigue load schedules. The Palmgren-Miner rule states unity summation of life fraction:

$$\frac{N_1}{N_{f1}} + \frac{N_2}{N_{f2}} + \frac{N_3}{N_{f3}} + ... = \sum \frac{N_j}{N_{fj}} = 1 \qquad (4\text{-}3)$$

where: N_j = number of cycles applied to a member at the bending moment M_j; N_{fj} = number of cycles to failure from the member material *S-N* curve for the bending moment M_j.

Therefore, the fatigue life of a back top rail could be estimated with equation (4.3):

$$\frac{25{,}000}{N_{f1}} + \frac{25{,}000}{N_{f2}} + \frac{25{,}000}{N_{f3}} + \frac{25{,}000}{N_{f4}} = 1 \tag{4-4}$$

The three identical loads, *P*, were applied at the center-point and at points 1/6 the span, *L*, from each supporting end. Therefore, the maximum bending M_j at the center point for each fatigue level is $M_j = \frac{5PL}{12}$.

The *S-N* curve equation of plywood#2 is $S = 5{,}796 \times (0.85 - 0.06 \times \log_{10} N_{fj})$. For a rectangular cross-section beam subjected to a bending moment, stress and moment have the following relationship:

$$S = \frac{6M_j}{bh^2} \tag{4-5}$$

Where: M_j = nominal applied moment (lb.-in.) in Table 4.6; *b* = beam member depth (in.); *h* = beam member thickness (in.).

Substituting the stress-moment equation into the *S-N* curve equation yielded the following relationship:

$$N_{fj} = 10^{\left(\frac{C}{D} - \frac{6M_j}{D \cdot b \cdot h^2}\right)} \tag{4-6}$$

Then, substituting N_{fj} into the Palmgren-Miner rule equation (4.4) yielded the following equation:

$$\frac{25{,}000}{10^{\left(\frac{C}{D}-\frac{6M_1}{D\cdot b\cdot h^2}\right)}}+\frac{25{,}000}{10^{\left(\frac{C}{D}-\frac{6M_2}{D\cdot b\cdot h^2}\right)}}+\frac{25{,}000}{10^{\left(\frac{C}{D}-\frac{6M_3}{D\cdot b\cdot h^2}\right)}}+\frac{25{,}000}{10^{\left(\frac{C}{D}-\frac{6M_4}{D\cdot b\cdot h^2}\right)}}=1 \qquad (4\text{-}7)$$

For a given rail member thickness of 3/4 inch, a minimum rail depth of 3.257 inches was resulted for plywood#2 material. Similarly, the depths of the specimens subjected to cyclic stepped load schedules were calculated using the above described calculation procedure.

Cyclic Stepped Load Testing Results

Table 4.7 summarizes the failed load level and its corresponding number of cycles to failure for each tested specimen. Table 4.8 summarizes average fatigue life results of back top rail specimens as observed cycles. Mean differences between the estimated and observed fatigue life values were determined and expressed as a percentage of estimated cycles. The results showed that, in general with *S*-*N* curve equations derived from low 5% data points, the Palmgren-Miner rule tended to overestimate the section size of the wood material in this study needed to achieve the intended acceptance level. This coincided with selecting the low 5% regression lines for conservative estimation of fatigue life of wood composites as furniture frame stock.

Table 4.7 Stepped cyclic load test results for each specimen at each service acceptance level [a]

Material type	No. of specimens	Service acceptance level					
		Light		Medium		Heavy	
		Load level (lb.)	Number of cycles	Load level (lb.)	Number of cycles	Load level (lb.)	Number of cycles
Plywood#2	1	150	15	225	4	200	664
	2	100	587	150	22,222	225	61
	3	125	20	225	2,211	175	96
OSB#2	1	150	11,087	150	2,397	275	8
	2	150	4,685	150	166	250	17,860
	3	125	4.083	175	5	275	3,345
OSB#3	1	125	1,297	175	8	250	214
	2	125	13,645	175	9	300	290
	3	125	71	175	8	275	13,284
OSB#4	1	125	224	175	1,544	250	696
	2	125	9,616	150	22,215	250	20,198
	3	125	2,202	175	41	275	5,657

[a] The load level column indicates the observed load where the specimen broke, and the number of cycle column indicates how many cycles the specimen survived before it failed at that load level.

Table 4.8 Comparisons between estimated and observed mean fatigue life of full-size back top rail specimens for each combination of material type and service acceptance level [a]

Service acceptance level	Est.	Material type							
		Plywood#2		OSB#2		OSB#3		OSB#4	
		Obs.	Diff. (%)	Obs.	Diff. (%)	Obs.	Diff. (%)	Obs.	Diff. (%)
Light	25,000	50,207	100	73,285	193	55,004	120	54,014	116
Medium	50,000	133,145	166	84,189	68	100,008	100	99,600	99
Heavy	100,000	125,273	25	198,737	98	204,596	104	192,183	92

[a] Est. stands for estimated cycles to failure; Obs. stands for observed cycles to failure; Diff. equals to (Obs. – Est.)/Est.

The stress ratio of MOR (the ultimate static bending stress of tested specimens) to the maximum fatigue stress occurred in each individual specimen was calculated as listed in Table 4.9. There are two columns for each acceptance level. The first column is the ratio of MOR to the maximum fatigue stress at which the tested specimen passed without failure, and the second column is the ratio of MOR to the maximum stress at which the specimen failed. The stress for each specimen was calculated by substituting its maximum moment and its depth into equation (4.5). For example, the calculated depth for OSB#2 to achieve heavy acceptance level was 4.062 inches. The specimen of this size tested under cyclic stepped load passed the load level of 250 pounds, and failed at 275 pounds (Table 4.7). Substitute the estimated depth and load level into equation (4.5) yielded the stress of the specimen, which were 3,795 psi at the load level of 250 pounds, and 4,174 psi at 275 pounds. Therefore, the stress ratio of MOR to the stress at passed load level was 1.21, and at failed load level was 1.10.

Table 4.10 summarizes the stress ratio ranges for the specimens tested in this study, and also the specimens tested in previous study (Zhang et al. 2005). The stress ratio of MOR to failed stress of plywood ranges from 0.75 to 1.85 for all three acceptance levels. The stress ratio of MOR to passed stress of plywood ranged from 0.85 to 2.32 for all three acceptance levels. This suggested that the stress ratio for design of upholstered furniture frame members to satisfy a given stress level using tested plywood should be greater than 1.85. In other words, the allowable design stress for plywood should be less than 54% of its MOR.

The stress ratio of MOR to failed stress of OSB ranges from 0.93 to 1.56 for all three acceptance levels. The stress ratio of MOR to passed stress of OSB ranges from 1.10 to 2.08 for all three acceptance levels. The stress ratio for design of upholstered furniture frame members using tested OSB should be greater than 1.56. In other words, the allowable design stress for OSB should be less than 64% of its MOR.

The stress ratio of MOR to failed stress of PB ranges from 1.22 to 1.46 for all three acceptance levels. The stress ratio of MOR to passed stress of PB ranges from 1.37 to 1.82 for all three acceptance levels. The stress ratio for design of upholstered furniture frame members using tested PB should be greater than 1.46. In other words, the allowable design stress for plywood should be less than 68% of its MOR.

Table 4.9 Ratios of MOR to stress occurred in each tested specimen at passed load level and failed load level

Material type		Service acceptance level					
		Light		Medium		Heavy	
		MOR/P *	MOR/F *	MOR/P *	MOR/F *	MOR/P *	MOR/F *
Plywood #2	1	1.02	0.85	0.85	0.75	1.46	1.28
	2	1.71	1.28	1.37	1.14	1.28	1.14
	3	1.28	1.02	0.85	0.75	1.71	1.46
OSB#2	1	1.20	1.00	1.60	1.34	1.21	1.10
	2	1.20	1.00	1.60	1.34	1.35	1.21
	3	1.50	1.20	1.60	1.15	1.21	1.10
OSB#3	1	1.51	1.20	1.34	1.15	1.35	1.21
	2	1.51	1.20	1.34	1.15	1.10	1.01
	3	1.51	1.20	1.34	1.15	1.21	1.10
OSB#4	1	1.51	1.20	1.34	1.15	1.35	1.21
	2	1.51	1.20	1.61	1.34	1.35	1.21
	3	1.51	1.20	1.34	1.15	1.21	1.10

* P is the stress at passed load level, and F is the stress at failed load level.

Table 4.10 Summary of the stress ratio ranges for each wood composite included

Material type	Ratio	
	MOR/Passed	MOR/Failed
Plywood#1	1.15 – 2.32	0.93 – 1.85
OSB#1	1.17 – 2.08	0.93 – 1.56
Particleboard	1.37 – 1.82	1.22 – 1.46
Plywood#2	0.85 – 1.71	0.75 – 1.46
OSB#2	1.20 – 1.60	1.00 – 1.34
OSB#3	1.10 – 1.51	1.01 – 1.21
OSB#4	1.21 – 1.61	1.10 – 1.34

A Simplified Evaluation of the *Schnadig* Frame

The Palmgren-Miner rule can be used to estimate the sizes of the members based on material *S-N* curves and stepped moment schedule. However, the frame itself constitutes a complex 3D structure in which the characteristics (especially the rigidity of the joints) are largely unknown (Zhang et al. 2000). Therefore, exact solutions of structural analyses of a sofa frame do not appear to be justifiable. A simplified analysis method is desirable for furniture engineers to perform daily quick design calculations to estimate structural member sizes without the need of assistance from expensive structural simulation software. One possible solution is to treat each member as a beam with either simple or fixed end support boundary condition. Taking the *Schnadig* frame as an example, its members were evaluated by using the aforementioned method.

Load Components in Front and Back Spring Rails

In GSA seat load foundation tests, the vertical sitting action load is transferred to the front and back spring rail through sinuous springs. The load can be broken down into

horizontal and vertical components. Tackett and Zhang (2007) investigated the horizontal and vertical components of an upholstered single-seat sofa equipped with five sinuous springs. A double-cantilevered, bi-axial, strain gage load cell was used to acquire the spring load data. When a 320-pound human subject was sitting still in the chair, the vertical components on the back spring rails were 25, 51, 55, 44, and 20 pounds in each of the five springs, and 15, 28, 31, 24, and 13 pounds in each of the five springs of the front spring rail. The middle springs carried the largest vertical load. The sum of vertical components (306 lb) was less than the weight of the sitter (320 lb) because the back of the seat and the sitter's legs carried part of the weight. Here, that small discrepancy was ignored, and 306 pounds was used. So the back spring rail carried 64% of the total weight (195 lb), and front spring rail 36% (111 lb).

The sum of the horizontal components of the back spring rail was 63 lb, and front spring rail was 66 lb, which was approximately 22% of the total weight of 306 lb for each spring. The horizontal component produced an out-of-plane bending moment, which was relatively small since the stretchers provide strong support in the horizontal direction. Using the beam models listed in Table 4.12, the maximum moment of a continuous bean with two middle supports (model 2a) is $M_h = \frac{7P_hL}{120}$, and the maximum moment of a simple support bean without middle support (model 1a) is $M_v = \frac{5P_vL}{12}$. The total of horizontal components P_h was 42% of P_v, which made the M_h 5% of M_v. In order to

simplify the analysis, the out-of-plane moment M_h was ignored, and only vertical components were considered.

The three-seat sofa frame was equipped with fifteen springs, which was modeled as three single-seat sofa investigated by Tackett and Zhang (2007). Figure 4.5a illustrates a simply-supported beam with fifteen evenly spaced concentrated loads, which represent three sets of the five loads measured for the single-seat chair. In beam A the maximum moment was 5,727 lb-in. To further simplify the calculation, two beams (Figure 4.5b and c) were analyzed with respect to the maximum moment. For all the beams, the sum of the loads was the same, 585 lb. This is three applications of the vertical load components measured for the single-seat sofa. First one was a simple support beam with three concentrated load, and each load was the sum of the five vertical components (195 lb). As shown in Figure 4.5b, the loads were applied at the center and at points $1/6^{th}$ the length of the open face of the sofa from each end, and the maximum moment was 5,850 lb-in. The other beam model was a simple support beam with evenly distributed load 8.125 lb/in as shown in Figure 4.5c, and the maximum moment was 5,265 lb-in. Comparing the maximum moment in beam B (5,850 lb-in) and C (5,265 lb-in) with the maximum moment in beam A (5,727 lb-in), beam B could be used as a simplified model of beam A with reasonable accuracy.

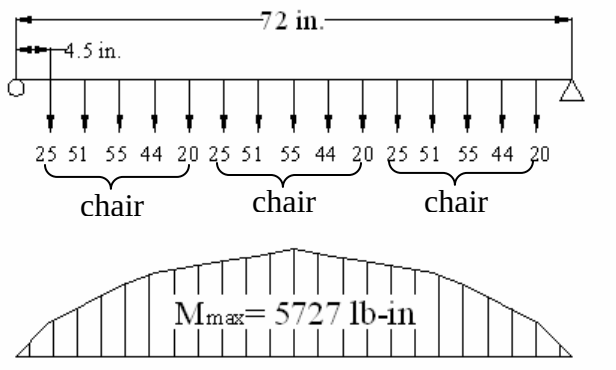

(a)

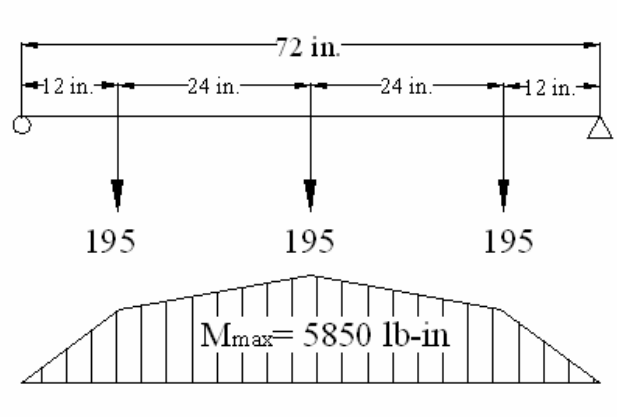

(b)

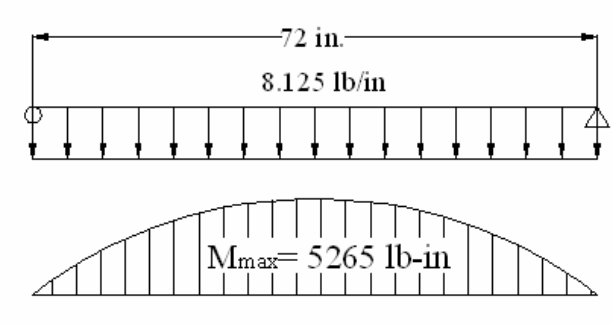

(c)

Figure 4.5 Maximum moment in three simply-supported beams

In conclusion, the load acting on back spring rail in the seat load foundation test could be simplified as three loads applied at the center and at points 1/6th the length of the rail from each end. The magnitude of each load was 64% of each "sitting action" load head, and the front spring rail carried 36% of the sitting load. Similarly, in horizontal direction, the magnitude of each load was 22% of sitting load for each spring rail. Table 4.11 lists the vertical and horizontal components in the front and back spring rails transferred from the GSA seat foundation load.

Table 4.11 Vertical and horizontal components in the front and back spring rails based on the GSA seat load foundation test schedule

Cyclic load P	Vertical component in front spring rails P× F_{vf} [a]	Vertical component in back spring rails P× F_{vb} [a]	Horizontal components in front and back spring rails P× F_h [a]	Number of loads	Acceptance level
	----------(lb.)----------				
150	54	96	33		
187.5	67.5	120	41.25		
225	81	144	49.5		
262.5	94.5	168	57.75		
300	108	192	66	3	Light
337.5	121.5	216	74.25		
375	135	240	82.5		Medium
412.5	148.5	264	90.75		Heavy

[a] F was defined as the seat load distribution factor. F_{vf} = 0.34 (the percentage of the load transferred to front spring rail in vertical direction), and F_{vb} = 0.68 (the percentage of the load transferred to back spring rail in vertical direction). F_h=0.22 (the percentage of the load transferred to front and back spring rails in horizontal direction).

Simplified Sofa Structural Member Analysis Models

Table 4.12 shows the beam models proposed to estimate bending moments for structural members in a sofa frame. Model 1ab are proposed as a simplified beam for

front rails, back top rails, front and back spring rails, with the span length L between two end supports spaced 78 inches apart. The maximum moment in a simply support beam (model 1a) is larger than that in a fixed end beam (model 1b). Therefore, the section size calculated based on model 1a could be used as a "conservative" design and model 1b a "progressive" design. The actual section size needed would be based on a moment that falls between these two values. Model 3 is a cantilever beam used to represent the front stumps with the length *L* 18 inches, and back posts with the length *L* 28 inches. Model 4 is used to simplify the stretchers with the *h* equal to the depth of front spring rails. The method of superposition (Ugural 1991) is applied to solve the statically indeterminate beam problems.

Table 4.13 to 4.19 list the stepped moment schedules for front spring rails, back spring rails, front rails, back top rails, stretchers, and front stumps. The load schedule for front rails is from seat load foundation test, and it is assumed that all the weights are applied on the front rails. The load schedule for stretcher is also derived from seat load foundation test, and the load is calculated as the reaction force in model 2b where *P* is the horizontal component in Table 4.11. The section sizes of the rails were calculated based on the stepped moment schedules and the *S*-*N* equation, $S = MOR(0.85 - H \times \log_{10} N_f)$, where H was 0.06 for plywood. Table 4.20 lists the calculated section sizes of the members based on simplified beam models.

Table 4.12 Simplified beam models to estimate bending moments for structural members in a sofa frame

Moment Diagram	Member Model and Formulae
Simple beam — End supports and three concentrated loads (model 1a) 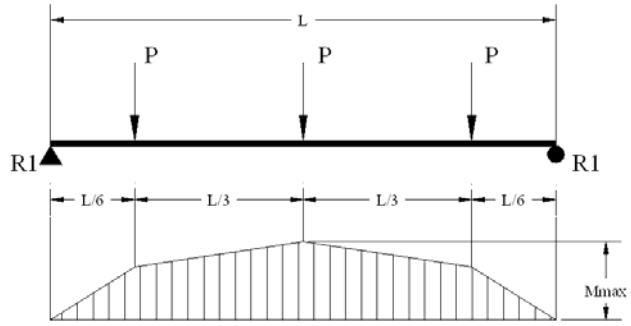	Front and back spring rails, back top rails, and front rails. (conservative) $M_{\max} = \frac{5PL}{12}$ $R_1 = \frac{3P}{2}$
Fixed end beam — End supports and three concentrated loads (model 1b) 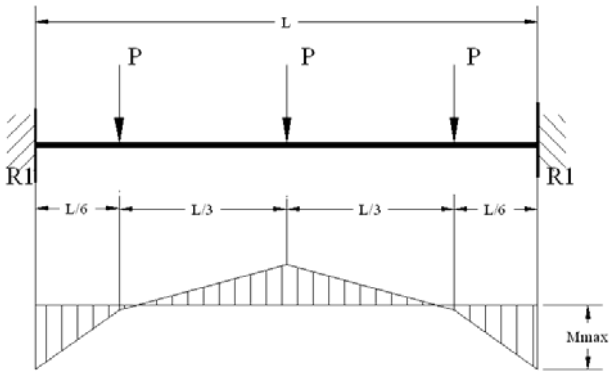	Front and back spring rails, back top rails, and front rails. (progressive) $M_{\max} = \frac{19PL}{72}$ $R_1 = \frac{3P}{2}$
Continuous beam — Four equally spaced supports and three concentrated loads (model 2a) 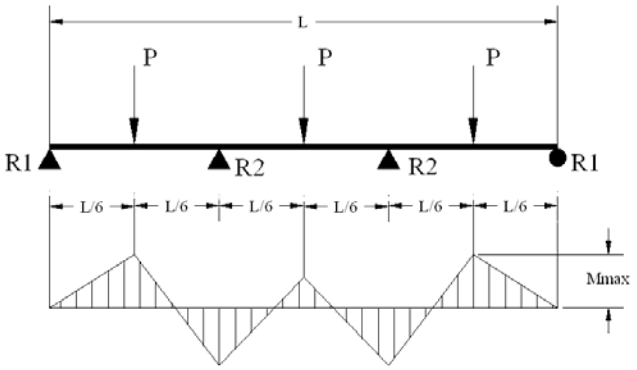	$M_{\max} = \frac{7PL}{120}$ $R_1 = \frac{7P}{20}$ $R_2 = \frac{23P}{20}$

Table 4.12 (continued)

Reaction forces of a simply supported beam — Two supports being L/3 from the end and three concentrated loads (model 2b) 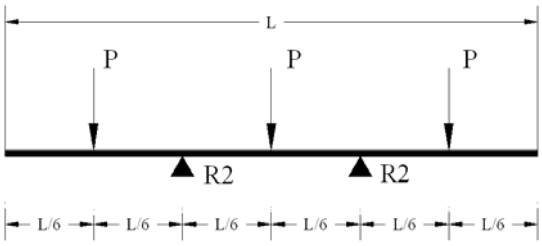	$R_2 = \frac{3P}{2}$
Cantilever beam — Concentrated end load (model 3) 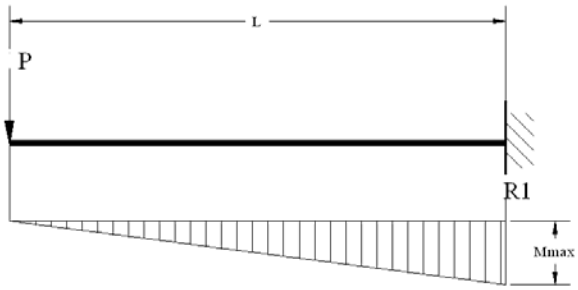	Front Stumps and back posts $M_{max} = PL$ $R_1 = P$
Simplified beam model for stretchers (model 4) 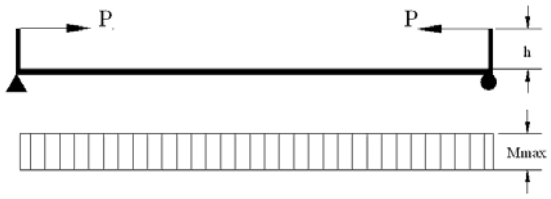	Stretchers $M_{max} = Ph$

Table 4.13 Stepped cyclic loading schedule for testing fatigue life of full-size front spring rails, and calculated maximum moments in front spring rails for each fatigue load level

j	Cyclic load	Cumulative cycles	Acceptance level	Mj	
				Simply	Fixed
	(lb.)			------- (lb.-in.) ------	
1	54	25,000		1755	1112
2	67.5	50,000		2194	1389
3	81	75,000		2633	1667
4	94.5	100,000		3071	1945
5	108	125,000	Light-Service	3510	2223
6	121.5	150,000		3949	2501
7	135	175,000	Medium-Service	4388	2779
8	148.5	200,000	Heavy-Service	4826	3057

Table 4.14 Stepped cyclic loading schedule for testing fatigue life of full-size back spring rails, and calculated maximum moments in back spring rails for each fatigue load level

j	Cyclic load	Cumulative cycles	Acceptance level	Mj	
				Simply	Fixed
	(lb.)			------- (lb.-in.) ------	
1	96	25,000		3120	1976
2	120	50,000		3900	2470
3	144	75,000		4680	2964
4	168	100,000		5460	3458
5	192	125,000	Light-Service	6240	3952
6	216	150,000		7020	4446
7	240	175,000	Medium-Service	7800	4940
8	264	200,000	Heavy-Service	8580	5434

Table 4.15 Stepped cyclic loading schedule for testing fatigue life of full-size front rails, and calculated maximum moments in front rails for each fatigue load level

j	Cyclic load	Cumulative cycles	Acceptance level	Mj	
				Simply	Fixed
	(lb.)			------- (lb.-in.) ------	
1	150	25,000		4875	3088
2	187.5	50,000		6094	3859
3	225	75,000		7313	4631
4	262.5	100,000		8531	5403
5	300	125,000	Light-Service	9750	6175
6	337.5	150,000		10969	6947
7	375	175,000	Medium-Service	12188	7719
8	412.5	200,000	Heavy-Service	13406	8491

Table 4.16 Stepped cyclic loading schedule for testing fatigue life of full-size back top rails, and calculated maximum moments in back top rails for each fatigue load level

j	Cyclic load	Cumulative cycles	Acceptance level	Mj	
				Simply	Fixed
	(lb.)			----- (lb.-in.) ----	
1	75	25,000	Light-Service	2438	1544
2	100	50,000	Medium-Service	3250	2058
3	125	75,000		4688	2573
4	150	100,000	Heavy-Service	4875	3088

Table 4.17 Stepped cyclic loading schedule for testing fatigue life of full-size back posts, and calculated maximums moments in back posts for each fatigue load level

j	Cyclic load	Cumulative cycles	Acceptance level	Mj
	(lb.)			(lb.-in.)
1	112.5	25,000	Light-Service	2,925
2	150	50,000	Medium-Service	3,900
3	187.5	75,000		4,875
4	225	100,000	Heavy-Service	5,850

Table 4.18 Stepped cyclic loading schedule for testing fatigue life of full-size stretchers, and calculated maximum moments in stretchers for each fatigue load level

j	Cyclic load	Cumulative cycles	Acceptance level	Mj[a]
	(lb.)			--(lb.-in.)--
1	49.5	25,000		49.5*h*
2	62	50,000		31*h*
3	74	75,000		74*h*
4	87	100,000		87*h*
5	99	125,000	Light-Service	99*h*
6	111	150,000		111*h*
7	124	175,000	Medium-Service	124*h*
8	136	200,000	Heavy-Service	136*h*

[a] *h* is the depth calculated for front spring rail at different levels.

Table 4.19 Stepped cyclic loading schedule for testing fatigue life of full-size front stumps, and calculated maximum moments in front stumps for each fatigue load level

j	Cyclic load	Cumulative cycles	Acceptance level	Mj
	(lb.)			----(lb.-in.)----
1	50	25,000		900
2	75	50,000	Light-Service	1350
3	100	75,000		1800
4	125	100,000		2250
5	150	125,000	Medium-Service	2700
6	175	150,000		3150
7	200	175,000	Heavy-Service	3600

Table 4.20 The depths of the *Schnadig* frame members calculated based on stepped cyclic load schedules

Frame Member	Performance-acceptance Level		
	Light	Medium	Heavy
	(simply supported/fixed end)		
	---------- (in.) ----------		
Front spring rails	2.879/2.291	3.223/2.565	3.382/2.692
Back spring rails	3.826/3.044	4.282/3.407	4.494/3.576
Front rails	4.238/5.326	4.748/5.966	4.967/6.263
Back top rails	2.396/1.906	2.767/2.202	3.390/2.698
Back posts	2.724	3.145	3.854
Stretchers	2.119/2.376	2.590/2.904	3.246/3.645
Front stumps	1.783	2.523	2.916

Summary

Selected wood materials were evaluated by subjecting them to edgewise static load, constant amplitude cyclic load, and cyclic stepped load in an effort to investigate the fatigue properties and their relationship with static properties. This is built on an earlier study by Zhang et al. (2005).

The regression equations of *S*-*N* curves through low 5% points were derived for all materials involved in this study and proposed as design equations for achieving a conservative design of furniture frame structural members considering fatigue effects. It was found that for the equation, $S = MOR(E - H \times \log_{10} N_f)$, the constant *E* was 0.85, and the constant *H* values were 0.06, 0.08, and 0.10, for plywood, OSB, and particleboard, respectively.

Cyclic stepped load tests of full-size back top rail specimens indicated that the Palmgren-Miner rule provided a conservative estimation of fatigue life of wood composites subjected to cyclic stepped bending stresses using their low 5% limit *S*-*N* curves. Results of stress ratio analyses suggested that the ratio of MOR to the fatigue stress level required to be passed for design of upholstered furniture frame members considering stepped fatigue effects could be set to various values for different types of wood composites, such as a minimum value of 1.85 for plywood, 1.56 for OSB, and 1.46 for PB. In other words, when considering cyclic stepped load effects, the allowable design stress for plywood, OSB, and PB should be no more than 54%, 64%, and 68% of their MOR, respectively. These numbers would provide furniture manufacturers a quick

reference to estimate the appropriate sizes of upholstered furniture structural members considering satisfaction of different GSA performance testing acceptance levels.

Finally, the section sizes of *Schnadig* frame members were calculated based on the stepped load schedule and material *S-N* equations. A simple support beam model and fixed end beam model were proposed as "conservative" and "progressive" design criteria, and the manufacturers can use this range as a reference in the design process. The study by Tackett and Zhang (2007) was referenced to derive the load schedules in front and back spring rails and stretcher from GSA seat load foundation test. Tackett and Zhang (2007) also found that the springs were stressed even where no sitting load was applied, which indicates that the springs exerted a constant load on the spring rails. This spring load will cause the creep of the spring rails during service. This creep was not covered by this study and should be of future research interest.

CHAPTER V

DIRECT WITHDRAW AND SHEAR RESISTANCE OF GLUE AND SINGLE STAPLE JOINTS IN PLYWOOD

The joints in the *Schnadig* frames were connected by staples. Some were also glued. The combination of staples and glue to connect furniture frame members is one of the most popular methods, especially in current upholstered furniture frame construction. As more wood-based composites such as plywood and OSB are used for upholstered furniture frame construction, the engineering data related to the load resistance capacity of the staple-glue joints in composite wood material become increasingly more important. The load resistance capacity of the staple-glue joints may be increased by the additive effects of glue and staple. Therefore, in order to analyze the load resistance capacity of staple-glue joints, it is necessary to study load resistance capacity of each connecting method separately. In this part, the direct withdraw load and shear load resistances of face to face and end to face plywood joints connected by glue or single staple are explored. It was anticipated that this preliminary experiment would provide useful information upon the structure of staple-glue joint, and aid in its design in the furniture industry.

Specimen Configurations and Materials

Glue Joints

The configurations of the face-to-face joint specimens in this study are shown in Figures 5.1. Both lateral and direct withdraw load test specimens of face-to-face joint type consisted of two principal structural members, a fastened member and a fastening member of the same type of material. For test specimens of the face-to-face joint type, both members had nominal dimensions of 12 inches long by 2 inches wide and by 0.75 inch thick. Two members of both lateral shear test and direct withdraw load test overlapped 2 inches in the fastening member length direction, so the glued contact area was 2 inches by 2 inches.

The configurations of the end-to-face joint specimens are shown in Figures 5.2. All test specimens of end-to-face joint type consisted of two principal structural members, a fastened member and a fastening member of the same type of material. For test specimens of the end-to-face joint type, both members had nominal dimensions of 8 inches long by 4 inches wide and by 0.75 inch thick. Therefore, the glued contact area was 4 inches by 0.75 inch.

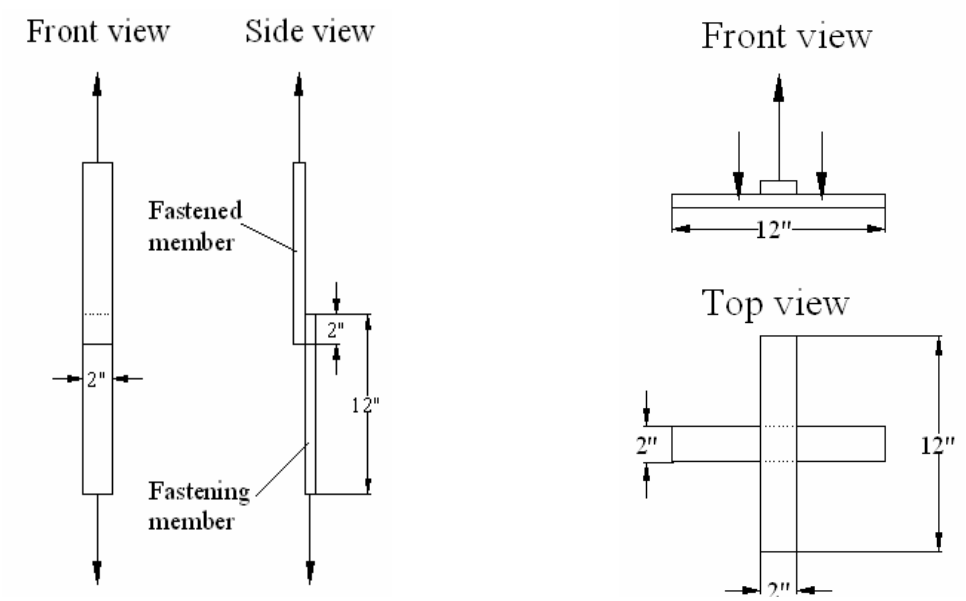

(a) (b)

Figure 5.1 General configurations of glued face-to-face joints for evaluating (a) lateral shear load, and (b) direct withdraw load

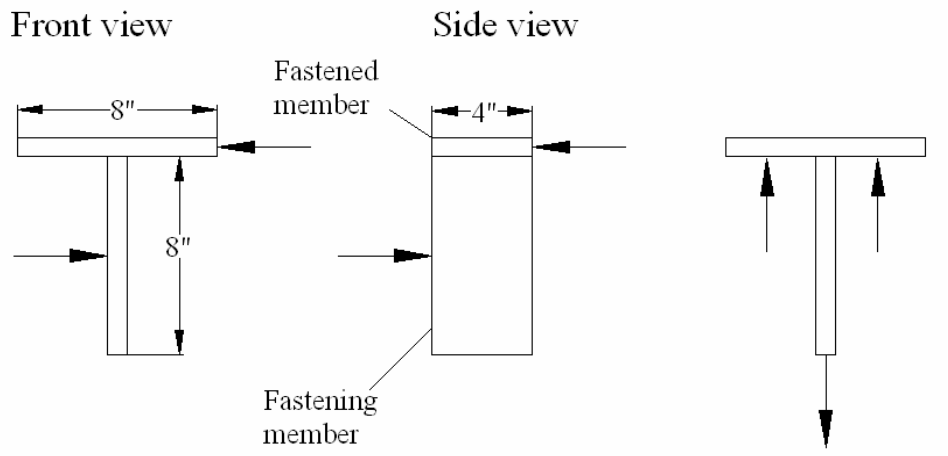

(a) (b) (c)

Figure 5.2 General configurations of glued end-to-face joints for evaluating (a) lateral parallel load, (b) lateral perpendicular load, and (c) direct withdraw load.

Single Staple Joints

The configurations of single staple face-to-face joint specimens subjected to lateral shear and direct withdraw load were the same with those glue joints as shown in Figure 5.1. For these two joints, the staples were 16-gage with the penetration depth of 0.75 inch, which was the thickness of the member. The staple crown orientation for both lateral shear and direct withdraw load tests was parallel to the fastening member face grain orientation as shown in Figure 5.3a,b.

The configurations of single-staple end-to-face joint specimens were the same with glue joints as shown in Figure 5.2. For all tested end-to-face specimens, the end penetration depth was 1 inch. The staple crown orientation for lateral perpendicular and parallel shear tests was perpendicular to the fastened member face grain orientation as shown in Figure 5.4a,b. The staple crown orientation for direct withdraw load test was at an angle of 45 degree to the fastened member face grain direction Figure 5.4c.

In addition to the lateral shear and direct withdraw load tests on single staple face-to-face and end-to-face joints, a tension test was performed on end-to-end single-staple joints as shown in Figure 5.3c. Both members had nominal dimensions of 12 inches long by 2 inches wide and by 0.75 inch thick. Different from face-to-face joints subjected to lateral shear load, the two members were aligned in a straight line with no overlap area. The staple was 16-gage with the penetration depth of 0.5 inch, and the crown of the staple was parallel with the grain orientation of both members.

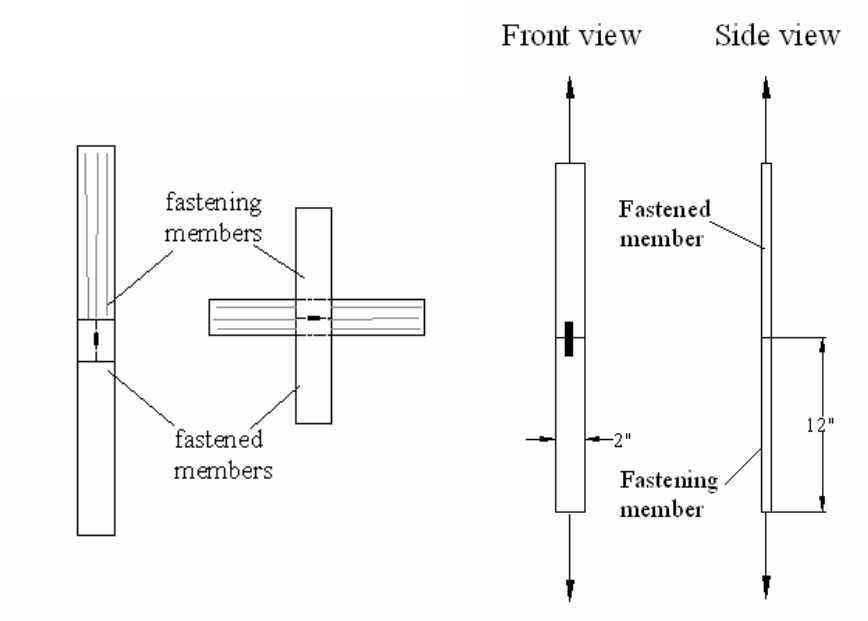

Figure 5.3 General configurations of single stapled face-to-face joints for evaluating (a) lateral shear load, (b) direct withdraw load, and (c) tension load for end-to-end joints

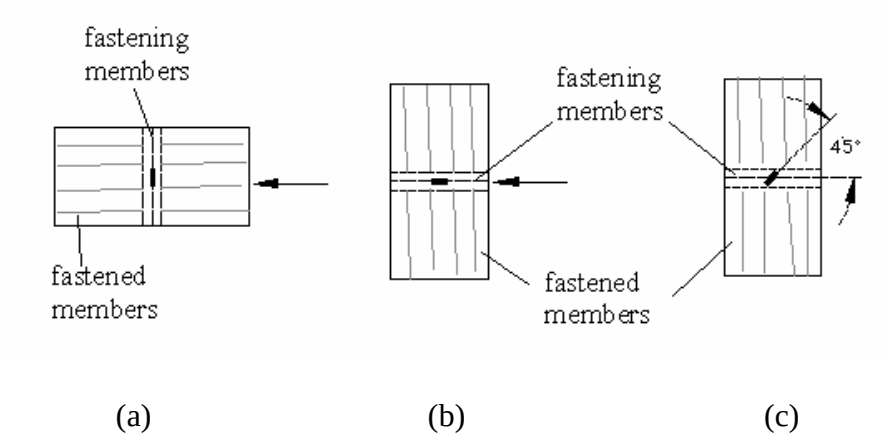

Figure 5.4 General configurations of single stapled end-to-face joints for evaluating (a) lateral parallel load, (b) lateral perpendicular load, and (c) direct withdraw load

Materials

The plywood was 6-ply southern yellow pine plywood. The full-size sheet (4 by 8 ft.) was constructed with the two center plies aligned parallel to the face plies and the two plies adjacent to face plies aligned perpendicular to the face. The face plies were aligned parallel to the 8-foot direction. Staples were SENCO 16 gage galvanized chisel-end-point types. Staple leg lengths of 1.5 and 1.75 inches were selected. Glue used was polyvinyl acetate (PVA) wood glue with solids content of 40%. All the materials were provided by *Schnadig*.

Experimental Design

Glue Joints

A complete random (CR) experiment with 3×2 factorial arrangement of treatments (Freund and Wilson 1997) was conducted to evaluate the load resistance capability of glued face-to-face joint. There were ten replicates per cell, so that a total of sixty specimens were tested. The treatments were face grain orientation of the members (parallel_parallel, parallel_cross, and cross_cross), and load direction (lateral shear load, Figure 5.1a, and direct withdraw load, Figure 5.1b). Parallel_parallel referred to the length of both members cut along the 8-foot full size direction, parallel_cross referred to the length of fastened member cut along 8-foot direction while the length of fastening member cut along 4-foot direction, and cross_cross referred to the length of both members cut along 4-foot direction.

A full linear model (5.1) for the two-factor factorial experiment was initially developed to test the influence of face grain orientation and load direction on the load resistances of face-to-face joint.

$$y_{ijk} = \mu + \alpha_i + \beta_j + (\alpha\beta)_{ij} + \varepsilon_{ijk} \quad (5\text{-}1)$$

Where:

y_{ijk} = response variable of ultimate stress (psi.)

μ = overall mean of ultimate stress (psi.)

α_i = discrete variable representing effect face grain orientation, i = parallel_parallel, parallel_cross, and cross_cross

β_j = discrete variable representing effect of load direction, j = lateral shear load and direct withdraw load

ε_{ijk} = random error term, k = 1~10 replicate; rest terms are two factor interactions

Since the two-factor interaction (face grain orientation × load direction) of the full model was found to be significant in the analysis of variance (ANOVA), the full model (5.1) was reduced to model (5.2):

$$y_{ijk} = \mu + (\alpha\beta)_{ij} + \varepsilon_{ijk} \quad (5\text{-}2)$$

A CR experiment with one treatment (Freund and Wilson 1997) was conducted on the glued end-to-face joint. The factor was load direction with three levels, which were, lateral parallel load (Figure 5.2a), lateral perpendicular load (Figure 5.2b), and

direct withdraw load (Figure 5.2c). With ten replicates per cell, there were thirty specimens tested altogether. The statistical model (5.3) was:

$$y_{ij} = \mu + \tau_i + \varepsilon_{ij} \tag{5-3}$$

Where:

y_{ij} = response variable of ultimate stress (psi.)

μ = overall mean of ultimate stress (psi.)

τ_i = discrete variable representing effect load direction, i = lateral parallel load, lateral perpendicular load, and direct withdraw load

ε_{ij} = random error term, j = 1~10 replicate

Single Staple Joints

A CR experiment with one treatment (load direction) was performed on the stapled face-to-face and end-to-face joints. For face-to-face joint type, there were two levels, i.e., lateral shear load (Figure 5.3a), direct withdraw load (Figure 5.3b). With twenty replicates per cell, a total of forty specimens were tested. For end-to-face joint type, the treatment load direction had three levels, i.e., lateral parallel load (Figure 5.4a), lateral perpendicular load (Figure 5.4b), and direct withdraw load (Figure 5.4c). With twenty replicates per cell, a total of sixty specimens were tested. All the members of stapled joints were cut along 8-foot direction.

The statistical models for both stapled face-to-face and end-to-face joint types were the same as indicated in equation (5.3). Where:

y_{ij} = response variable of ultimate load (lb.)

μ = overall mean of ultimate load (lb.)

τ_i = discrete variable representing effect load direction, for face-to-face joint i = lateral parallel load, and direct withdraw load; and for end-to-face joint i = lateral parallel load, lateral perpendicular load, and direct withdraw load

ε_{ij} = random error term, j = 1~20 replicate

For single staple end-to-end joints, twenty replicates were tested to attain the mean maximum load resistance without statistical analysis.

Specimen Preparation and Test

Prior to joint construction, all cut plywood blanks were conditioned in an equilibrium moisture content chamber at $77 \pm 4^{\circ} F$ and 41 ± 1 percent relative humidity. Moisture content of the plywood averaged 7.1 percent and, and density averaged 36.9 pcf. The glue was applied to both fastened member and fastening member and the two members were clamped for 48 hours before testing. The amount of glue applied was approximately 0.2 ounce and 0.19 ounce per joint for face-to-face and end-to-face joints, respectively.

All specimens were tested on a hydraulic SATEC universal-testing machine at a loading rate of 0.10 in./min. Figures 5.5 ab and 5.6 show the test setups for face-to-face and end-to-face joint types, respectively. Figure 5.5c shows the set up for end-to-end

single staple joint under tensile load. Ultimate lateral and direct withdraw loads and joint failure modes were recorded.

(a)

(b)

(c)

Figure 5.5 Test setups for evaluating load resistance of face-to-face joint type, (a) lateral shear test, (b) direct withdraw load test, and (c) tension test for single staple end-to-end joints

(a)

(b)

(c)

Figure 5.6 Test setups for evaluating load resistance of end-to-face joint type, (a) joints loaded parallel to the fastening member thickness direction, (b) joints loaded perpendicular to the fastening member thickness direction, and (c) direct withdraw load test

Results and Discussion

Glue Joints

Table 5.1 summarizes the mean ultimate stresses of glued face-to-face joint and their coefficients of variation (COV). Each value represents a mean of 10 replicates tested. The joints failed because of the bond failure between glue and plywood. A two-factor analysis of variance (ANOVA) general linear mode procedure was performed on individual joint data with the full model (model 5.1) to analyze main effects and the interaction on the mean ultimate stresses of face-to-face joint type. The ANOVA results indicated that the two-factor interaction, face grain orientation times load direction, was statistically significant at the 5 percent significance level. Hence, the tests for main effects were ignored, and the reduced model (model 5.2) was employed to explore the significant two-factor interaction on the response variable.

Table 5.1 shows mean comparisons of ultimate stresses for load direction effect for each face grain orientation. Tables 5.2 gives the mean comparisons for face grain orientation effect for each load direction. The results were based on a one-way classification with six treatment combinations. The protected least significant difference (LSD) multiple comparisons procedure at the 5 percent significance level was performed to determine the mean differences of those treatment combinations. The error mean square from the full model factorial analysis was employed for all comparisons, i.e., the LSD value of 70 psi was calculated based on the error mean square of the full model.

Results indicated that for all the face grain orientations, the lateral shear load resistance of face-to-face glued joint is significantly higher than direct withdraw load resistance (Table 5.1). This finding might suggest that a furniture frame would be much stronger if it is constructed as glued joints being subjected to lateral loads instead of direct withdrawal loads. For lateral shear load, the face grain orientation has a significant effect on the mean value of ultimate stresses. It appears that parallel cut members exhibiting more "glue capabilities" because the parallel_parallel joint reflects the highest load resistance while the cross_cross the lowest. However, for direct withdraw load, there is no significant difference among face grain orientations (Table 5.2).

Table 5.3 summarizes the mean ultimate stresses and their COV for glued end-to-face joint. Each value represents a mean of 10 replicates tested. The joints failed because of the bond failure between the glue and plywood. The LSD value of 91 psi was calculated based on the error mean square of model 5.3. The ANOVA test results show that the load direction has a significant role on the mean value of ultimate stresses of glued end-to-face joint, with lateral perpendicular shear load resistance being the highest and direct withdraw load resistance lowest.

Table 5.1 Mean ultimate stresses of glued face-to-face joint type, and mean comparisons of ultimate stresses for load direction [a]

Face grain orientation	Mean ultimate stress for different load directions (psi.)	
	Lateral shear load	Direct withdraw load
Parallel_parallel	510 (15) A	130 (19) B
Parallel_cross	328 (24) A	101 (9) B
Cross_cross	245 (18) A	99 (11) B

[a] Values in parentheses are coefficients of variation in percent; values with the same capital letter are not statistically significant at 5 percent significance level.

Table 5.2 Mean comparisons of ultimate stresses of glued face-to-face joint type for face grain orientation [a]

Load direction	Mean ultimate stress for different face grain orientations (psi.)		
	Parallel_parallel	Parallel_cross	Cross_cross
Lateral shear load	510 A	328 B	245 C
Direct withdraw load	130 A	101 A	99 A

[a] Values with the same capital letter are not statistically significant at 5 percent significance level.

Table 5.3 Mean comparisons of ultimate stresses of glued end-to-face joint type for each load direction [a]

Mean ultimate stress for different load directions (psi.)		
Lateral perpendicular shear load	Lateral parallel shear load	Direct withdraw load
490 (10) A	345 (23) B	224 (38) C

[a] Values in parentheses are coefficients of variation in percent; values with the same capital letter are not statistically significant at 5 percent significance level.

Single Staple Joints

Table 5.4 summarizes the mean ultimate stresses and their COV for single stapled face-to-face and end-to-face joint. Each value represents a mean of 20 replicates tested. The LSD value was calculated based on the error mean square of model 5.3. It is 22 lb and 30 lb for face-to-face and end-to-face joint, respectively.

The ANOVA test results show that the load direction has a significantly role on the mean ultimate load of single stapled face-to-face joint, but not on the end-to-face joint. For the single stapled face-to-face joint, the same with the glued joint, lateral shear load resistance is significantly higher than tensile load resistance

For the single staple end-to-end joint (Figure 5.3c), the average tension force was 123 pounds with the COV of 15.

Table 5.4 Mean ultimate loads of single stapled face-to-face and end-to-face joint type, and mean comparisons of ultimate stresses for each load direction [a]

Joint type	Mean ultimate load for different load directions (lb.)		
	Lateral shear load	Direct withdraw load	
Face-to-face	216 (10) A	175 (25) B	
	Lateral perpendicular shear load	Lateral parallel shear load	Direct withdraw load
End-to-face	192 (18) A	176 (18) A	180 (27) A

[a] Values in parentheses are coefficients of variation in percent; values with the same capital letter are not statistically significant at 5 percent significance level.

Summary

Lateral shear, direct withdraw tests were conducted on face-to-face joint and T-shaped, end-to-face joint in southern yellow pine plywood. Two connection methods were investigated in this study, which were glue and single staple. And a tension test was performed on the single-staple end-to-end joints.

Two factors, load direction and face grain orientation, were included in the glue face-to-face joint type. Experimental results indicate that the load-to-grain direction has a significant role on the mean ultimate stresses. For all the face grain orientation, the lateral shear load resistance is significantly higher than direct withdraw load resistance. However, the face grain orientation affects the mean ultimate stresses only when the joints being subjected to lateral shear load.

One factor, load direction, was included in the glued end-to-face and both single staple face-to-face and end-to-face joints. For glued end-to-face joints, the load direction affects the mean ultimate stresses significantly, with lateral perpendicular shear load resistance being the highest and direct withdraw load resistance lowest. For single staple face-to-face joint type, the lateral shear load resistance is significantly higher than tensile load resistance. For single staple end-to-face joint, no difference is found among lateral perpendicular load, lateral parallel load, and tensile load resistance.

In next chapter, FE models were developed to explore the internal forces of critical joints and members when the frames were subjected to GSA performance test load and boundary conditions. Combining the testing results on frames, members, and

joints, proper measures were taken to strength those weak parts in order to achieve the medium or above acceptance level.

CHAPTER VI

NUMERICAL ANALYSIS OF CRITICAL COMPONENTS AND IMPROVEMENT SUGGESTIONS

Through conducting GSA performance tests on *Schnadig* frames, critical components were identified. The weak joints were the front stump to bottom side rail, front stump to side center rail, and top arm rail to back post. The weakest member was the back spring rail. In this part of study, finite element models were developed to simulate the GSA testing on bare frames, so that the internal forces at the critical joints and members were obtained. When the cyclic load effects were considered, the static/fatigue ratio of 2 was used for the joint design, and the procedures described in Chapter IV were applied to the estimation of member sizes. Based on the experimental and numerical results, measures were taken to strengthen those weak components so that the medium or above acceptance level can be satisfied.

A model of a three-seat sofa frame including key structural members was developed using FEM software I-DEAS. The members included the top rail, back post, back upright, top arm rail, bottom side rail, side center rail, front stump, front rail, front spring rail, back rail, back spring rail, stretcher, and leg, Figure 6.1. The dimensions of each member are listed in Table 6.1. Four sets of load and boundary conditions were applied based on GSA testing, which were horizontal side-thrust arm load test (inward),

horizontal side-thrust arm load test (outward), backrest frame test, and vertical load test on back spring rail. For each test, the four legs were constrained as no translations in X, Y, and Z directions, but were free to rotate.

It was assumed that the material is homogeneous and the joint is rigid. Young's modulus of the material was $E = 1.22 \times 10^6$ psi, and Poisson's ratio $\upsilon = 0.29$. The element used was 3-D solid linear element. For each simulation model, a 100-pound load was applied to the frame at each load head.

Table 6.1 Dimensions of each member

Members	Dimension (in.)		
	Length	Depth	Thickness
Top rail	90	3	
Back post	27.75	5.25	
Back upright	27.75	3	
Top arm rail	25.5	5.25	
Side center rail	29.25	3	
Bottom side rail	29.25	3	
Front stump	18	5.25	0.75
Front rail	90	5.25	
Front spring rail	79.5	3	
Back rail	79.5	1.5	
Back spring rail	79.5	3	
Stretcher	25.5	3	
Leg	3.75	0.75	

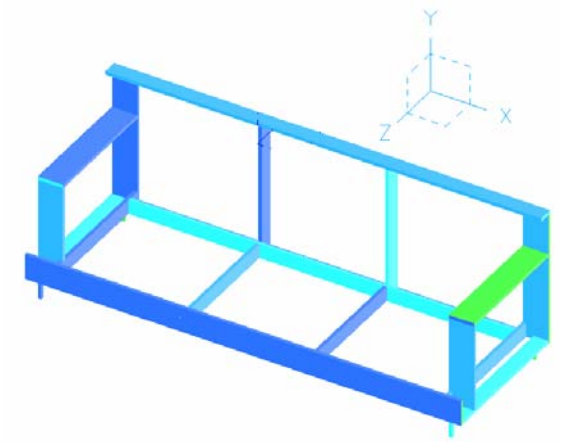

Figure 6.1 A three-seat sofa frame model develop by I-DEAS

Joint of Front Stump to Bottom Side Rail

A horizontal side-thrust arm load test (inward) model was developed to study the stress at the joint of front stump to bottom side rail, Figure 6.2a. A load of 100 pounds was applied at the outside surface of one arm at a point as near as possible to the intersection of the stump with the arm. Figure 6.2b shows the deformation and stress concentration, and Figure 6.2c illustrates the load distribution among joints. As shown in Figure 6.2b and c, the 100-pound load acting upon the arm rail in an inward direction caused a bending moment of 1,137 lb-in at the joint of front stump to bottom side rail, a torsion of 348 lb-in at the joint of bottom side rail to front rail, and a torsion of 254 lb-in at the joint of arm rail to back post.

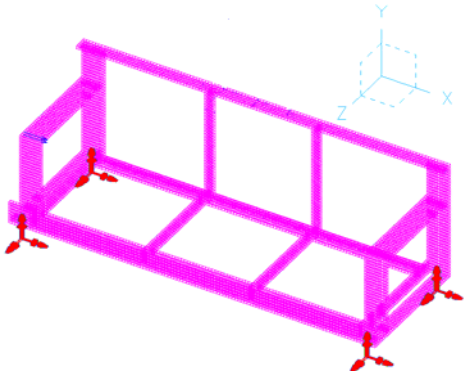

(a)

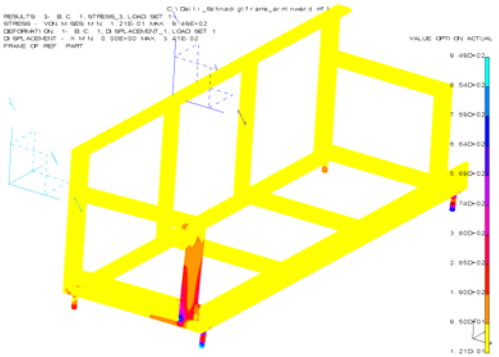

(b)

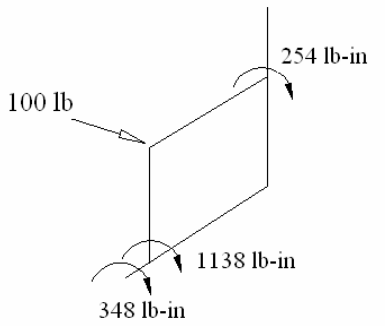

(c)

Figure 6.2 Horizontal side-thrust arm load test (inward), (a) FE model, (b) deformation and stress distribution, and (c) load distribution among joints

The joint of front stump to bottom side rail was a critical joint under GSA testing load, and its element forces on the end surface of front stump were obtained as shown in Figure 6.3. The tension force summed up to 505 lb, and the moment was 1,138 lb-in for each unit load applied. The three frames tested achieved an average load level of 100 pounds, and the failure mode observed was the withdrawal of staples from the material because of the tension force (Table 5.2). The medium acceptance level is 175 pounds (Table 2.1), and at that load level the bending moment would be 1,992 lb-in, which will produce a tension force of 884 lb.

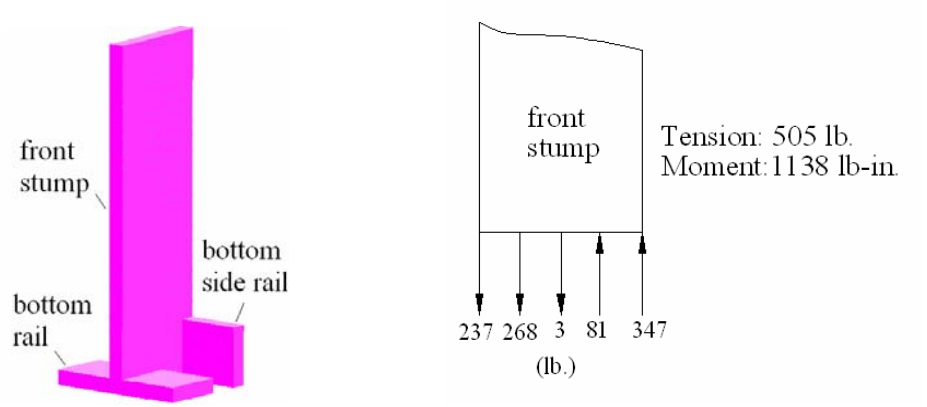

Figure 6.3 Joint of front stump to bottom side rail and its 2D sketch of element force at the end of front stump

Zhang et al (2002b) proposed the equation $y = S \times N^{0.75}$ to predict the direct withdrawal strength of multi-staple joints based on the strength of single-staple joints. Here S is the load capacity of the single staple and N is the number of staples. There were two staples driven through the block to the bottom side rail face and two driven through the edge to the end of front stump, and the penetration depth was 0.5 inch. The

direct load capacity of single staple with penetration depth of 0.5 inch was 142.5 pounds (Zhang et al. 2002b), so the direct withdraw load resistance of front stump to bottom side rail would be 403 lb by using this formula, only 46% of the desired strength of 884 lb. It was obvious that the joint was not strong enough, and the GSA test also showed it as a critical joint. Moreover, the load resistance should be doubled for design purpose when the cyclic load effects were considered. In other words, to guarantee a medium acceptance level, the joint the front stump to bottom side rail should be able to resist the bending moment of 3,984 lb-in (1,922 × 2), and which would cause a tensile load of 1,768 lb (884 × 2).

In order to strengthen the joint, it is necessary to increase the number of staples and also the depths of staple penetration. The bottom side rail in *Schnadig* frame was 1.5 inches thick so that the staples could be only driven through the block to the bottom side rail face and driven through the bottom side rail edge into front stump end (Figure 3.7). It is suggested that the bottom side rail be reduced because the bottom side rail itself was not a critical structural member based on GSA tests. If the depth of bottom side rail were 0.75 inch, as shown in Figure 6.4, the staples could be driven through bottom side rail into front stump end and the block. Doing this would have two benefits for a staple-glued joint. One would be an increase of the penetration depth of staples, which can better secure the joint before the glue dries out. Second would be that the staples can help prevent the delamination of plywood. However, if only staples were used, almost twenty staples would be needed in order to reach a tensile strength of 1,768 lb with the

staples with 0.75 inch penetration, which was obviously not practical. For this reason, glue is recommended to strengthen the connection.

Figure 6.4 shows the suggested construction of the joint of front stump to bottom side rail. Glue would be applied to the block on both contact surfaces with bottom side rail and front stump, and also the end of front stump. Staples would be driven through the rails to the block and front stump end. If the blocks were 2.5 inches by 2.5 inches with the depth of 1.5 inches, and the staples were 16-gage with the leg of 1.5 inches, the penetration depth would be 0.75 inch. By putting four staples from bottom side rail into the block and two staples from bottom side rail into the end of front stump at tension side, there would be six staples to resist the direct withdraw force. As listed in Table 5.4, the mean load resistances of single staple direct withdraw from plywood end and face was 180 lb and 175 lb respectively, so the resistance of the six staples would be approximately 690 lb. The glue area of front stump to bottom side rail was 3 inches by 0.75 inch, and with the glued end-to-face direct withdraw stress of 224 psi (Table 5.3) the direct withdraw resistance would be 504 lb. If the glue area of block to bottom side rail were 2.5 inches by 1.5 inches, and the direct withdraw stress between the block (yellow poplar) and plywood would be tested in order to calculate the load resistance. Figure 6.5 shows the test set up. The test was conducted on a hydraulic SATEC universal-testing machine at a loading rate of 0.10 in./min. The specimens would be cut as 2 inches by 2 inches, and the yellow poplar specimen and plywood specimen was glued together. Chapter V showed that ten replicates were tested with the mean ultimate stress 145 psi.

Therefore, the direct withdraw resistance of glued block and bottom side rail would be 544 lb. Adding the direct withdraw load resistance of staples and glue, the predicted tensile strength of the joint of front stump to bottom side rail would be 1,738 lb.

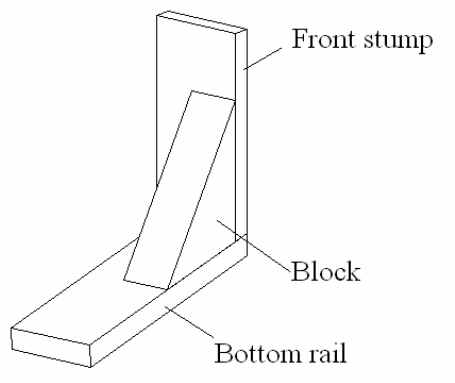

Figure 6.4 Suggestion of improved design of the joint of front stump to bottom side rail

Figure 6.5 Direct withdraw stress test set up for glued yellow poplar and plywood

Figure 6.6 shows a static bending test for the improved joint of front stump to bottom side rail. Loads were applied to the rail 10 inches from the bottom side rail, i.e.,

the moment arm was 10 inches. Three replicates were tested with the average ultimate load of 496 lb, and the joint broke because of the failure of the glue bond. Also, the staples pulled out of the material. The moment arm was 10 inches, so the moment capacity of the glue-staple joint of front stump to bottom side rail was 4,960 lb-in. Therefore, the suggested joint construction was considered as being able to meet medium acceptance level under side-thrust inward load test on arms, where the moment was required to be 3,984 lb-in or above. Moreover, the moment capacity of the tested joints could be 1.94 the static moment at 225 pound load level (Table 2.1). With this ratio, most probably the joint can meet heavy acceptance level when considering cyclic load effects.

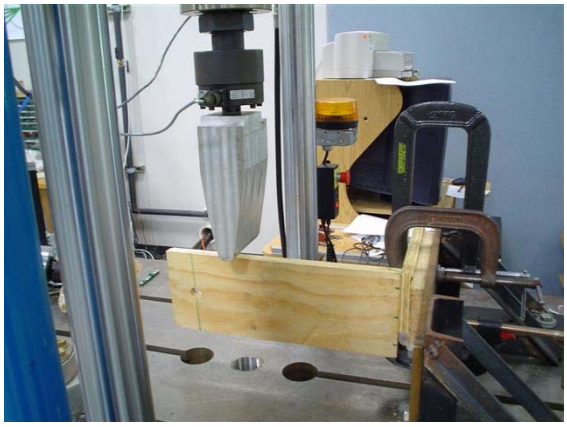

Figure 6.6 Bending test on improved front stump to bottom side rail joint

Joint of Front Stump to Side Center Rail

A FE model of horizontal side-thrust arm load test (outward) was developed to study the stress at the joint of front stump to side center rail, Figure 6.7a. A 100-pound

load was applied at the inside surface of one arm at a point as near as possible to the intersection of the stump with the arm. Figure 6.7b shows the deformation and stress concentration, and Figure 6.7c shows the load distribution among the joints. As shown in Figure 6.7b and c, the load acting upon the arm rail in an outward direction caused a bending moment of 941 lb-in at the joint of front stump to side center rail, a torsion of 396 lb-in at the joint of side center rail to front rail, and a torsion of 302 lb-in at the joint of arm rail to back post.

The element forces on the edge of front stump are illustrated as in Figure 6.8. The tension force summed up to 387 lb, and the moment was 942 lb-in for each 100-pound load applied. The medium acceptance level is 150 pounds (Table 2.1), and at this load level the moment would be 1,413 lb-in, and the tension force would be 581 lb. The three frames tested under GSA horizontal side-thrust arm load test (outward) all passed light acceptance level, with an average load of 83 pounds (Table 5.2). For the joint of front stump to side center rail of *Schnadig* frames, there were two staples driven through the side center rail into front stump edge with the penetration depth of 0.75 inch. The direct withdraw load resistance was calculated as 303 lb, which was 52% of the load resistance at medium acceptance level (581 lb). It was obvious the joint was not strong enough, and the GSA tests also showed it as a critical joint. Moreover, when cyclic load effects were considered, the joint of front stump to side center rail would have a bending moment of 2,826 lb-in (1413 × 2), which would cause a tension force of 1,162 lb (581 × 2).

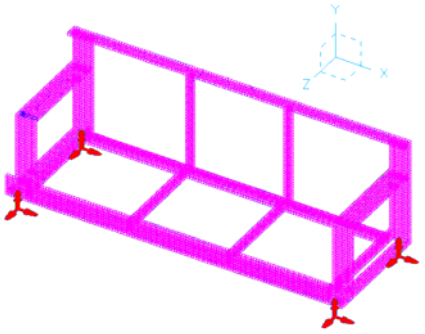

(a)

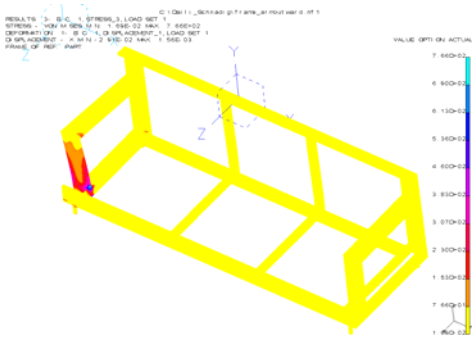

(b)

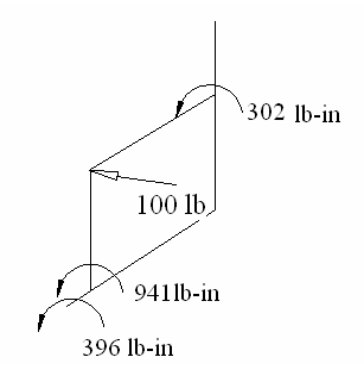

(c)

Figure 6.7 Horizontal side-thrust arm load test (outward), (a) FE model, (b) deformation and stress distribution, and (c) load distribution among joints

In order to strengthen the joint, it is suggested to use a corner block. The use of a corner block will increase the glue contact area, which, as stated before, can ensure a stiffer joint. Figure 6.9 shows the suggested configuration of the joint of front stump to side center rail. The block should be aligned with the upper edge of side center rail, where the maximum tension force occurred, as shown in Figure 6.8. Five staples should be driven through side center rail into the block, and three driven through side center rail into the edge of front stump. If the blocks were 2.5 inches by 2.5 inches with the depth of 1.5 inches, 16-gage staples would penetrate to a depth of 0.75 inch. There would be six staples at the tension force area, so the direct withdraw load resistance of staples would be 690 lb. The contact glue area between the side center rail and the front stump subjected to tension force would be 1.5 inches by 0.75 inch, so with the end-to-face direct withdraw stress of 224 psi (Table 5.3) the direct withdraw resistance would be 252 lb. The direct withdraw load resistance of the connection between the block and the side center rail was 544 lb. Adding the load resistances of staples and glue, the predicted direct withdraw load resistance would be 1,486 lb.

Figure 6.10a shows a static test set up, with a bending moment arm of 10 inches. Three tested samples had an average ultimate load of 414 pounds. The joint failed because of the glue bonding between the upper sides (tension area) failed and the staples pulled out of the side center rail edge. At this load level, the moment capacity would be 4,140 lb-in, which can meet the medium acceptance level requirement of 2,826 lb-in. The heavy acceptance level for side-thrust outward load on arms is 200 pounds (Table

2.1), and the moment at this load level when considering cyclic load effects would be 3,768 lb-in. Hence, the improved joints can be considered as being able to meet heavy acceptance level under side-thrust outward load test on arms.

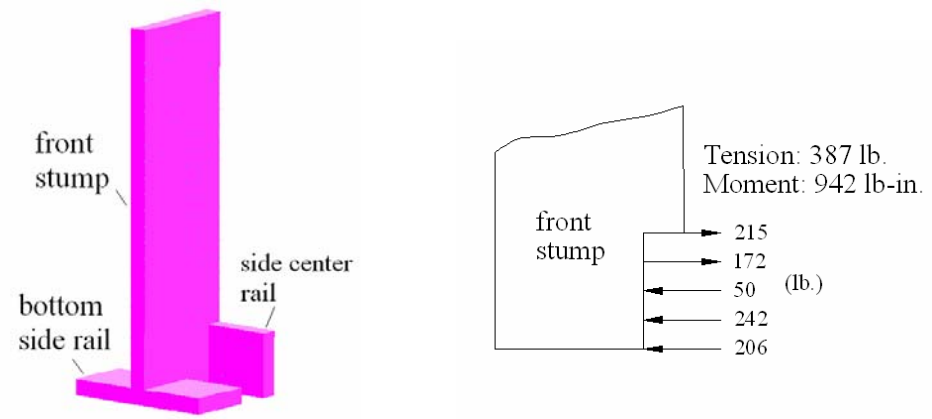

Figure 6.8 Joint of front stump to side center rail and its 2D sketch of element force at the edge of front stump

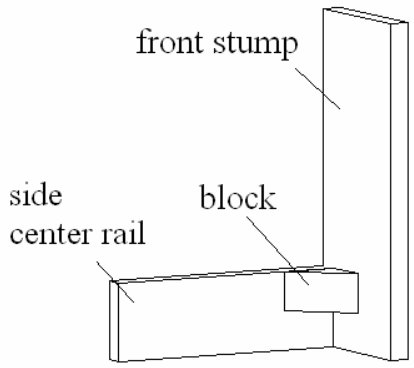

Figure 6.9 Suggestion of improved design of the joint to resist horizontal side-thrust arm load in outward direction

Finally, a cyclic stepped load test was performed on the joint of front stump to side center rail. The testing schedule was horizontal side-thrust load test on the arms (Table 2.1). Two specimens were tested. Figure 6.10b shows the test set up. One joint failed at the sixth load level (175 lb), which was considered as achieving a medium acceptance level (150 lb), but not a heavy acceptance level (200 lb). The other joint passed heavy acceptance level (200 lb) and failed at 225 lb. Both specimens failed because the staples withdraw from the front stump edge and from the block, and the glue bonding between the block and front stump to the side center rail failed.

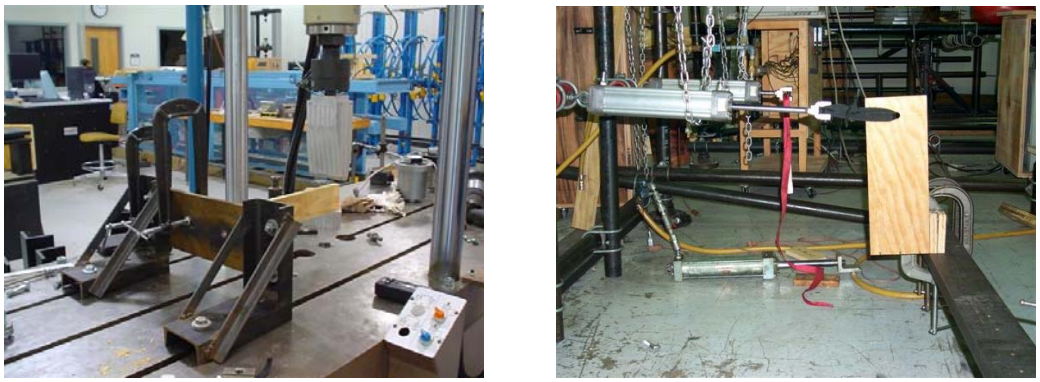

(a) (b)

Figure 6.10 Tests on improved front stump to side center rail joint, (a) static bending test, and (b) cyclic stepped load test

Joint of Top Arm Rail to Back Post

A FE model of backrest frame test was developed to study the stress at the joint of top arm rail to back post, Figure 6.11a. Three 100-pound loads were applied on the top rail at the center and at points 1/6th the length of the open face of the sofa from each end.

Figure 6.11b shows the deformation and its stress distribution. Figure 6.11c illustrates the load distribution among the joints.

As shown in Figure 6.11c, for three 100-pound loads applied on the top rail, the shear force at the back post would be 98 lb and at the back upright 50 lb. Thus, the end supports carried approximately 2/3 of the load while mid supports carried 1/3 of the load. The moments produced at the joint of top arm rail to back post, the joint of bottom side rail to back post, and the joint of back upright to back spring rail was 728, 639, and 1,307 lb-in, respectively. Of those three joints, the joint of top arm rail to back post was identified as a critical joint in GSA backrest frame tests.

The maximum computed moment in the top rail was in the mid-span, which was 2,300 lb-in for three 100-pound loads (Figure 6.12a). Table 6.2 shows the moment at every GSA backrest frame test load level based on the simulation application of three 100-pound loads. By using the aforementioned Palmgren-Miner rule, the depths needed for different acceptant levels were calculated and listed in Table 6.2. Also listed are the results calculated using simplified beam models in Chapter IV. It can be seen that the depths calculated from computer model fell between the results of the fixed end beam model and the simple support beam model. Hence, the simplified beam models could be served as an effective tool to give a conservative estimation of the moment range for the top rail under GSA load conditions. In the original *Schnadig* frame, the top rail was 2.75 inches in depth, which was large enough to allow medium duty classification based on the calculation.

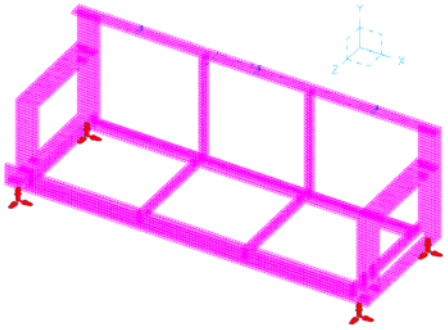

(a)

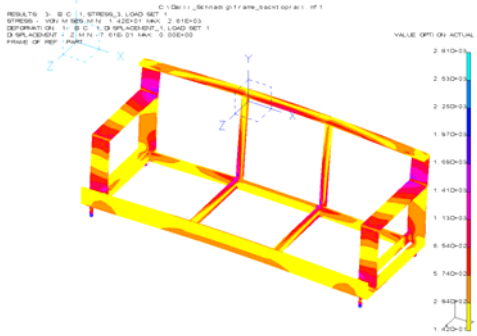

(b)

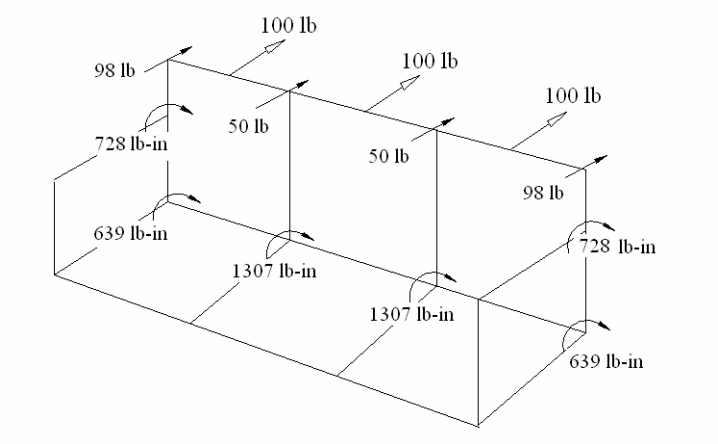

(c)

Figure 6.11 Backrest frame test, (a) FE model, and (b) deformation and stress distribution, and (c) load distribution among joints

Table 6.2 Maximum moment in the back top rail for GSA backrest frame test load schedule and calculated depths for different acceptance levels

j	P (lb.)	Number of loads	Cumulative cycles	Service-acceptance level	M_j $P \times M_u$[a] (lb.-in.)	Estimated depths (in.)		
						C[a]	F[a]	S[a]
1	75	3	25,000	Light-Service	1,725	2.016	1.906	2.396
2	100	3	50,000	Medium-Service	2,300	2.328	2.202	2.767
3	125	3	75,000		2,875			
4	150	3	100,000	Heavy-Service	3,450	2.852	2.698	3.390

[a] M_u = 2,300 (lb-in.)/100 (lb.) (moment caused by unit load)
C stands for depths calculated based on computer models; F stands depths calculated from fixed end beam model, and S stands for depths calculated from simply supported beam model.

Figure 6.12b shows the element force on the end of the back upright at the joint of back upright to back spring rail, where the computed tension force was 499 lb. The medium acceptance level of backrest frame tests was 100 lb, so the tension force of this joint at medium load level would also be 499 lb. The joint of back upright to back spring rail had four staples driven through the back spring rail into the back upright edge, and two driven through the back center rail to back upright edge. The direct withdraw load resistance of six staples with the penetration depth of 0.75 inch was found to be 690 lb, which was 1.4 the strength of the minimum specified load resistance of 499 lb. The joint of back upright to back spring rail was not a critical joint under GSA backrest frame test.

Figure 6.12c shows the element force on the end of bottom side rail at the joint of bottom side rail to back post, where the computed tension force was 228 lb. The medium acceptance level of backrest frame tests is 100 lb, so the required tension resistance of this joint at medium load level would also be 228 lb. If there were four staples driven though the back post into bottom side rail end, giving a penetration depth of 0.75 inch,

the direct withdraw load resistance would be 509 lb, which was 2.2 the strength of minimum specified load resistance of 228 lb. And the joint of bottom side rail to back post was not a critical joint under GSA backrest frame test.

The joint of top arm rail to back post was a critical joint, and its element forces on the end of top arm rail are illustrated in Figure 6.13. The tension force was 935 lb, and the bending moment was 728 lb-in for three 100-pound loads acting upon the back top rail. Ten and nine staples were counted on the joint of top arm rail to back post on frame #2 and #4, which passed heavy and medium acceptance level, respectively. For frame #8, six staples were used, which achieved light acceptance level (75 lb) and failed at the medium acceptance load level (100 lb). Glue was applied to the mortise and tenon joint. However, very little or none was found on the contact surfaces. Therefore, it is suggested to use at least ten staples to ensure adequate direct withdrawal strength. However, proper application of glue on the contact surface would make the joint much stronger so that fewer staples would be needed.

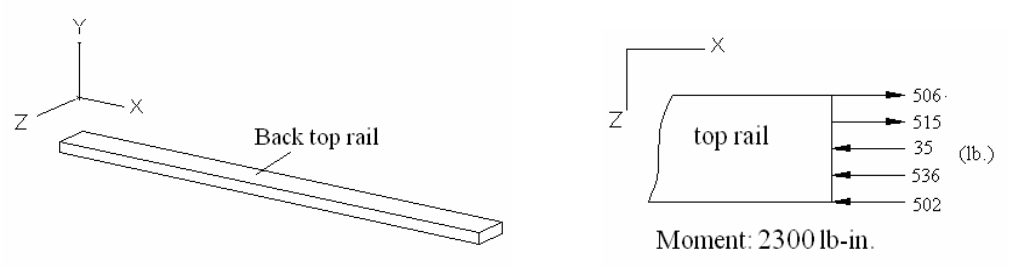

(a)

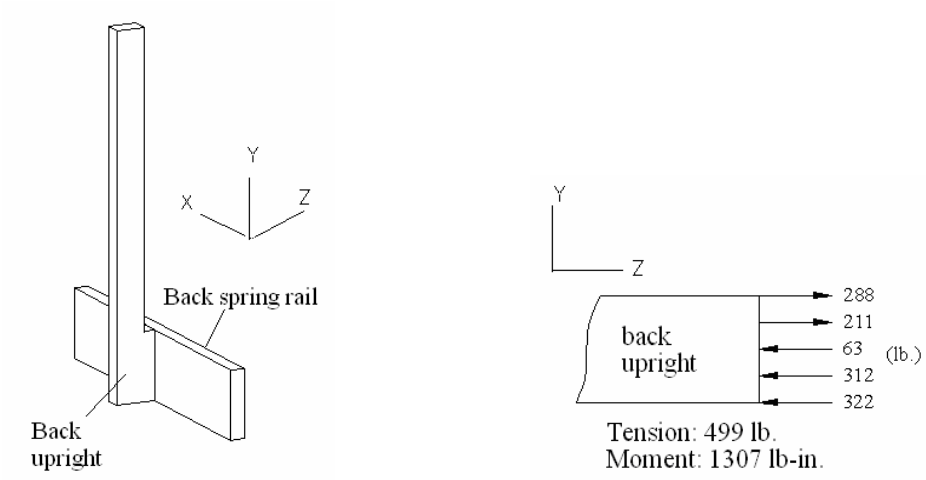

(b)

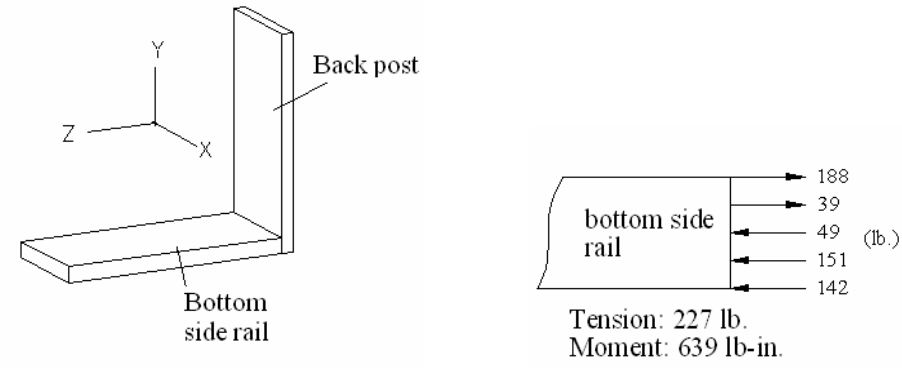

(c)

Figure 6.12 The element force at (a) mid span of top rail, (b) end of back upright, and (c) end of bottom side rail

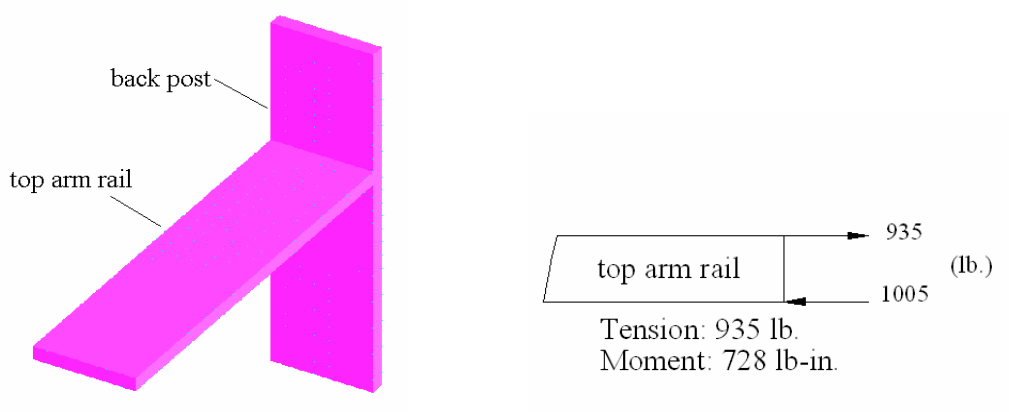

Figure 6.13 Joint of top arm rail to back post and its 2D sketch of element force at the end of top arm rail

The joint of top arm rail to back post was also a critical joint under GSA backrest foundation tests. However, there were only four to five staples at the joint for the frames used in the backrest foundation tests, while in the backrest frame tests the number of staples on the same joint of the frame tested were ten, nine and six. The difference in the number of staples used appears to be the cause of the inconsistent performance behavior. As stated in Chapter III, the direct withdraw load at each joint of top arm rail to back post can be assumed as half of the total load applied on the backrest foundation. The medium acceptance level for backrest foundation test was 125 pounds, so the direct withdraw load at the joint of top arm rail to back post would be 188 pounds.

In general, taking the cyclic load effects into consideration, the joint of top arm rail to back post would have a bending moment resistance of 1,456 lb-in (728 × 2), and tensile load resistance of 1,870 lb (935 × 2). It is suggested that at least ten staples should be used, with the application of glue to guarantee a strong enough joint to achieve

medium or above acceptance level for both backrest frame test and backrest foundation test.

Figure 6.14 shows sample joints and set up for the tests. The L-shape joint was made for bending test, and the T-joint was made for direct withdraw test. No changes were made in the configurations of the joints except that glue was used to strengthen the connection. Glue was applied to the contact surfaces and ten staples were driven through back post into arm rail end. The staples were 16-gage with penetration depth of 0.75 inch. The direct withdraw load resistance of 10 staples with the penetration depth of 0.75 inch would be 1,012 lb, and the direct withdraw load resistance of glued top arm rail to back post would be 882 lb. Thus the predicted direct withdraw load resistance of the connection would be 1,894 lb. The three replicates were tested in bending, giving an average ultimate load of 152 pounds. The joints failed because of the glue bonding were detached and the staples were pulled out of the arm rail end. With the bending moment arm of 10 inches, the moment capacity would be 1,520 lb-in, which can meet the requirement of medium acceptance level of backrest frame test. The three replicates were tested direct staple withdrawal. An average ultimate load of 1,934 pounds was achieved, which meets the medium acceptance level for backrest frame test and heavy acceptance level requirement for backrest foundation test.

Figure 6.14 Bending and direct withdrawal test set up for the improved top arm rail to back post joint

Back Spring Rail

Figure 6.15 shows the FE model and its deformation and stress concentration. Three 100-pound vertical loads were applied to the back spring rail to compute the bending moment in the edge-wise direction. These loads were applied at the center and at points $1/6^{th}$ the length of the open face of the sofa from each end. The maximum moment occurred at the mid-span of the back spring rail. Figure 6.16 shows the element forces on the cross section at the mid-span of back spring rail when it was subjected to three 100-pound vertical loads. For this load, the bending moment was calculated as 2,230 lb-in.

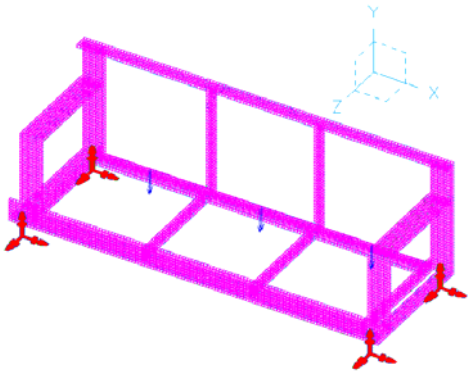

(a)

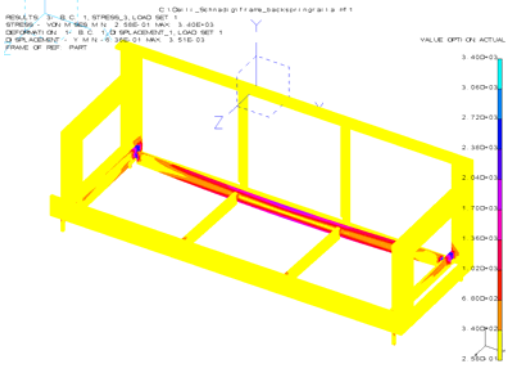

(b)

Figure 6.15 Back spring rail vertical load test, (a) FE model, and (b) deformation and stress distribution

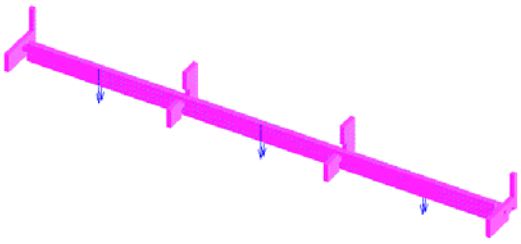

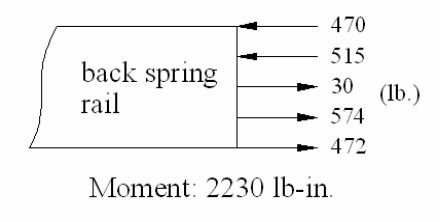

Figure 6.16 Back spring rail and its 2D sketch of element force at the middle section

With the seat load foundation schedule (Table 2.1), the bending moment produced by three 100-pound loads applied on the back spring rail, the percentage of vertical force component, and the moment at each load level can be calculated. The method of Palmgren-Miner rule was applied to estimate the section size of the back spring rail needed to meet the designated GSA acceptance levels. Table 6.3 lists the schedule of seat load foundation test, the corresponding vertical load component in the back spring rail, the resulting moment, and the estimated section sizes. The depths in the last two columns were calculated from simplified beam models, using both simply supported beam and fixed end beam as described in Chapter IV. As listed in Table 6.3, the depths calculated from the computer models are between the depths calculated from simplified beam models, and were more close to the depths from fixed end beam model (F^*=96% C*). It might indicate that for a quick estimation, simplified fixed end beam model can be used to predict the maximum moment in the back spring rail beam.

The back spring rail of the *Schnadig* frame was 3 inches deep. In the seat load tests, two frames passed light acceptance load level, and one failed at light acceptance load level. As listed in Table 6.3, the estimated depth for light acceptance level was 3.169 inches, and medium was 3.547 inches. In order to achieve a medium or above acceptance level, the back spring rail should be at least 3.547 inches in depth. Considering the internal voids in the plywood panel, a greater depth would be needed. One suggestion is to use a back spring rail with the depth of at least 3.547 inches as calculated. Another suggestion is to give the back spring rail some support in the vertical

direction. Figure 6.17a shows the construction of back spring rail in *Schnadig* frame, where the back spring rail was connected to the stretchers and back uprights. In this way, the stretchers and back uprights would provide some restrains in the vertical direction. However, should the joints loosen, only a small part of the load would be transferred and the back spring rail would carry most of the vertical load. In order to improve the vertical support, it is recommended that the stretcher be connected to the back upright directly as shown in Figure 6.17b (the back spring rail could be laid across over the stretcher). By connecting the stretcher to back upright, the stretcher could be viewed as a two-end-fixed beam. The vertical load would transfer from the back spring rail directly to the stretcher. It would give more support and reduce the moment in the back spring rail. With the construction of Figure 6.17b, the maximum moment produced by the three 100-pound loads on the back spring rail would be 1,492 lb-in if it is assumed that the connection of stretcher to back upright be rigid. For this case, the calculated depth of the back spring rail would be 2.611 inches for light, 2.922 inches for medium, and 3.067 inches for heavy acceptance level.

Table 6.3 Estimation of the back spring rail in GSA seat load foundation test

Cyclic load P (lb.)	Vertical component in the back spring rail $P\times F_b$[a] (lb.)	Number of loads	Moment in the back spring rail $P\times F_b\times M_u$[a] (lb.-in.)	Acceptance level	Estimated depth (in.)		
					C[a]	F[a]	S[a]
150	96	3	2141				
187.5	120		2676				
225	144		3211				
262.5	168		3746				
300	192		4282	Light	3.169	3.044	3.826
337.5	216		4817				
375	240		5352	Medium	3.547	3.407	4.282
412.5	264		5887	Heavy	3.722	3.576	4.494

[a] F_b = 0.68 (the percentage of the load transferred to back spring rail).
M_u = 2,230 (lb-in.)/100 (lb.) (moment caused by unit load).
C stands for depths calculated based on computer models; F stands depths calculated from fixed end beam model, and S stands for depths calculated from simply supported beam model.

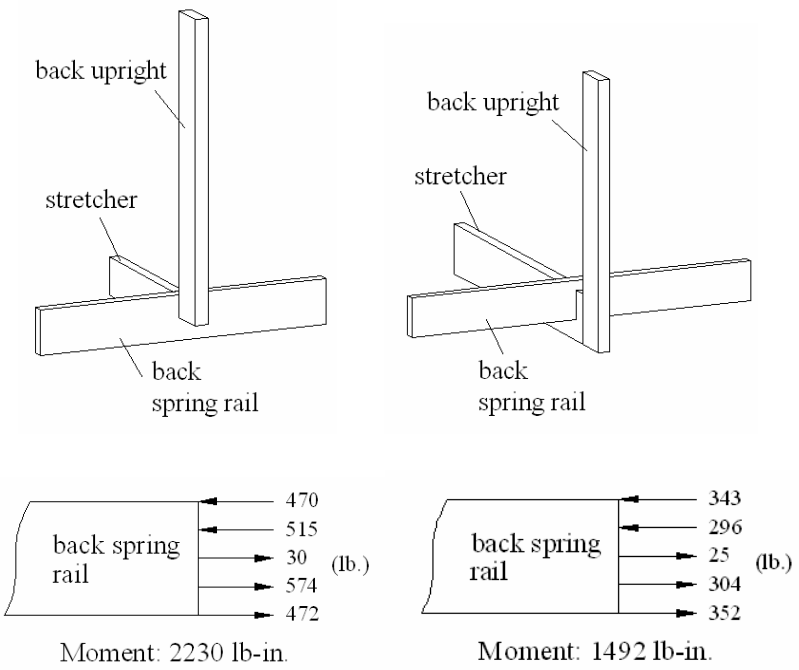

(a) (b)

Figure 6.17 The back spring rail and the maximum moment at the mid-span in (a) *Schnadig* frame construction, and (b) suggested frame construction

Summary

In this section of research, numerical analyses were carried out on a three-seat sofa frame models in order to obtain the internal forces produced at critical components. A solid 3D three-seat sofa frame model was developed using I-DEAS software. GSA load tests were simulated. These were horizontal side-thrust arm load test (inward and outward), backrest frame test, and vertical load on back spring rail. The joint of front stump to bottom side rail, joint of front stump to side center rail, joint of top arm rail to back post, and back spring rail were analyzed because they were identified as weak parts under GSA performance tests. A ratio of two was applied when considering the cyclic load effects for designing the joint. Palmgren-Miner rule was used to estimate the section size of members needed to satisfy GSA acceptance standards.

Recommendations for the improved frame construction were proposed based on the numerical analysis, GSA performance test on frames, and all the tests on components described in the previous chapters. For joints, the improved application of glue and staples was proposed as one way to improve the strength. These were the two major connectors in the original *Schnadig* frames. Samples of the suggested joint constructions were made and tested under bending loads and direct withdrawal loads. Testing results indicated that all of the improved joints allowed the sofas to achieve the medium acceptance level, and some even achieved the heavy acceptance level. The joint of front stump to side center rail was tested under GSA side-thrust load test on arms (outward) schedule. One specimen passed medium acceptance level and the other one reached

heavy acceptance level. For back spring rail, it was found that vertical support would reduce the moment in the rail member so that the medium or above acceptance level could be achieved.

CHAPTER VII

CONCLUSIONS AND RECOMMENDATIONS

Conclusions

The objectives of this research were to evaluate the structure of *Schnadig* three-seat sofa frames, summarize current available information related to engineering design, derive cyclic schedules for durability evaluation of frame components, and develop frame design loads. The target goal of medium or above acceptance level was selected for the improved design. The design procedures and testing results in the study are applicable on other frames, and serve as a guideline for product engineering and reengineering. This research was divided into four parts: (1) evaluation of the frames; (2) evaluation of wood composites as frame stock members; (3) evaluation of the strength of glue joints and single staple joints; and (4) numerical analyses on the frames.

The following conclusions are drawn from the performance test on the *Schnadig* frames:

- Generally the frames did not reach the anticipated medium acceptance level except for the arm vertical test, where all the tested frames passed heavy duty.
- Weak joint connections were the major cause of failure. The weak joints identified were the front stump to bottom side rail joint, the front stump to side center rail joint, and the top arm rail to back post joint.

- Only one member was overstressed during the tests. this was the back spring rail under the seat load foundation test.
- It was found that although glue was applied to the joints when the frames were assembled, little or none of the glue got into the interface of the joints. Therefore, only the staples were considered carrying loads.
- A ratio of two can be applied to static loads use for the design of joints to account for the effect of cyclic loading.

The following conclusions are drawn from evaluation of static and fatigue properties of wood composites:

- Regression analysis of *S-N* data of constant amplitude cyclic load tests on selected wood composites yielded a linear relationship between applied nominal stress and the logarithm of number of cycles to failure.
- The regression equations of *S-N* curves through low 5% points were derived for all selected wood composite materials and proposed as design equations for achieving a conservative design of furniture frame structural members considering fatigue effects. It was found that for the equation, $S = MOR(E - H \times \log_{10} N_f)$, the constant E was 0.85, and the constant H values were 0.06, 0.08, and 0.10, for plywood, OSB, and particleboard, respectively.
- Cyclic stepped load tests of full-size back top rail specimens indicated that the Palmgren-Miner rule provided a conservative estimation of fatigue life of

wood composites subjected to cyclic stepped bending stresses using their low 5% limit *S-N* curves.

- When cyclic stepped load effects were considered, the allowable design stress for plywood, OSB, and PB should be no more than 54%, 64%, and 68% of their MOR, respectively.
- The required sizes of members in S*chnadig* frame were estimated based on the *S-N* curves and the moment schedule derived from GSA seat load foundation test. Simple support beam model and fixed end beam model were proposed as conservative and progressive, respectively, design criteria.

The following conclusions are drawn from evaluation of lateral shear and direct withdraw strengths of face-to-face and end-to-face joints:

- Two factors, load direction and face grain orientation, were included in the glue face-to-face joint type. Experimental results indicate that the load-to-grain direction has a significant role on the mean ultimate stresses. For all face grain orientations, the lateral shear load resistance is significantly higher than direct withdraw load resistance. However, the face grain orientation affects the mean ultimate stresses only when the joints are subjected to lateral shear load.
- Load direction was included in the glue end-to-face, staple face-to-face, and end-to-face joints. For glue end-to-face joint, the load direction affects the mean ultimate stresses significantly, with lateral perpendicular shear load

resistance being the highest and direct withdraw load resistance the lowest. For single staple face-to-face joint type, the lateral shear load resistance is significantly higher than direct withdraw load resistance. For single staple end-to-face joint, no difference is found among lateral perpendicular load, lateral parallel load, and direct withdraw load resistance

The following conclusions are drawn from the numerical analyses of the critical components:

- A solid 3D frame model was developed using I-DEAS software to predict the internal forces on critical components.
- Computer analyses were used to come up with the recommendations for strengthening the weak parts so that the medium or above acceptance level could be achieved.
- Testing results of improved joints indicated that all of them reached the medium acceptance level, and some even achieved the heavy acceptance level.

Recommendations for *Schnadig* Frames

Through performance testing on *Schnadig* frames, the weak components were identified. Recommendations and suggestions were proposed based on the numerical analysis, performance test on frames, and all the tests on components stated in the previous chapters.

In general, the tested frames did not achieve desired medium acceptance level except for those tested under cyclic vertical load on arms, where all three frames passed

heavy acceptance level. Weak connections were the major cause of failure. The weak joints were, (1) joint of front stump to bottom side rail under side-thrust load on arms in an inward direction, (2) joint of front stump to side center rail under side-thrust load on arms in an outward direction, (3) joint of arm rail to back post under backrest frame test and backrest foundation test. The failure modes of the joints were observed as staples direct withdrawal from member face, end and edge. In addition to the weak joints, one member was found to be over stressed. This was the back spring rail under seat load foundation test, where the back spring rail broke in the mid-span in an edgewise direction. Based on these experiment observations, numerical analysis, and experience, the following suggestions and recommendations are made:

During the frame assembly operation, glue must be applied so that the contact surfaces are adequately coated. Glue was used during the manufacture of the tested frame assemblies. However, little or none was found on the contact surfaces of the connecting members, especially the contact surfaces between the mortise and tenon. Study results indicated that proper glue application can significantly improve joint performance. Therefore, it is suggested that glue should be applied appropriately on the contact surfaces of the critical joints as described in the preceding chapters.

The correct number of staples must be used. In this research, the number of staples used in the joint of arm rail to back post varied from four to ten. The three frames subjected to backrest frame test had six, nine, and ten staples on the joint of arm rail to back post. The three tested frames reached light, medium and heavy acceptance level

respectively. For the backrest foundation test, there were only four or five staples on the same joint, and all the frames did not reach light acceptance level. It is obvious that the inconsistent application of staples was the cause of the wide performance variation in frame performance behaviors. Hence the proper application of staples on the critical joints is recommended in order to attain a stable behavior.

For the critical joints, the improvement suggestions are to use staples and glue together to ensure a strong connection. For the joint of front stump to side rail, a glue block is also suggested to increase the glue area and to allow more staples to be used.

Joints made using these improvement suggestions were tested under static load, and all of them reached anticipated medium acceptance level. In addition to the static load test, two samples of joints of front stump to side center rail were tested under cyclic stepped load, and they reached medium and heavy acceptance level respectively according to side-thrust load on arms (outward) schedule.

For the critical back spring rail member, one suggestion is to increase the depth of the rail to at least 3.547 inches. This will enable the seat load foundation to achieve medium acceptance level. The other suggestion is to modify the construction so that more vertical supports can be provided to the back spring rail. One way to do this is to place an extra leg in the middle of the back spring rail. It is also suggested to use pine plywood in lieu of hardwood plywood for the front and back spring rails. As shown in Table 4.1, hardwood plywood is weak along its cutting (8-foot) direction, with its MOR (5,835 psi) almost identical to that of pine plywood (5,796 psi). Its strong direction

(perpendicular to the cutting direction) with a MOR of 8,547 psi, nonetheless, could not be utilized because the maximum 48-inch length is not long enough. So that the hardwood plywood offers no performance advantage. Replacing the hardwood plywood with pine plywood would save on material costs.

For less critical members, smaller section sizes can be used. Another possibility is to use cheaper material such as OSB if minimum section sizes are needed for upholstery purposes. For example in the original design, the bottom side rail consisted of two plywood members with an overall depth of 1.5 inches (0.75 each). Since the bottom side rail was not found to be a critical structural member in the performance tests, it is suggested that its overall depth be reduced to 0.75 inch using one plywood member only. By this means, the staples could be driven through the bottom rail into the block and front stump end, which can better secure the joint, and at the same time could save materials cost. In the same fashion, the section size of the front stump could also be reduced, or cheaper material could be used. As listed in Table 4.18, the depth of the front stump needed to pass heavy duty is about 3 inches, and the fixed end beam model has already considered the maximum moment. The original front stump with the depth of 7 inches is obviously an over-design.

Generally speaking, improved quality control during frame assembly is recommended, especially for the critical joints. Improvements of the weak components were proposed to meet medium or above acceptance level. On the other hand, some less

critical members can be made from fewer or cheaper materials to maximize the performance/cost ratio.

LITERATURE CITED

Adkins, D. W. and R. G. Kander. 1988. Fatigue performance of glass reinforced thermoplastics. Proceeding of the 4th Annual Conference on Advance Composites, September 1988, Dearborn, MI. Paper No. 8808-010. Sponsored by ASM International, Materials park, OH.

American Society for Testing and Materials. 2001a. Standard test methods for mechanical properties of lumber and wood-base structural material. ASTM D 4761-96. ASTM, West Conshohocken, PA.

American Society for Testing and Materials. 2001b. Standard test methods for specific gravity of wood and wood-based material. ASTM D 2395-93. ASTM, West Conshohocken, PA.

Bao, Z. and C.A. Eckelman. 1995. Fatigue life and design stresses for wood composites used in furniture. Forest Prod J 45(7/8): 59-63.

Cai, Z, J. P. Bradtmueller, M. O. Hunt, K. J. Fridley, and D. V. Rosowsky. 1996. Fatigue behavior of OSB in shear. Forest Prod. J. 46 (10):81-86.

Dowling, N. E. 1999. Mechanical Behavior of Materials. Prentice-Hall, Inc, New Jersey: 401-411.

Eckelman, C. A. 1971. Designing joints with gusset plates. Furniture Design and Manufacturing 43(9).

Eckelman, C. A. 2003. Strength design of furniture. Tim Tec. Inc. West Lafayette. Ind.

Eckelman, C. A. and J. E. Winandy. 1978. *The* Performance Test Method for Upholstered Furniture. FEHS-78-125. Federal Supply Service, General Services Administration. Washington, D.C.

Eckelman, C. A. 1988a. Performance testing of furniture. Part I. Underlying concepts. Forest Prod. J. 38(3):44-48.

Eckelman, C. A. 1988b. Performance testing of furniture. Part II. A multipurpose universal structural performance test method. Forest Prod. J. 38(4):13-18.

Eckelman, C. A. 1988. The withdrawal strength of screws from a commercially available medium density fiberboard. Forest Prod. J. 38(5):21-24.

Eckelman, C. A. and Y. A. Erdil. 2000. Joint design for furniture frames constructed of plywood and oriented strand board. FNR 170.35pp.

Eckelman, C. A., Y. A. Erdil, and J. Zhang. 2002. Withdrawal and bending strength of dowel joints constructed of plywood and oriented strandboard. Forest Prod. J. 52(9):66-74.

Eckelman. C. A., H. Akcay, R. Leavitt, and E. Haviarova. 2002. Demonstration building constructed with round mortise and tenon joints and salvage material from small-diameter tree stems. Forest Prod. J. 52(11/12):82-86.

Eckelman, C. A., E. Haviarova, A. Tankut, N. Denizli, H. Akcay, and Y. Erdil. 2004a. Withdrawal capacity of pinned and unpinned round mortise and tenon furniture joints. Forest Prod. J. 54(12):185-191.

Eckelman, C. A., E. Haviarova, Y. Erdil, A. Tankut, and N. Denizli, H. Akcay. 2004b. Bending moment capacity of round mortise and tenon furniture joints. Forest Prod. J. 54(12):192-197.

Eckelman, C. A. and J. Zhang, 1995, Uses of the General Service Administration performance test method for upholstered furniture in the engineering of upholstered furniture frames. Holz als Roh und Werkstoff 53 (1995):261-267.

Efe H., J. Zhang, Y. Z. Erdil, and A. Kasal. 2005. Moment capacity of traditional and alternative T-type end-to-side-grain furniture joints. Forest Prod. J.55(5):69-73.

Erdil, Y. Z., A. Kasal, and C. A. Eckelman. 2005. Bending moment capacity of rectangular mortise and tenon furniture joints. Forest Prod. J. 55 (12):209-213.

Erdil, Y. Z., J. Zhang, and C. A. Eckelman. 2002. Holding strength of screws in plywood and oriented strandboard. Forest Prod. J. 52(5):55-62.

Erdil, Y. Z., J. Zhang, and C. A. Eckelman. 2003. Withdrawal and bending strength of dowel-nuts in plywood and oriented strandboard. Forest Prod. J. 53(6):54-57.

Freund, R. J. and W. J. Wilson. 1997. Statistical methods. Academic Press, Inc, San Diego, CA.

Fridley. K. J. 1992. Design for creep in wood structures. Forest Prod. J. 42(3):23-28.

General Services Adminstration 1981: FNAE-80-204. Upholstered furniture test method. Furniture commodity center, Federal supply services. Washington D. C.

General Services Adminstration 1989: FNEW-83-259E. Performance test method for intensive use chairs. Furniture commodity center, Federal supply services. Washington D. C.

General Services Adminstration. 1998. FNAE-80-214A. Upholstered furniture test method. Furniture commodity center, Federal supply services. Washington D. C.

Gustafsson, S. I. 1995. Furniture design by use of the finite element method. Holz als Roh-und Werkstoff 53(1995):257-260.

Gustafsson, S. I. 1996a. Finite element modeling versus reality for birch chairs. Holz als Roh-und Werkstoff 54: 355-359.

Gustafsson, S. I. 1996b. Stability problems in optimized chairs. Wood Sci. and Technol. 30(5): 339-345.

Gustafsson, S. I. 1997. Optimsing ash wood chairs. Wood Sci. and Technol.31(4):291-301.

Hoover, W. L., J. M. Ringer, C. A. Eckelman, and J. A. Youngquist. 1987. Material design factors for hardwood laminated-veneer-lumber. Forest Prod. J. 37(9):15-23.

Hoover, W. L., C. A. Eckelman, J. M. Ringer, and J. A. Youngquist. 1988. Design and specification of hardwood laminated-veneer-lumber for furniture applications. Forest Prod. J.38(1):31-34.

Janowiak, J. J, and R. F. Pellerin. 1990. An empirical investigation of impact loading of reconstituted wood plates. Forest Prod. J. 40(6):21-28.

Kommers, W. J. 1943. The fatigue behavior of wood and plywood subjected to repeated and reversed bending stresses. Rept. No. 1327. USDA Forest Serv., Forest Prod. Lab., Madison, WI.

Kurt R. 2003. The strength of press-glued and screwed-glued wood-plywood joints. Holz als Roh-und Werkstoff 61:269-272.

Miner, M.A. 1945. Cumulative damage in fatigue. J of Applied Mechanics 12 (3): A159-164.

Palmgren, A.1924. Die lebensdauer von kugallagern. Ver. Deut Ingr. 68:339-341.

Smardzewski, J. 1998. Numerical analysis of furniture constructions. Wood Sci. and Technol. 32(4):273-286.

Tackett, B. and J. Zhang. 2007. A biaxial load cell design for simultaneous measurement of horizontal and vertical spring forces in sinuous spring-supported seating. J. of Testing and Evaluation. 35(4): xxx-xxx.

Ugural, A. C. 1991. Mechanics of materials. McGraw-Hill, Inc, New York.

Zhang, J., B. Chen, and S. R. Daniewicz. 2005. Fatigue performance of wood-based composites as upholstered furniture frame stock. Forest Prod J 55(6):53-59.

Zhang., J., Y. Z. Erdil, and C. A. Eckelman. 2002a. Lateral holding strength of dowel joints constructed of plywood and oriented strandboard. Forest Prod. J. 52(7/8):83-89.

Zhang., J., Y. Z. Erdil, and C. A. Eckelman. 2002b. Torsional strength of dowel joints constructed of plywood and oriented strandboard. Forest Prod. J. 52(10):89-94.

Zhang, J, F. C. Lin, C. Eckelman, and H. Gibson. 2000. A structural design model for sofa seat frames equipped with sinusoidal-type springs. Forest Prod. J. 50(3): 49-57.

Zhang. J, D. E. Lyon, F. Quin, and B. Tackett. 2001. Bending strength of gusset-plate joints constructed of wood composites. Forest Prod. J. 51(2): 29-35.

Zhang, J, G. Li, and T. Sellers, Jr.. 2003a. Withdrawal and bending performance of dowel joints in furniture grade pine plywood. Forest Prod. J. 53(7/8):41-49.

Zhang, J, G. Li, and T. Sellers, Jr.. 2003b. Bending fatigue life of two-pin dowel joints in furniture grade pine plywood. Forest Prod. J. 53(9):33-39.

Zhang. J. and M. Maupin. 2004. Face lateral and withdrawal resistances of staple joints in furniture-grade pine plywood. Forest Prod. J. 54(6):40-46.

Zhang. J, F. Quin, and B. Tackett. 2001. Bending fatigue life of two-pin dowel joints constructed of wood and wood composites. Forest Prod. J. 51(10): 73-78.

Zhang. J, F. Quin, and B. Tackett. 2001. Bending strength and stiffness of two-pin dowel joints connected of wood and wood composites. Forest Prod. J. 51(5): 40-44.

Zhang, J., F. Quin, B. Tackett, and S. Parkt. 2002a. Direct withdrawal strength of single-staple joints in pine plywood. Forest Prod. J. 52(2):86-91.

Zhang, J., F. Quin, B. Tackett, and S. Parkt. 2002b. Direct withdrawal strength of multiple-staple joints in pine plywood. Forest Prod. J. 52(5):61-66.

Zhang. J., F. Quin, and H. Chen. 2004. Edge lateral resistance of staple joints in furniture-grade pine plywood. Forest Prod. J. 54(7/8):85-95.

Zhang. J., Y. Yu, and F. Quin. 2005. Moment capacity of metal-plate-connected joints in furniture grade pine plywood. Forest Prod. J. 55(5):45-51.

APPENDIX A

SCHNADIG FRAME PART DETAILS

Table A.1 *Schnadig* frame part details

Part name	Quantity	Material	Size (Length by Width by Depth) ----------in. ----------
End upright	2	Pine	23 5/32 by 1 3/8 by 3/4
Back center rail	2	Pine	78 15/16 by 6 3/64 by 3/4
Back rail filler	2	Pine	82 41/64 by 7 5/32 by 3/4
Back spring rail	2	Hardwood	78 15/16 by 3 by 7/8
Top rail	2	Pine	78 3/64 by 2 3/4 by 3/4
Arm spacer	2	Pine	4 1/32 by 1 45/64 by 3/4
Back filler block	2	Pine	3 59/64 by 1 5/8 by 3/4
Bottom arm filler	2	Pine	14 25/32 by 1 19/64 by 3/4
Stump tack strip	2	Pine	9 11/16 by 1 9/64 by 3/4
Front filler spacer	2	Pine	6 1/2 by 3 29/32 by 3/4
Wing	2	Pine	8 33/64 by 3 27/32 by 3/4
Front spring rail	2	Hardwood	78 15/16 by 2 by 7/8
Top arm filler	2	Pine	27 21/64 by 3 19/64 by 3/4
Side center rail	2	Pine	27 3/32 by 2 by 3/4
Side skirt rail	2	Pine	25 3/64 by 1 3/8 by 3/4
Bottom front rail filler	2	Pine	45 13/64 by 6 17/32 by 3/4
Back post	2	Pine	28 11/64 by 5 51/64 by 3/4
Top arm filler	2	Pine	25 5/8 by 4 5/32 by 3/4
Center support	2	Pine	28 33/64 by 7 37/64 by 3/4
Leg stretcher left	2	Pine	27 57/64 by 2 1/2 by 3/4
Leg stretcher right	2	Pine	27 57/64 by 2 1/2 by 3/4
Leg stretcher filler	2	Pine	26 19/32 by 2 1/2 by 3/4
Stump	2	Pine	15 1/16 by 7 by 3/4
Arm spacer	2	Pine	4 1/32 by 1 45/64 by 3/4
Side rail	2	Pine	27 9/16 by 3 by 3/4
Seat stretcher	2	Pine	26 15/16 by 4 3/4 by 7/8
Front rail	2	Pine	90 27/64 by 4 5/8 by 3/4